ABSTRACT

Title of Document: ULTRAFAST NONLINEAR PLASMONICS

Sanghee Nah, Doctor of Philosophy, 2012

Directed By: Professor John T. Fourkas
Department of Chemistry and Biochemistry

Metal nanostructures can enhance the optical signals by orders of magnitude due to surface plasmon resonance. This field enhancement of the plasmonic nanostructures has led to optical detection and light manipulation beyond the free space diffraction limit. However, the significant enhancement of optical signals of the nanostructures has not been fully understood. In order to examine field-enhanced phenomena, this dissertation studies a variety of plasmonic nanostructures using two nonlinear optical processes, multiphoton-absorption-induced luminescence (MAIL) and metal-enhanced multiphoton absorption polymerization (MEMAP).

Nonlinear absorption of near-infrared light can lead to luminescence of metal nanostructures. This luminescence can be observed at localized areas of the nanostructures because of localized surface plasmon resonance and the “lightning

rod" nanoantenna effect. In the presence of a prepolymer resin, luminescence generated from the nanostructures can induce polymerization by exciting a photoinitiator. The strong correlation between MAIL and MEMAP is demonstrated by using different excitation wavelengths and different types of prepolymer resins.

While localized surface plasmon resonance plays a pivotal role in field-enhanced optical phenomena observed at local areas of gold nanoparticles, nanowires, and nanoplates, surface plasmon propagation is essential to understanding of the nonlinear optical properties in silver nanowires. As silver nanowires can support surface plasmon propagation for many microns, excitation of NIR light at one end of the nanowire can induce luminescence at the other end of the nanowire. This broadband luminescence can excite a photoinitiator, inducing polymerization. The luminescence-induced polymerization in remote positions can be used to assemble nanostructures.

Nonlinear luminescence and its correlation to polymerization are also studied using carbon nanostructures. While metal nanostructures exhibit plasmonic field enhancement, carbon nanotubes have strong Coulomb interactions between excited electrons and holes, which results in luminescent emission. Additionally, the high density of electron states of carbon nanotubes can increase the probability of the recombination of the excited electron and hole, which in turn induce luminescence. The luminescence emission and photopolymerization are studied using different kinds of carbon nanostructures.

ULTRAFAST NONLINEAR PLASMONICS

By

Sanghee Nah

Dissertation submitted to the Faculty of the Graduate School of the
University of Maryland, College Park, in partial fulfillment
of the requirements for the degree of
Doctor of Philosophy
2012

Advisory Committee:
Professor John T. Fourkas, Chair
Professor Neil Blough
Professor Amy Mullin
Professor Ray Phaneaf
Professor YuHuang Wang

Acknowledgements

First and foremost, I would like to gratefully thank my adviser, Dr. John Fourkas, for his support, advice, and guidance throughout my graduate study. Without his guidance, none of the work in this thesis would have been possible. His incredible ideas, keen observation, intuition, and incredible memory about everything always brought solutions of my work. Whenever I faced unexpected research difficulties, he was always there to guide and support me. His patience and optimism has encouraged me immensely both in research and in person. I am very fortunate to meet him as my adviser and to see when he brings brainstorming ideas out and develops inspiration and creativity. I believe that all he has taught me will continue to guide me in my future career.

I would like to thank my family for their support. They always gave me warmth, confidence, and encouragement to overcome hard moments of studying. Their cheers and jokes were the best cure of my difficult moments.

I would like to thank all the members of the Fourkas group. I was very lucky to work with Dr. Linjie Li who taught me how to start the work when I first joined the group. I would like to thank Dr. George Kumi who has been an excellent mentor. Dr. Kumi was the most considerate and kind person I have ever known. I would like to thank Dr. Qin Zhong, Dr. Feng Ding, Dr. Rafael Gatass and Dr. Kathleen Monaco for sharing good tips on the experiments and being good friends. I am grateful to Dr. Michael Stocker for being a good friend throughout the graduate program since we joined the Fourkas group together, and for inviting me to his beautiful wedding. My special thanks go to Xiaoxiao He and Sijia Qin who were good friends for many years.

Their encouragement helped me to get through difficult moments. I would like to thank Floyd Bates II with whom I enjoyed talking about research and interesting subjects. I would like to express my warmest thanks to Xiaoyu Sun for being such a great friend. I won't forget the beautiful postcards she sent from many fantastic places. I am very grateful to Junjie Hao for performing the experiments using gold nanoplates and his sharing delicious chocolates. I also thank Zulya Tomova for helping me to finish several experiments and focus on this dissertation. I am very much indebted to Dr. Christopher Rivera for his great support to complete this dissertation with valuable and critical comments. I am very grateful to Dr. Samrat Dutta for sharing ideas on the research, setting up the spectrometer, and collecting data together. I would like to thank Dr. Farah Dawood for setting up the spectrometer for many times and sharing valuable advice on graduate work. I would like to thank John Bender for creating a program to collect spectra and cheering us with super funny jokes. I would like to thank Alison Sikorsky, Dr. Carlos Toro, Jarrett Leeds, Meghan Driscoll, and Michael Hsu for being good friends. I am very grateful to Katherine Manfred and Emily Lin for being such great friends, sharing delicious Kolaczki, Focaccia, and cupcakes, and cheering me up with humorous jokes and good songs.

Table of Contents

List of Figures

Chapter 1: Surface plasmons with nonlinear optical processes

1.1 Introduction

Metal nanostructures with at least one dimension that is 1-100 nm in size have received a great deal of attention over the last few decades due to their electron confinement properties, which are distinct from those in bulk systems or individual atoms.[1] On the surface of metal nanostructures, free electrons in the conduction band collectively oscillate within tens of nanometers from the surface, in a mode called a surface plasmon (SP). When incident light at a wavelength much larger than the size of the metal nanostructures excites the nanostructures, it can couple to these collective oscillations, driving an electromagnetic field resonance at a metal-dielectric interface. This localized surface plasmon resonance (LSPR) leads to a localized electromagnetic field enhancement.

SPs can propagate along the metal-dielectric interface as the conduction electrons move on the metal surfaces. These propagating plasmons are known as surface plasmon polaritons (SPPs). SPPs can travel along a metal nanostructure surface for up to hundreds microns.[2,3] However, SPPs are confined to within tens to hundreds of nanometers of the surfaces because electromagnetic field of the SPs exponentially decays in z-direction.[2-5] The LSPR and SPPs from metal nanostructures offer the capability of manipulating the light beyond the free-space optical diffraction limit.[6,7]

It has been shown that SPs on metal structures can provide more than five

orders of magnitude enhancement in optical signals such as scattering,[8-11] absorption,[12] and fluorescence.[13-15] The field enhancement has been used widely for applications including single molecule spectroscopic sensing,[16-20] photothermal therapy,[21-23] optical imaging,[24] and photolithography.[25,26] In addition, the conversion from far-field incident light (light exciting the sample with a distance much larger than the wavelength) to the near-field of SPs (light exciting the sample within a distance smaller or of the order of the wavelength) has led to the development of faster and more efficient optical sensors than the currently available.[27,28]

The electromagnetic field enhancement observed to date has largely exceeded the values predicted by theory. For example, strong optical scattering from single molecules has been detected by surface enhanced Raman spectroscopy (SERS),[16,20] while the theory behind this phenomenon has not clearly predicted the same result. In order to investigate field-enhanced phenomena, we studied two nonlinear optical processes, multiphoton-absorption-induced luminescence (MAIL) and metal-enhanced multiphoton absorption polymerization (MEMAP) on a variety of plasmonic metal nanostructures.

In this Chapter, the fundamentals of surface plasmon resonance (SPR) on metal nanostructures and the background of MAIL and MEMAP will be discussed. The contribution of SPPs to nonlinear processes and the relationship between MAIL and MEMAP will also be discussed with examples.

1.2 Properties of LSPR and SPPs

1.2.1 Fundamentals

Figure 1.1 illustrates how the free electrons in a metal sphere oscillate with the incident light. The interaction between light and the metal nanospheres generates the LSPR. As seen in Figure 1.1, the wavelength of the incident light should be larger than the size of the metal nanostructures to induce optical SPR. SPs are confined to within 50 nm from the surface in the case of gold and silver nanostructures.[1]

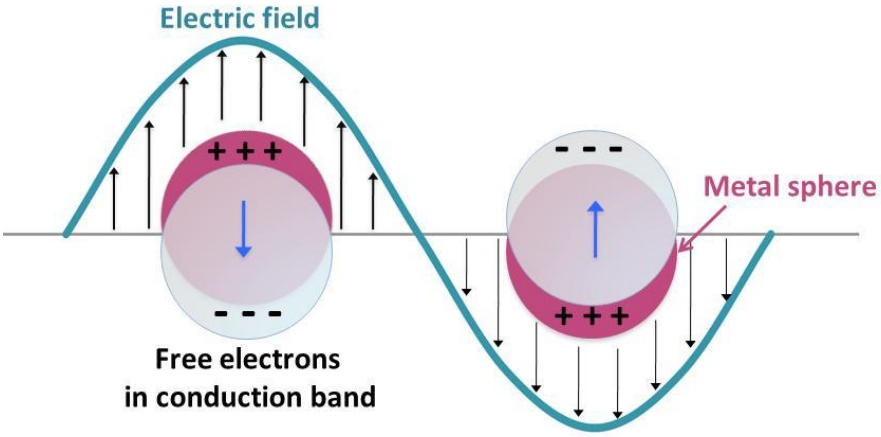

Figure 1.1. Schematic of a localized SPs. (Reproduced from reference[2]).

The most extensively studied metals in regard to the SP-associated field enhancement are gold and silver, because their surface plasmon absorption cross-section is located in the visible region of the spectrum. The field enhancement of metal nanospheres can be explained by considering the electric-field permittivity of the metal nanostructure and that of the environment. When we consider light of wavelength λ exciting a metal nanosphere of radius *a* (*a* is much smaller than λ), the electromagnetic field[5,9] outside the particle is given by

$$E_{out}(x,y,z) = E_0\hat{\boldsymbol{z}} - \left[\frac{\varepsilon_{in}-\varepsilon_{out}}{(\varepsilon_{in}+2\varepsilon_{out})}\right] a^3 E_0 \left[\frac{\hat{\boldsymbol{z}}}{r^3} - \frac{3z}{r^5}(x\hat{\boldsymbol{x}} + y\hat{\boldsymbol{y}} + z\hat{\boldsymbol{z}})\right] \quad , (1.1)$$

where ε_{in} is the dielectric constant of the metal nanosphere and ε_{out} is the dielectric constant of the environment.[2] The dielectric constant (ε) is a relative permittivity that indicates how an electric field affects or is affected by the dielectric medium. It is a complex quantity, i.e. $\varepsilon = \varepsilon' + i\varepsilon''$. In the case of a material with low permittivity, a stronger electric field exists inside the medium than outside of it. For example, the relative permittivity for gold at 830 nm is $\varepsilon_m \approx -29 + 2.1i$, so there is a large, negative real part.[3] The dielectric field resonance condition is determined by the ε_{in} in Eq (1.1), because ε_{in} is strongly wavelength-dependent and ε_{out} is much weaker than ε_{in}.[2] When ε_{in} is roughly equal to $-2\varepsilon_{out}$, the electric field can be enhanced.[2] Since this resonance condition is met at the wavelengths in visible and NIR region of the spectrum for the gold and silver nanostructures,[2] these metal nanostructures have been studied using typical optical systems with visible to NIR light.

This LSPR is sensitive to changes in the local environment. The optical signals of surface plasmon absorption, scattering and luminescence can be tuned by modifying the shape,[29] size,[30,31] and geometry[15,26,32] of nanostructures as well as the refractive index (n, $n = \sqrt{\varepsilon}$)[30,33,34] of the surrounding medium. For example, the plasmon absorption band moves markedly to longer wavelengths as gold nanostructures are elongated. Figure 1.2a shows a typical plasmon absorption spectrum of a solution of gold nanorods with an aspect ratio of 3 to 5. The scanning electron microscope (SEM) image of the gold nanorods (along with a small amount

of nanospheres) is shown in Figure 1.2b.

In Figure 1.2a, the absorption band at 516 nm is a transverse mode from the 16 nm short axis of the nanorods. The absorption band at 800 nm is a longitudinal mode from 45 nm long axis of the nanorods. As the nanorods become longer, the longitudinal mode can be shifted to longer wavelength. An absorption band from the gold nanospheres is also seen at 548 nm due to their 43 nm diameters.

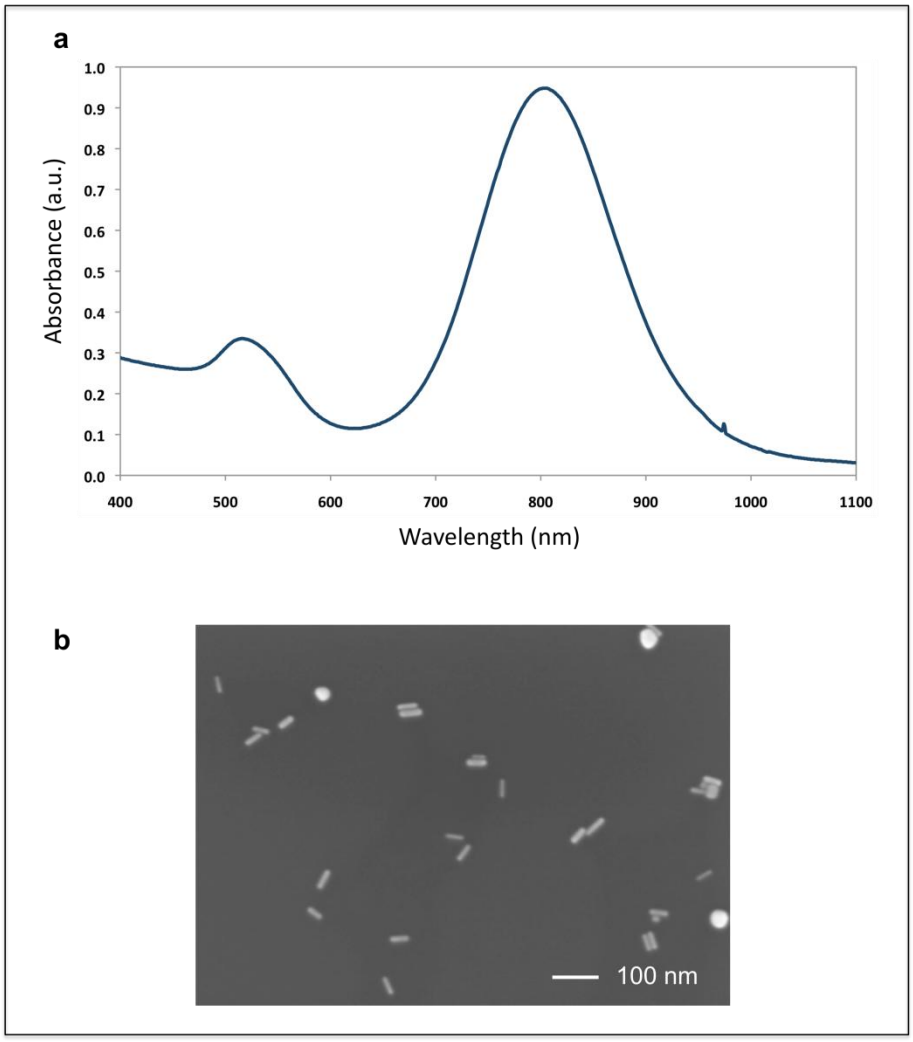

Figure 1.2. (a) UV/vis absorption spectrum of gold nanorods. (b) SEM image of gold nanorods and nanospheres. The absorbance spectrum in (a) was measured using the nanostructures shown in (b).

Visible to NIR light can not only be localized at nanostructures to generate LSPR, but also can be guided along the nanostructures by SPPs. Figure 1.3 illustrates propagating SPPs on a metal-dielectric interface. SPPs can travel many microns along an interface until the energy decays. The propagation length in z is limited due to the exponential decay of the evanescent wave.[2-5]

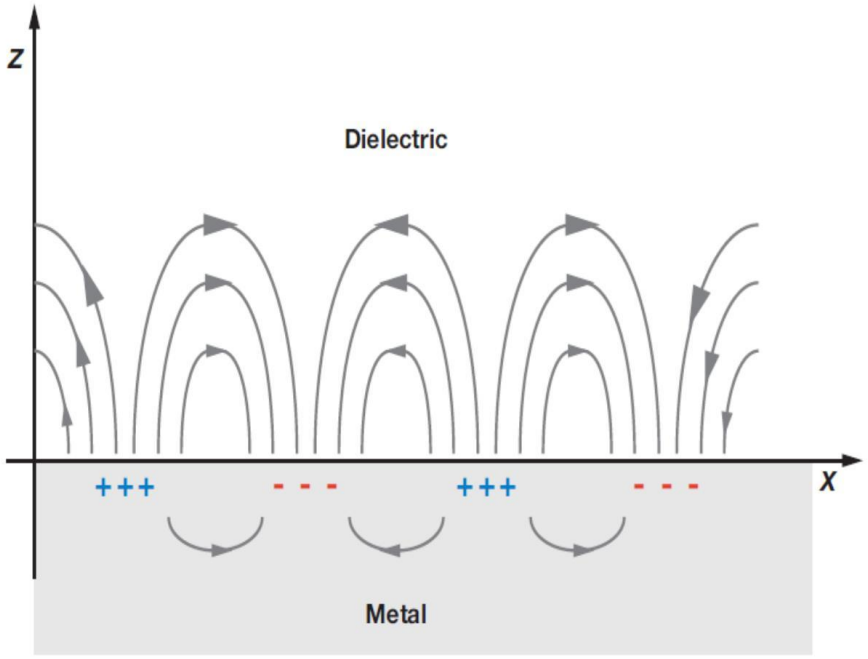

Figure 1.3. Schematic of SPPs at a metal-dielectric interface. (Reproduced from reference [2]).

SPPs have been observed from different kinds of nanostructures.[35] For example, when light excites one end of a 100 nm-thick silver nanowire, the electric field is confined on the surface and propagates along the nanowire up to 40 μm.[35] The localization and propagation of SPs are unique properties of metal nanostructures that enable the observation and manipulation of light beyond the diffraction limit.[6,7]

1.2.2 Applications of SPs

The localized SP modes on metal nanostructures have played a pivotal role in optical and biological applications[2,14] and have provided the optical detection sensitivity necessary for single molecule applications.[16-20] For example, hydrogen gas molecules have been detected at the field-enhanced gap between palladium and gold triangular nanostructures.[32] As a photothermal therapy tool,[21-23] gold nanorods have been used as a minimally-invasive treatment of tumor cells due to the heat created by the field-enhanced absorption in gold nanorods.[22] SERS signals have been detected from a single dye molecule in a colloidal silver solution.[18]

Moreover, SPPs have led to advances in the development of optoelectric sensors because the incident light can be converted into SPP modes, which can turn into electrical signals. For instance, photonic circuits made with metal nanostructures result in faster than typical electrical sensors,[28] because circuits designed with nanostructures can detect incident photons by the electric signals generated by the conversion of SPPs into electron-hole pairs. The SPP-combined electric circuit can overcome the conventional, far-field detection limit including the detection of plasmon states in which coupling to the far-field is suppressed by symmetry.[28,36]

Despite the extensive studies on SP modes, the field enhancement experimentally observed is still not fully understood. In order to study SP-assisted field enhancement, we have employed two nonlinear optical processes, MAIL and MEMAP. The fundamentals and applications of these nonlinear processes will be discussed in the following section.

1.3 Multiphoton absorption

1.3.1 Fundamentals

In 1931, Maria Göppert-Mayer first theoretically predicted the multiphoton absorption (MPA) process.[37] Due to the requirement of high photon intensities, two-photon absorption was first experimentally observed when the laser was developed in 1961.[38] In a typical two-photon absorption process, two photons of about equal energy are simultaneously absorbed by a molecule. This absorption leads to an electronic transition, and any resulting fluorescence emission occurs at the same wavelengths where it can be observed following single-photon absorption of photons of twice the energy.

In general, the absorption probability is proportional to the excitation intensity to the power of the number of photons required for the excitation transition. Quantum mechanical Perturbation theory can explain the absorption probability in MPA.[39,40] When an electron is excited from the initial state |i> to the final state |f>, the transition can be explained using the electric field vector E_γ, and the position vector r.[39,40] Equation (1.2) shows an example of the transition probability for two-photon absorption.

$$P \approx \left| \sum_m \frac{\langle f | \vec{E}_\gamma \cdot \vec{r} | m \rangle \langle m | \vec{E}_\gamma \cdot \vec{r} | i \rangle}{\varepsilon_\gamma - \varepsilon_m} \right|^2 \qquad (1.2)$$

In this equation, ε_γ is the energy of E_γ and ε_m is the energy difference between the ground state and the virtual state m. At the virtual state m, because the lifetime of the excited electrons is only a few femtoseconds, simultaneous absorption of photons is crucial to reach the excited state.[39,40] This equation shows the transition probability is

proportional to the light intensity squared.

In order to drive the MPA process, ultrafast lasers are commonly used due to their high photon intensity.[41] A typical ultrafast Ti:sapphire oscillator produces pulses with temporal widths of tens of femtoseconds at a repetition rate of 80 MHz (a 12.5 ns interpulse separation time).[41] When the femtosecond pulses are focused through a microscope objective, the high intensity drives the MPA process at the focal region. Since MPA only occurs efficiently in the small focal volume of laser beam, the region that undergoes MPA can be controlled in three dimensions.

When employing MPA, it is common to utilize objectives with high numerical aperture (NA) to create high photon density at the focal volume. At the focal point, the number of photons absorbed per molecule per pulse[42] can be calculated as shown in Eq (1.3).

$$n_a \approx \frac{p_0^2 \delta}{\tau f_p^2} \left(\frac{(\mathrm{NA})^2}{2\hbar c \lambda} \right)^2 \qquad (1.3)$$

In this equation, p_0 is a time-averaged laser power, τ is a pulse duration, f_p is a pulse repetition rate, and δ is the two-photon absorption cross-section, which is defined in SI units as 1 GM = 10^{-58} m^4 s photon^{-1}, named after Göppert-Mayer[42].

1.3.2 Applications of MPA

1.3.2.1 Optical imaging in biology

Multiphoton microscopy has been used widely in fluorescence imaging of tissue specimens[42] and living animals.[43-45] Because multiple photons are simultaneously absorbed in the fluorescent molecules, a fluorescence microscope can

utilize visible or near-infrared (NIR) ultrafast pulses to excite the molecules instead of harmful ultraviolet (UV) light. The tightly focused pulses used for the imaging can alleviate out-of-focus photobleaching and photodamage since the tissue is transparent to the low-frequency radiation.[14]

Since commercial multiphoton microscopes were introduced in 1996, applications of multiphoton fluorescence imaging have increased exponentially.[14] For example, neuroscientists have directly imaged serotonin, one type of neurotransmitter, in cells by three-photon excitation with infrared light.[44] Embryologists have monitored a developing hamster embryo using multiphoton microscopy to study its development over a day.[46] Nanosurgery has been demonstrated using a femtosecond laser to cut single axons inside the roundworm *C. elegans* in order to study nerve regeneration.[47] Gene expression in tumor cells was monitored *in vivo* using multiphoton microscope.[48] Using quantum dots, multicolor fluorescence imaging has been performed to study different biological environments in the skin of living mice.[43]

1.3.2.2 Three-dimensional polymerization

One of the most important applications of the multiphoton absorption process is fabrication of three-dimensional polymer structures. In a typical polymerization process, a prepolymer resin, including monomers and a photoinitiator, absorbs UV light. The UV excitation leads to the excitation of the photoinitiator. When a MPA process is used for this transition, the photoinitiator can be excited with visible to NIR light. The resulting radicals or cations lead to cross-linking among monomers.

Because MPA occurs in a tightly focused spot, the resulting polymer features can be as small as the focal volume of the excitation light. Figure 1.4 shows high resolution polymer structures in three dimensions fabricated by multiphoton absorption polymerization (MAP)[41].

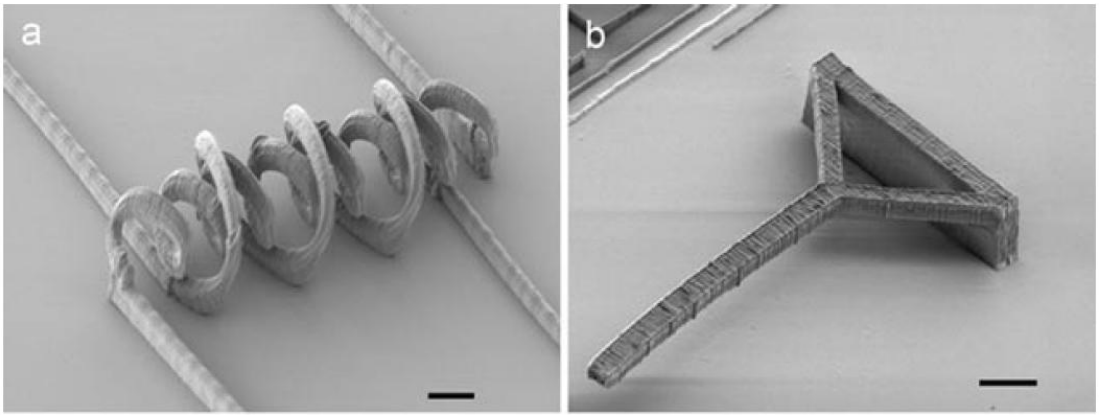

Figure 1.4. Three-dimensional polymer structures fabricated by MAP. (a) SEM image of interpenetrating coils. (b) SEM image of a cantilever. The scale bars are 10 μm. (Reproduced from reference [41]).

In order to decrease the polymer sizes for fabricating high resolution devices, many methods have been developed utilizing the principles of MAP. For example, a polymer feature of 80 nm, which is λ/10, where λ is an excitation wavelength, has been fabricated by combining MAP and modifications of the development process.[49] Shorter excitation wavelengths can increase the resolution (d) as shown in Eq (1.4),[27]

$$d = \frac{\lambda}{2n \sin \alpha} \tag{1.4}$$

where α is the half angle over which light is focused. However, the feature size along

the z-axis is roughly three times bigger than that in lateral xy- axis.[14,27] A recent paper reported the achievement of λ/20 polymer features using resolution augmentation through a photo-induced deactivation (RAPID) method.[50] The use of RAPID lithography with visible light can make high resolution integrated circuits with reduced manufacturing cost than what is required by conventional lithography using UV light.[50]

1.4 Multiphoton absorption of plasmonic nanostructures

MAIL is a result of an MPA process performed using plasmonic metal nanostructures. MAIL was first observed from noble metal surfaces in 1986.[51] Boyd *et al.* further showed that field enhancement by SPs was strengthened at rough surfaces.[51] Because an MPA process is involved, MAIL from metal nanostructures can be observed with NIR excitation. For example, gold nanoparticles have been found to luminesce in the visible after absorbing three NIR photons simultaneously.[52] MAIL has been observed from a variety of metal nanostructures such as gold nanoparticles,[52] nanorods,[53] and nanoantennas.[54] As the SPR changes with the different shapes of nanostructures examined, the respective MAIL intensities are also modified. It is well known that SPs become stronger at the sharp edges of the nanostructures due to the crowding of the electromagnetic fields, also known as the "lightning rod" nanoantenna effect.[54-56] As a result, the sharp edges on single nanostructures[53] and small gaps[54] between multiple nanostructures show very efficient MAIL.

MAIL from metal nanostructures has been extensively used in nonlinear optical biological imaging. For example, two-photon luminescence imaging was used with individual gold nanorods to follow flow in mouse ear blood vessels.[45] Cancer cells in the 500 μm-deep tissue have also been imaged by two-photon luminescence of gold nanorods.[14]

In MEMAP, the presence of metal nanostructures can induce MAP at a much lower excitation intensity than required for typical polymerization due to the field enhancement by SPR. MEMAP can create polymer features as small as a few nanometers due to the LSPR. For example, when light excites a gap of a few nanometers in a gold bowtie nanoantenna, a polymer feature of 30 nm in size can be created.[26] MEMAP has also been observed from gold nanorods,[57] and a metal-coated AFM tip.[58]

Nonlinear optical processes such as MAIL and MEMAP highlight the significance of controlling the properties of SPR on metal nanostructures, because the luminescence and polymerization occur efficiently where field enhancement is strongest. However, these nonlinear optical properties have previously been observed from randomly dispersed nanostructures[52] or nanostructures in uniform arrays.[57] In this dissertation, I present studies of MAIL and its correlation to individual nanostructures of different shapes. The relationship between the MAIL and MEMAP will be examined.

1.5 Thesis outline

Plasmonic metal nanostructures exhibit unique optical signals over a broad range of spectral wavelengths. The optical fields from the nanostructures are enhanced due to the LSPR and SPPs. To study the SP-associated field enhancement, we used plasmonic gold and silver nanostructures. Two nonlinear optical processes, MAIL and MEMAP, were examined using different shapes of the nanostructures. Chapter 2 will show MAIL and its correlation to MEMAP in gold nanoparticle aggregates. The relationship between the efficient MAIL intensities and the polymer features created from each nanoparticle will be discussed.

In order to further examine our observation of MAIL and its correlation to MEMAP, we used uniform gold nanowires. Chapter 3 will discuss how plasmonic nanowires exhibit MAIL. In addition, I will discuss how polymerization occurs from luminescent nanowires when three different kinds of photoresists are employed.

Chapter 4 will present the observation of MAIL and MEMAP using gold nanoplates. The polarization-dependent MAIL intensity patterns from single triangular and hexagonal nanoplates will be discussed. I will present the luminescence and its correlation to the polymerization induced in localized areas of the nanoplates.

In addition to the study of LSPR using gold nanostructures, I will also present the study of SPPs using silver nanowires in Chapter 5. Because the silver nanowires can support SPP propagation for many microns, I was able to observe MAIL and MEMAP at remote positions from the light excitation areas. I will also discuss how the SPPs of silver nanowire can be used to assemble nanostructures in a controlled

manner.

Chapter 6 will discuss the nonlinear optical properties of carbon nanomaterials. To date the optical properties of carbon nanotubes (CNTs) were studied using CNTs in solutions or using randomly dispersed nanotubes. The optical signals measured from these samples contain information from aggregated nanotubes. In Chapter 6, I will present MAIL signals from individual multiwalled nanotubes. In addition, MAIL and its correlation to polymerization using single-walled nanotubes and graphene multiple sheets will be presented.

References

(1) Eustis, S.; El-Sayed, M. A.: Why gold nanoparticles are more precious than pretty gold: Noble metal surface plasmon resonance and its enhancement of the radiative and nonradiative properties of nanocrystals of different shapes. *Chem. Soc. Rev.* **2006**, *35*, 209-217.

(2) Willets, K. A.; Van Duyne, R. P.: Localized surface plasmon resonance spectroscopy and sensing. *Annu. Rev. Phys. Chem.* **2007**, *58*, 267-297.

(3) Barnes, W. L.: Surface plasmon-polariton length scales: A route to sub-wavelength optics. J. Opt. a-Pure Appl. Opt. **2006**, *8*, S87-S93.

(4) Knoll, W.: Interfaces and thin films as seen by bound electromagnetic waves. *Annu. Rev. Phys. Chem.* **1998**, *49*, 569-638.

(5) Kelly, K. L.; Coronado, E.; Zhao, L. L.; Schatz, G. C.: The optical properties of metal nanoparticles: The influence of size, shape, and dielectric environment. *J. Phys. Chem. B* **2003**, *107*, 668-677.

(6) Gramotnev, D. K.; Bozhevolnyi, S. I.: Plasmonics beyond the diffraction limit. *Nature Photon.***2010**, *4*, 83-91.

(7) Kawata, S.; Inouye, Y.; Verma, P.: Plasmonics for near-field nano-imaging and superlensing. *Nature Photon.* **2009**, *3*, 388-394.

(8) Kneipp, K.; Kneipp, H.; Itzkan, I.; Dasari, R. R.; Feld, M. S.: Ultrasensitive chemical analysis by Raman spectroscopy. *Chem. Rev.* **1999**, *99*, 2957-2976.

(9) Schatz, G. C.: Theoretical-studies of surface enhanced Raman-scattering *Accounts Chem. Res.* **1984**, *17*, 370-376.

(10) Zou, S. L.; Schatz, G. C.: Silver nanoparticle array structures that produce giant enhancements in electromagnetic fields. *Chem. Phys. Lett.* **2005**, *403*, 62-67.

(11) Haynes, C. L.; Van Duyne, R. P.: Plasmon-sampled surface-enhanced Raman excitation spectroscopy. *J. Phys. Chem. B* **2003**, *107*, 7426-7433.

(12) Jain, P. K.; Eustis, S.; El-Sayed, M. A.: Plasmon coupling in nanorod assemblies: Optical absorption, discrete dipole approximation simulation, and exciton-coupling model. *J. Phys. Chem. B* **2006**, *110*, 18243-18253.

(13) Mohamed, M. B.; Volkov, V.; Link, S.; El-Sayed, M. A.: The 'lightning' gold nanorods: fluorescence enhancement of over a million compared to the gold metal. *Chem. Phys. Lett.* **2000**, *317*, 517-523.

(14) Zipfel, W. R.; Williams, R. M.; Webb, W. W.: Nonlinear magic: Multiphoton microscopy in the biosciences. *Nature Biotech.* **2003**, *21*, 1368-1376.

(15) Kinkhabwala, A.; Yu, Z.; Fan, S.; Avlasevich, Y.; Muellen, K.; Moerner, W. E.: Large single-molecule fluorescence enhancements produced by a bowtie nanoantenna. *Nature Photon.* **2009**, *3*, 654-657.

(16) Kneipp, K.; Wang, Y.; Kneipp, H.; Perelman, L. T.; Itzkan, I.; Dasari, R.; Feld, M. S.: Single molecule detection using surface-enhanced Raman scattering (SERS). *Phys. Rev. Lett.* **1997**, *78*, 1667-1670.

(17) Nie, S. M.; Chiu, D. T.; Zare, R. N.: Probing individual molecules with confocal fluorescence microscopy. *Science* **1994**, *266*, 1018-1021.

(18) Kneipp, J.; Kneipp, H.; Kneipp, K.: SERS - a single-molecule and nanoscale tool for bioanalytics. *Chem. Soc. Rev.* **2008**, *37*, 1052-1060.

(19) Storhoff, J. J.; Lucas, A. D.; Garimella, V.; Bao, Y. P.; Muller, U. R.: Homogeneous detection of unamplified genomic DNA sequences based on colorimetric scatter of gold nanoparticle probes. *Nature Biotech.* **2004**, *22*, 883-887.

(20) Nie, S. M.; Emery, S. R.: Probing single molecules and single nanoparticles by surface-enhanced Raman scattering. *Science* **1997**, *275*, 1102-1106.

(21) Wu, X.; Ming, T.; Wang, X.; Wang, P.; Wang, J.; Chen, J.: High-photoluminescence-yield gold nanocubes: For cell imaging and photothermal therapy. *Acs Nano* **2010**, *4*, 113-120.

(22) Huang, X. H.; El-Sayed, I. H.; Qian, W.; El-Sayed, M. A.: Cancer cell imaging and photothermal therapy in the near-infrared region by using gold nanorods. *J. Am. Chem. Soc.* **2006**, *128*, 2115-2120.

(23) Kim, J.-W.; Galanzha, E. I.; Shashkov, E. V.; Moon, H.-M.; Zharov, V. P.: Golden carbon nanotubes as multimodal photoacoustic and photothermal high-contrast molecular agents. *Nature Nanotech.* **2009**, *4*, 688-694.

(24) Zijlstra, P.; Chon, J. W. M.; Gu, M.: Five-dimensional optical recording mediated by surface plasmons in gold nanorods. *Nature* **2009**, *459*, 410-413.

(25) Srituravanich, W.; Fang, N.; Sun, C.; Luo, Q.; Zhang, X.: Plasmonic nanolithography. *Nano Lett.* **2004**, *4*, 1085-1088.

(26) Sundaramurthy, A.; Schuck, P. J.; Conley, N. R.; Fromm, D. P.; Kino, G. S.; Moerner, W. E.: Toward nanometer-scale optical photolithography: Utilizing the near-field of bowtie optical nanoantennas. *Nano Lett.* **2006**, *6*, 355-360.

(27) Fourkas, J. T.: Nanoscale photolithography with visible light. *J. Phys.*

Chem. Lett. **2010**, *1*, 1221-1227.

(28) Falk, A. L.; Koppens, F. H. L.; Yu, C. L.; Kang, K.; Snapp, N. d. L.; Akimov, A. V.; Jo, M.-H.; Lukin, M. D.; Park, H.: Near-field electrical detection of optical plasmons and single-plasmon sources. *Nature Phys.* **2009**, *5*, 475-479.

(29) Mock, J. J.; Barbic, M.; Smith, D. R.; Schultz, D. A.; Schultz, S.: Shape effects in plasmon resonance of individual colloidal silver nanoparticles. *J. Chem. Phys.* **2002**, *116*, 6755-6759.

(30) Haynes, C. L.; Van Duyne, R. P.: Nanosphere lithography: A versatile nanofabrication tool for studies of size-dependent nanoparticle optics. *J. Phys. Chem. B* **2001**, *105*, 5599-5611.

(31) Jensen, T. R.; Malinsky, M. D.; Haynes, C. L.; Van Duyne, R. P.: Nanosphere lithography: Tunable localized surface plasmon resonance spectra of silver nanoparticles. *J. Phys. Chem. B* **2000**, *104*, 10549-10556.

(32) Liu, N.; Tang, M. L.; Hentschel, M.; Giessen, H.; Alivisatos, A. P.: Nanoantenna-enhanced gas sensing in a single tailored nanofocus. *Nature Mater.* **2011**, *10*, 631-636.

(33) Miller, M. M.; Lazarides, A. A.: Sensitivity of metal nanoparticle surface plasmon resonance to the dielectric environment. *J. Phys. Chem. B* **2005**, *109*, 21556-21565.

(34) Hulteen, J. C.; Vanduyne, R. P.: Nanosphere lithography - A materials general fabrication process for periodic particle array surfaces. *J. Vac. Sci. Technol. A-Vac. Surf. Films* **1995**, *13*, 1553-1558.

(35) Yan, R.; Pausauskie, P.; Huang, J.; Yang, P.: Direct photonic-

plasmonic coupling and routing in single nanowires. *Proc. Natl. Acad. Sci. U.S.A.* **2009**, *106*, 21045-21050.

(36) Nordlander, P.; Oubre, C.; Prodan, E.; Li, K.; Stockman, M. I.: Plasmon hybridization in nanoparticle dimers. *Nano Lett.* **2004**, *4*, 899-903.

(37) Göppert-Mayer, M.: Über elementarakte mit zwei quantensprüngen. *Annalen der Physik* **1931**, *9*, 273-295.

(38) Kaiser, W.; Garrett, C. G. B.: Two-photon excitation in CaF2:Eu2+. *Phys. Rev. Lett.* **1961**, *7*, 229-232.

(39) So, P. T. C.; Dong, C. Y.; Masters, B. R.; Berland, K. M.: Two-photon excitation fluorescence microscopy. *Annu. Rev. Biomed. Eng.* **2000**, *2*, 399-429.

(40) Nakamura, O.: Fundamental of two-photon microscopy. *Microsc. Res. Tech.* **1999**, *47*, 165-171.

(41) LaFratta, C. N.; Fourkas, J. T.; Baldacchini, T.; Farrer, R. A.: Multiphoton fabrication. *Angew. Chem. Int. Ed.* **2007**, *46*, 6238-6258.

(42) Denk, W.; Strickler, J. H.; Webb, W. W.: Two-photon laser scanning fluorescence microscopy. *Science* **1990**, *248*, 73-76.

(43) Larson, D. R.; Zipfel, W. R.; Williams, R. M.; Clark, S. W.; Bruchez, M. P.; Wise, F. W.; Webb, W. W.: Water-soluble quantum dots for multiphoton fluorescence imaging in vivo. *Science* **2003**, *300*, 1434-1436.

(44) Maiti, S.; Shear, J. B.; Williams, R. M.; Zipfel, W. R.; Webb, W. W.: Measuring serotonin distribution in live cells with three-photon excitation. *Science* **1997**, *275*, 530-532.

(45) Wang, H. F.; Huff, T. B.; Zweifel, D. A.; He, W.; Low, P. S.; Wei, A.;

Cheng, J. X.: In vitro and in vivo two-photon luminescence imaging of single gold nanorods. *Proc. Natl. Acad. Sci. U.S.A.* **2005**, *102*, 15752-15756.

(46) Squirrell, J. M.; Wokosin, D. L.; White, J. G.; Bavister, B. D.: Long-term two-photon fluorescence imaging of mammalian embryos without compromising viability. *Nature Biotech.* **1999**, *17*, 763-767.

(47) Yanik, M. F.; Cinar, H.; Cinar, H. N.; Chisholm, A. D.; Jin, Y. S.; Ben-Yakar, A.: Neurosurgery - Functional regeneration after laser axotomy. *Nature* **2004**, *432*, 822-822.

(48) Brown, E. B.; Campbell, R. B.; Tsuzuki, Y.; Xu, L.; Carmeliet, P.; Fukumura, D.; Jain, R. K.: In vivo measurement of gene expression, angiogenesis and physiological function in tumors using multiphoton laser scanning microscopy. *Nature Med.* **2001**, *7*, 864-868.

(49) Xing, J.-F.; Dong, X.-Z.; Chen, W.-Q.; Duan, X.-M.; Takeyasu, N.; Tanaka, T.; Kawata, S.: Improving spatial resolution of two-photon microfabrication by using photoinitiator with high initiating efficiency. *Appl. Phys. Lett.* **2007**, *90*, 131106.

(50) Li, L.; Gattass, R. R.; Gershgoren, E.; Hwang, H.; Fourkas, J. T.: Achieving lambda/20 resolution by one-color initiation and deactivation of polymerization. *Science* **2009**, *324*, 910-913.

(51) Boyd, G. T.; Yu, Z. H.; Shen, Y. R.: Photoinduced luminescence from the noble-metals and its enhancement on roughened surfaces. *Phys. Rev. B* **1986**, *33*, 7923-7936.

(52) Farrer, R. A.; Butterfield, F. L.; Chen, V. W.; Fourkas, J. T.: Highly

efficient multiphoton-absorption-induced luminescence from gold nanoparticles. *Nano Lett.* **2005**, *5*, 1139-1142.

(53) Imura, K.; Nagahara, T.; Okamoto, H.: Photoluminescence from gold nanoplates induced by near-field two-photon absorption. *Appl. Phys. Lett.* **2006**, *88*, 023104.

(54) Muhlschlegel, P.; Eisler, H. J.; Martin, O. J. F.; Hecht, B.; Pohl, D. W.: Resonant optical antennas. *Science* **2005**, *308*, 1607-1609.

(55) Schumacher, T.; Kratzer, K.; Molnar, D.; Hentschel, M.; Giessen, H.; Lippitz, M.: Nanoantenna-enhanced ultrafast nonlinear spectroscopy of a single gold nanoparticle. *Nature Comm.* **2011**, *2*:333.

(56) Novotny, L.; Beversluis, M. R.; Youngworth, K. S.; Brown, T. G.: Longitudinal field modes probed by single molecules. *Phys. Rev. Lett.* **2001**, *86*, 5251-5254.

(57) Murazawa, N.; Ueno, K.; Mizeikis, V.; Juodkazis, S.; Misawa, H.: Spatially selective nonlinear photopolymerization induced by the near-field of surface plasmons localized on rectangular gold nanorods. *J. Phys. Chem. C* **2009**, *113*, 1147-1149.

(58) Yin, X. F., Nicholas; Zhang, Xiang; Martini, Ignacio B.; Schwartz, Benjamin J.: Near-field multiphoton nanolithography using an apertureless optical probe. *In nonlinear optical transmission and multiphoton processes in organics.*; Yeates, A. T., Belfield, K. D., Kajzar, F., Lawson, C. M., Ed., 2003; Vol. 5211; pp 96-103.

Chapter 2: Nonlinear optical properties of plasmonic gold nanoparticles[†]

2.1 Introduction

Due to the localized surface plasmon resonance (LSPR), metallic nanostructures are well known to enhance electromagnetic fields by orders of magnitude.[1,2] This field enhancement has led to the ability to detect single molecules in many analytical techniques.[3-5] For example, surface-enhanced Raman scattering (SERS) signals have been observed from single molecules due to the SPR of metal nanoparticles.[6-11] Additionally, surface-enhanced infrared absorption (SEIRA) technique has provided up to a three order of magnitude increase in vibrational absorption signals.[12-16]

Despite the wealth of experimental studies on field-enhanced phenomena of noble-metal nanostructures, theory has yet to explain fully the extreme enhancements of signals that, for instance, make possible the detection of single molecules via SERS.[6-11] It is clear that aggregates of nanoparticles can provide considerably larger field enhancements than do individual particles, but even the multiple-particle structures that have been examined theoretically do not appear capable of generating the enhancements required to explain many of the phenomena that have been observed.[11,17,18]

An important experimental tool for understanding field enhancement is the

correlation of different field-enhanced phenomena with one another and with nanostructure geometry. This type of strategy, for example, led to the realization that aggregates of particles can have considerably larger SERS signals than do single particles.[11,19,20] Here we apply such an approach to two other phenomena involving field enhancement, multiphoton-absorption-induced luminescence (MAIL) and metal-enhanced multiphoton absorption polymerization (MEMAP) using gold nanoparticles.

MAIL has been observed to be a two-photon process for 800 nm excitation in most studies of gold nanostructures.[21-24] However, some gold nanoparticles have been found to have extremely large MAIL signals, and in this case MAIL is a three-photon process with 800 nm excitation.[25] On the other hand, MAIL from silver nanoparticles is a two-photon process with 800 nm excitation.[26] One recent paper has proposed that the efficient luminescence following three-photon excitation at 800 nm arises from nanoparticles that have shapes that lead to particularly large electric field enhancements.[26]

In multiphoton absorption polymerization (MAP)[27-29] the absorption of two or more photons of light is used to excite photoinitiator molecules that drive polymerization in a prepolymer resin. The photons are of too long of a wavelength to be absorbed individually, and so must be absorbed simultaneously. As a result, the absorption probability scales as the light intensity to the power of the number of photons required for excitation. Excitation, and therefore polymerization, can thus be constrained to occur within the focal volume of a tightly focused laser beam. By using an ultrafast laser, which produces short, intense pulses with a low duty cycle,

MAP can be accomplished at low average laser power.

Because multiphoton absorption is a nonlinear optical process, its probability can be increased substantially by field enhancement. The idea behind MEMAP is to take advantage of this field enhancement to perform MAP at laser intensities that would normally be below the threshold for causing polymerization. MEMAP has been reported on gold nanostructures created by shadow-sphere lithography,[30] in the controlled gaps of nanoscale gold structures[23,31] and at a metal-coated AFM tip.[32] MEMAP has also been observed in arrays of gold nanostructures using incoherent light.[31]

In this Chapter we present the results of studies in which MAIL and MEMAP were performed on the same set of gold nanoparticles on glass substrates. The particles were also imaged with scanning electron microscopy (SEM) to correlate optical properties with structure. We find that both MAIL and MEMAP are most efficient in small clusters of nanoparticles, and that there is a strong correlation between the two phenomena. Wavelength-dependent studies indicate that the dominant mechanism for MEMAP in our systems is not field-enhanced two-photon absorption, but rather that polymerization is driven by the excitation of photoinitiators by MAIL.

2.2 Experimental Section

2.2.1 Nanoparticle Synthesis

The preparation of gold nanoparticles was carried out through the citrate-

reduction method.[33] As an initial step, 0.139 g of HAuCl4 was dissolved in 250 mL of distilled water. The solution was brought to a boil, and then 20 mL of a 1 wt% sodium citrate solution was added under rapid stirring. To induce further reduction, boiling was continued for about 20 min. The size of the synthesized gold nanoparticles (26 nm) was determined by both UV/visible absorption and transmission electron microscopy.

Gold nanoparticles were coated with silica shells following literature methods.[34,35] A 500 μL sample of an aqueous solution of 1 mM (3-aminopropyl)trimethoxysilane (APTS) was added slowly to 100 mL of an Au nanoparticle solution under vigorous stirring and allowed to react for 15 min. Next 1 g of sodium silicate solution was diluted to 50 mL with distilled water. The pH of the sodium silicate solution was adjusted to 10 by addition of a cation exchange resin. The active silica solution (4 mL) was added to the APTS/gold nanoparticle suspension under vigorous stirring. Further polymerization of active silica in the solution (at pH ~8.5) was allowed to proceed for one day. The resulting silica shells on the gold nanoparticles were imaged by transmission electron microscopy, and had an average thickness of 2 nm.

2.2.2 Sample Preparation

To disperse the nanoparticles for experiments, a 3 μL sample of gold nanoparticle solution was placed on a coverslip that had been first treated with an oxygen plasma and with a solution of 2 vol% of (3-acryloxypropyl) trimethoxysilane, 5 vol% of deionized water, and 93 vol% of ethanol for 12 hr to improve adhesion of

the final polymeric structures.[36] The sample was then placed in an oven at 110 ℃ for 3 min to evaporate the solvent.

The acrylic resin used was composed of 54 wt% dipentaerythritol pentaacrylate esters (SR 368 Sartomer), 43 wt% tris(2- hydroxyethyl) isocyanurate triacrylate (SR 399 Sartomer), and 3 wt% Lucirin TPO-L (BASF) as a photoinitiator. The chemical structures of each monomer and the photoinitiator are shown in Figure 2.1a. Figure 2.1b is a schematic of the polymerization process of the acrylate monomers with the photoinitiator. After thorough mixing, one drop of the resin was placed on the nanoparticle-coated substrate. A layer of Scotch tape was placed on the coverslip as a spacer, and then a second coverslip was placed on top of the tape. The sandwiched sample was mounted on a computer-controlled, 3D, piezoelectric nanostage (Physik Instrumente).

2.2.3 Imaging and Fabrication

A tunable Ti:sapphire laser (Coherent Mira 900-F) produced pulses of 150 fs duration at a repetition rate of 76 MHz. The beam was introduced into an inverted microscope (Zeiss Axiovert 100) through the reflected light-source port and was directed to the objective by a dichroic mirror. A 1.45 NA, 100×, oil-immersion objective (Zeiss R Plan-FLUAR) was used for MAIL imaging and multiphoton fabrication. Scanning was performed with the piezoelectric sample stage or with a set of galvanometric mirrors. The luminescence signal was collected by a single-photon-counting avalanche photodiode (EG&G) and the signal was transferred to a computer with a data acquisition board (National Instruments). Data collection and image

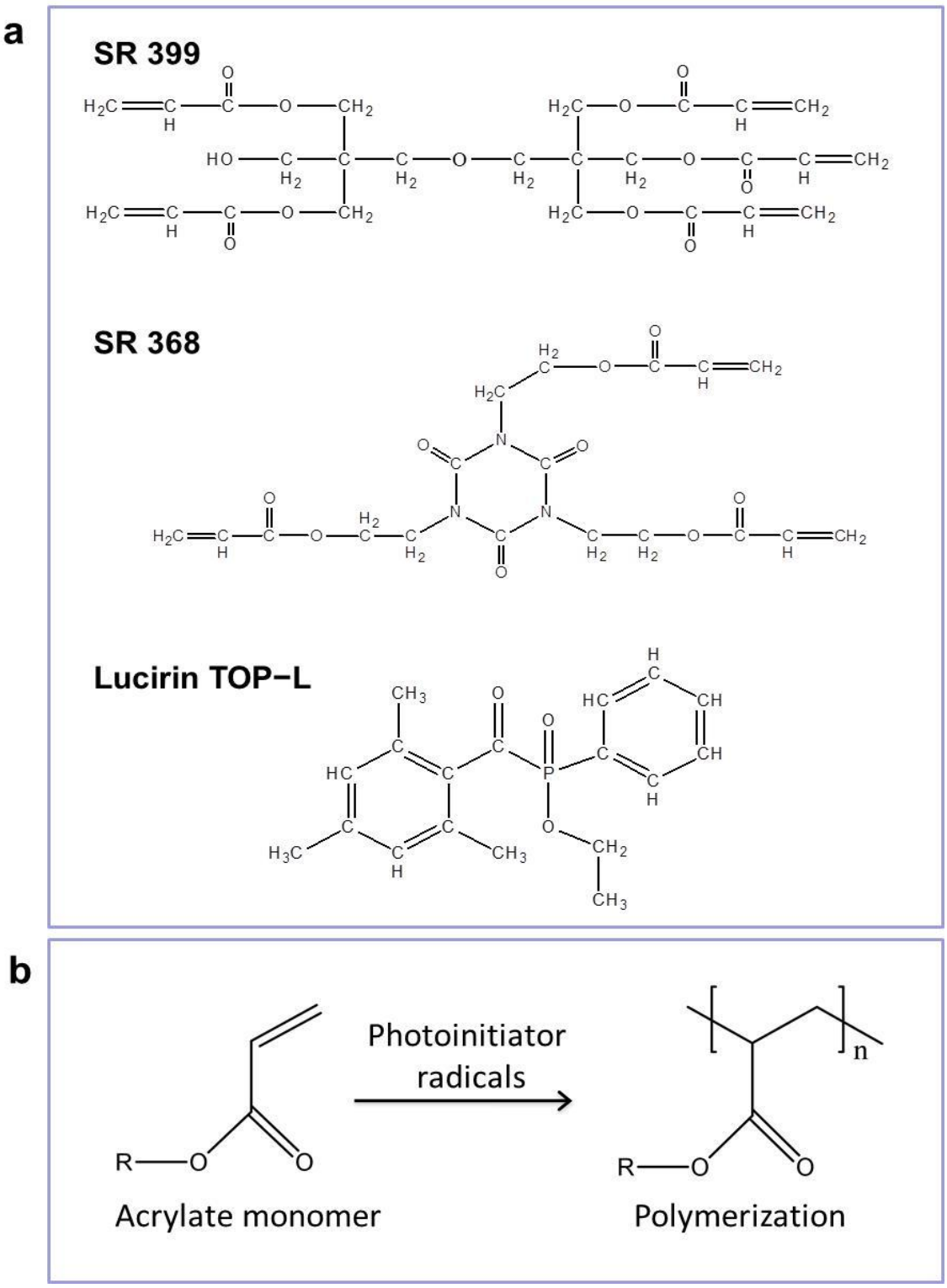

Figure 2.1. (a) Chemical structures of SR 399, SR 368, and Lucirin TPO-L. (b) A typical polymerization of acrylate monomers.

construction were performed with software written in LabView (National Instruments).

For MAIL imaging, typically an area of 30 μm^2 was scanned with 140 × 140 pixel resolution in ~10 s. Filters that cut off the excitation light were placed before the detector. MEMAP was performed under similar conditions or simultaneously with MAIL imaging. MAP was used to create markers on the substrate so that the same sample region could be located reproducibly. For SEM imaging, samples were sputter-coated with approximately 10 nm of Pt/Pd. Shown in Figure 2.2 are a typical gold MAIL spectrum[25] along with the one-photon absorption and two-photon

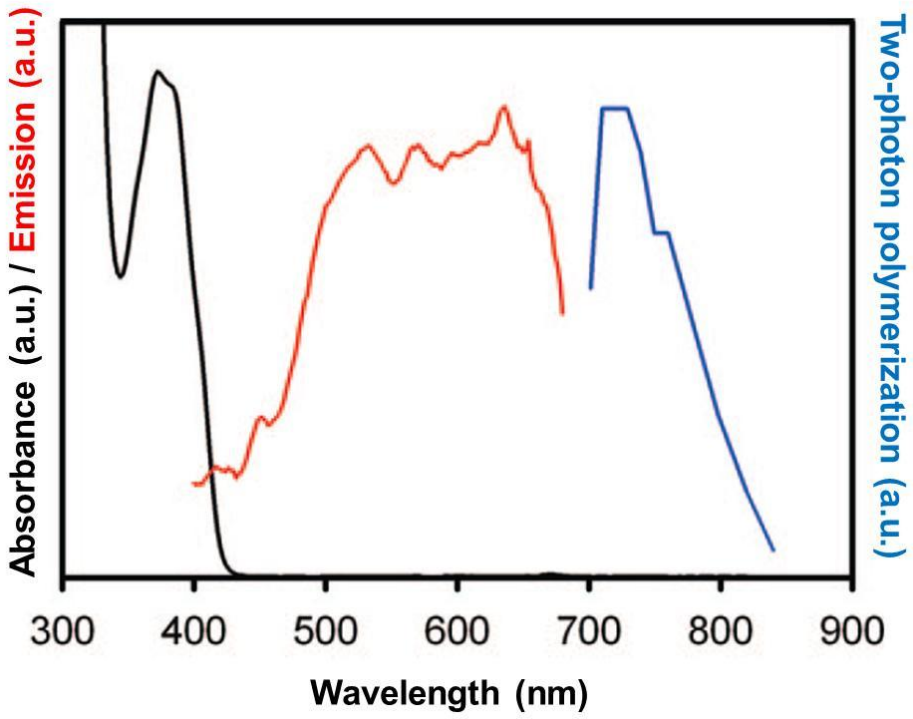

Figure 2.2. Linear absorption spectrum (black) and two-photon polymerization action spectrum (blue) of Lucirin TPO-L and a typical MAIL emission spectrum for gold nanoparticles (red).

polymerization action spectra of Lucirin TPO-L.[34] The two-photon polymerization action spectrum is the inverse of the square of minimum laser excitation intensity that can induce polymerization and the fabrication threshold was measured at different excitation wavelengths.[34]

2.3 Results and discussion

Our initial experiments focused on correlating MAIL efficiency with nanoparticle morphology. Gold nanoparticles were coated on a glass coverslip and MAIL experiments were performed with 800 nm excitation. The excitation intensity was less than 2 mW at the sample. Typical MAIL data are shown as 3D and contour plots in panels a and b of Figure 2.3, respectively. The luminescent regions span a broad range of intensities, as has been observed previously.[25] An SEM image of the same region of the gold nanoparticle sample is shown in Figure 2.3c. It is apparent from this image that there are significant aggregates of nanoparticles on the substrate. In general, the regions of brightest luminescence correspond with the positions of aggregates.

To explore this correspondence in more detail, Figure 2.4 is an overlay of the matching regions of the MAIL image and the electron micrograph. The aggregate of three nanoparticles marked A has only modest MAIL intensity, whereas the larger aggregates B and C both exhibit considerably brighter luminescence. The luminescence intensity does not appear to be linear in the number of particles in an

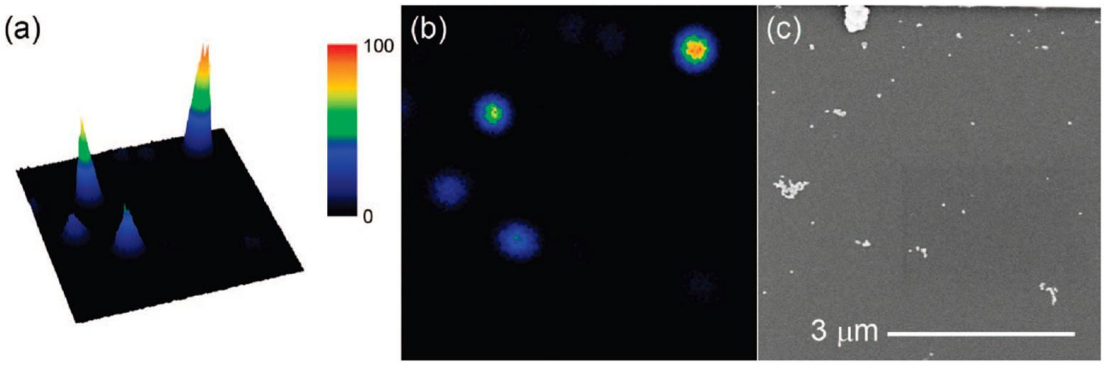

Figure 2.3. (a) 3D and (b) contour plots of MAIL from gold nanoparticles deposited on a glass substrate and excited with 800 nm light. The intensity scale is the same for both images. (c) An SEM image of the same region of the sample.

aggregate. For example, the most aggregated cluster D shows the modest MAIL intensity and the brightest MAIL intensity is shown from the aggregate E in the figure. However, the MAIL intensity depends upon the aggregate structure as well. This enhancement of emission due to aggregation is reminiscent of the effects that have been seen in SERS, in which aggregates can have considerably larger field enhancements than do single nanoparticles.[11,20]

To investigate the origin of MAIL further, we studied particles with a 2 nm coating of silica. As we observed previously,[25] the silica coating does not lead to any significant change in MAIL behavior. SEM studies of samples of silica-coated particles indicated the presence of aggregates similar to those observed for uncoated nanoparticles. As also was the case for the uncoated nanoparticles, we found a strong correlation between aggregation and luminescence intensity in the coated particles. The aggregate shape again plays an important role in determining the luminescence intensity of the silica-coated nanoparticles. The MAIL intensity measured from the

nanoparticle aggregates was up to 2000 photon counts, which was the detection limit of the photodiode. This result demonstrated that MAIL signals from the aggregates were enhanced by at least three orders of magnitude comparing to those from single nanoparticles.

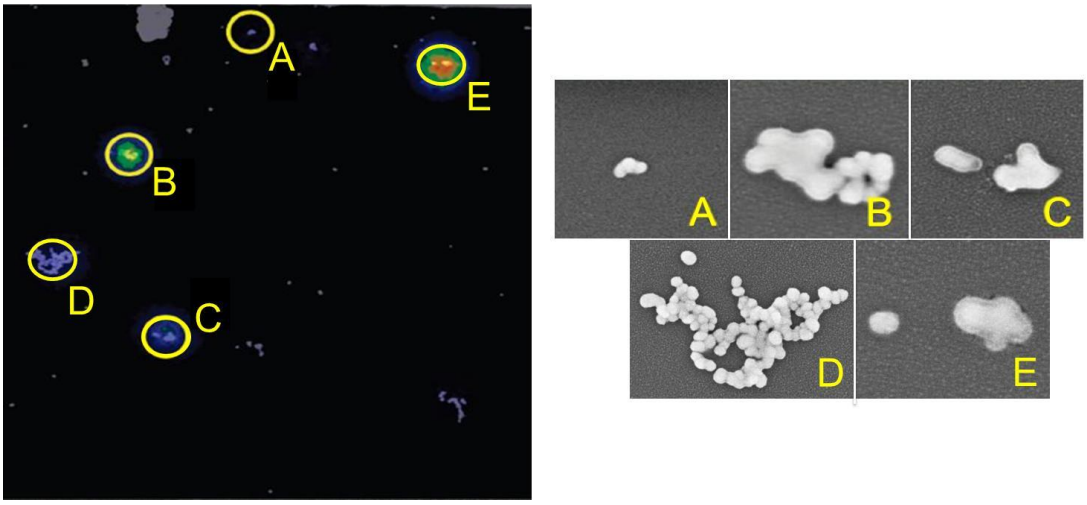

Figure 2.4. An overlay of the MAIL and SEM images from Figure 2.3 (top) and close-up SEM images of selected emitting aggregates (bottom). The magnifications of the close-ups vary.

We also examined the effect that the 10-nm coating of Pt/Pd that was applied to the samples for SEM imaging had on MAIL. Pt/Pd films on glass do not exhibit MAIL, and gold nanoparticles that are encapsulated completely in Pt/Pd would not be expected to luminesce. However, the majority of particles that luminesced before coating the substrate with Pt/Pd also luminesced afterward, albeit with a somewhat diminished intensity. Thus, coating particles and aggregates on one side with another metal does not have a substantial influence on MAIL efficiency. There was no

obvious correlation of particle shape or aggregation with the areas in which the MAIL did disappear upon Pt/Pd coating.

Our previous studies have demonstrated that MAIL from gold nanoparticles involves a three-photon excitation process at 800 nm.[25] Similar results were obtained for 900 nm excitation.[25] This observation is surprising, since other studies have shown MAIL from different gold structures to arise from two-photon excitation at 800 nm.[21,23,37,38] Furthermore, neither 800 nor 400 nm light is within the plasmon band of the gold nanoparticles employed here, so plasmonic enhancements would not be expected to be significant. We believe that the implication of these results is that our experimental protocol selects for particles or aggregates of particles that have a particularly large three-photon-absorption cross-section.[26] It is additionally possible that the aggregates that exhibit strong MAIL with 800 nm light have collective plasmon bands that are red-shifted enough to have significant absorption at this wavelength.

If the efficiency of MAIL depends upon shifted plasmon bands in aggregates, then the MAIL efficiency of different aggregates would be expected to be a function of excitation wavelength. To explore this issue, we performed MAIL experiments on the same region of a sample with 725, 800, and 890 nm excitation. The MAIL emission taken at the three wavelengths ranged from the near-infrared to the visible region of the spectrum and appeared to be independent to the number of photons absorbed by the gold nanoparticles because no significant changes in spectral shapes were observed with different excitation intensities. The MAIL intensities from each aggregate were examined using single photon counting photodiode. Representative

MAIL intensity images from one such study are shown in Figure 2.5. For 725 and 800 nm light, the excitation power was less than 2 mW at the sample, whereas for 890 nm light the excitation power was on the order of 10 mW at the sample. The images for 725 and 800 nm excitation are similar. With 890 nm excitation, the most prominent MAIL emission arises from regions that do not luminesce as strongly with shorter wavelength excitation. Comparison with an SEM image of the same region did not reveal a clear correlation between structure and the wavelength dependence of the MAIL efficiency, but our results suggest that at least for long wavelength excitation aggregates with significantly red-shifted plasmon bands may be involved.

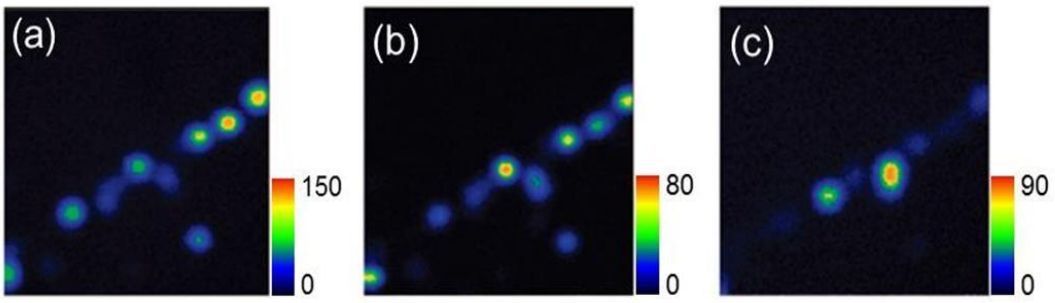

Figure 2.5. Contour plots of MAIL from gold nanoparticles on the same region of a glass substrate excited with (a) 725, (b) 800, and (c) 890 nm light.

We next turn to MEMAP and its correlation with MAIL. The radical photoinitiator used for these studies, Lucirin TPO-L, has a two-photon polymerization action spectrum that has a peak at 725 nm (Figure 2.2). The polymerization action spectrum is negligibly small at wavelengths longer than 850 nm.[36] We first performed experiments at 800 nm, a wavelength at which MAP can easily be performed with this photoinitiator.[34] Prepolymer resin was placed on top of a substrate that had been coated with gold nanoparticles. The laser beam was scanned

over the sample at an intensity too low to lead to polymerization in the pure prepolymer resin but high enough to obtain high-quality MAIL images. A MAIL image from a representative sample is shown in 3D form in Figure 2.6a and as a contour plot in Figure 2.6b. An SEM image of the same sample area (Figure 2.6c) demonstrates the presence of both individual nanoparticles and aggregates. Overlapping the MAIL and SEM images reveals that once again the brightest emission arises from regions that contain aggregates of particles (Figure 2.7). Nanoparticles that do not show strong MAIL emission, such as particle A in Figure 2.7, do not exhibit any polymerization. However, particles or aggregates that do exhibit MAIL such as B and C in Figure 2.7, also have a polymer coating. Similar results were obtained with excitation at 725 nm.

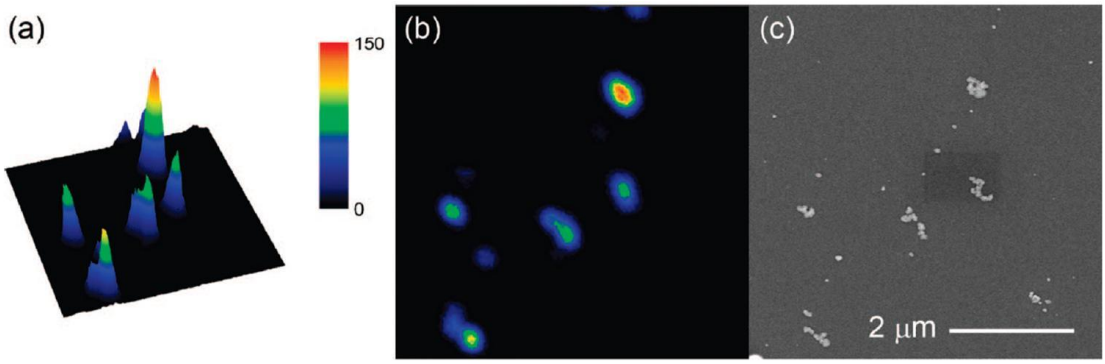

Figure 2.6. (a) 3D and (b) contour plots of MAIL from gold nanoparticles deposited on a glass substrate, immersed in prepolymer resin, and excited with 800 nm light. The intensity scale is the same for both images. (c) An SEM image of the same region of the sample.

If the prepolymer resin is prepared without any photoinitiator, MAIL emission is observed but polymerization does not occur even at high laser intensity. We can

therefore conclude the photoinitiator is essential for MEMAP. This result implies that multiphoton excitation does not lead to ejection of electrons from the gold nanoparticles, at least in quantities sufficient to cause polymerization.

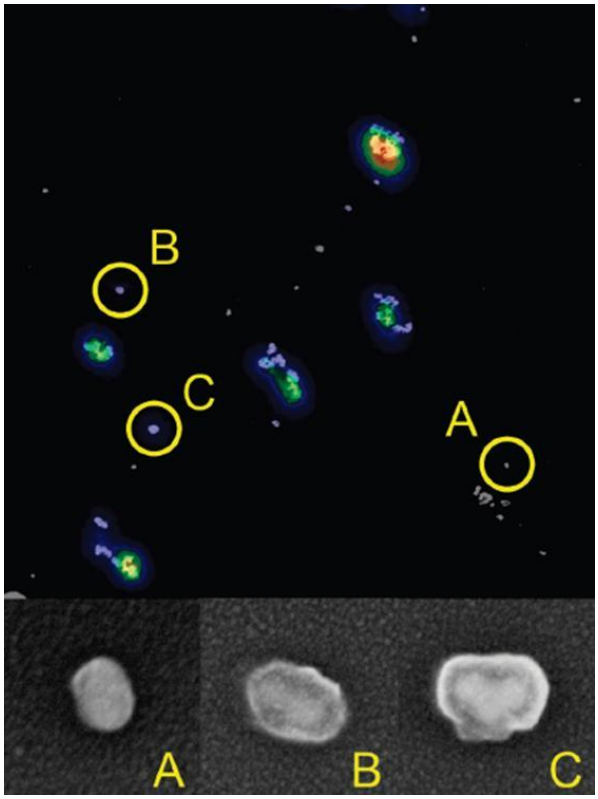

Figure 2.7. An overlay of the MAIL and SEM images from Figure 2.6 (top) and close-up electron micrographs of selected particles and aggregates without a polymer shell (bottom left) and with a polymer shell (bottom center and bottom right). The magnifications of the close-ups vary.

Our results indicate that there is a direct correspondence between MAIL and MEMAP. This conclusion is consistent with the results of previous studies in indicating that field enhancement can lead to being able to perform MAP at lower intensities than is possible in the absence of noble-metal structures.[23,30-32] However, we must still establish the role played by field enhancement in MEMAP. One

possibility is that field enhancement increases the effective two-photon absorption cross section of nearby photoinitiator molecules. This mechanism has been assumed to be the source of MEMAP in previous reports.[23,30-32] However, MAIL from gold occurs across the visible spectrum,[25] and so it is also possible that the emitted light causes polymerization directly by exciting the photoinitiator molecules. Indeed, it is due to this second potential mechanism that we call the effect metal-enhanced MAP rather than field-enhanced MAP.

Our observations offer a number of clues into the mechanism of MEMAP in gold nanoparticles and aggregates. First, field enhancement is expected to occur in localized hot spots in nanoparticle aggregates. Because polymerization takes place in a solvent-free resin in our system, radicals do not diffuse over a significant distance before reacting. Thus, field-enhanced two-photon absorption would be expected to lead to asymmetric polymerized regions around aggregates with hot spots. However, the polymerized region is generally spread uniformly about the aggregates for which MEMAP occurs. Second, the pattern of field enhancement is expected to be dependent upon the polarization of the light. We have observed no preference for the polymerized pattern to be stretched or otherwise affected along the polarization axis of the excitation light. Third, silica coating of the nanoparticles does not have any appreciable effect on the efficiency of MEMAP. Taken together, these factors suggest that MEMAP in this system does not arise from field-enhanced two-photon absorption of the photoinitiator.

To seek more definitive evidence for the origin of MEMAP, we performed experiments using 890 nm excitation. Because the two-photon absorption cross

section of Lucirin TPO-L is vanishingly small at this wavelength, in the absence of gold nanoparticles we were not able to observe MAP in the prepolymer resin even at very high laser powers (~100 mW) of 890 nm light.

Shown in panels a and b of Figure 2.8 are 3D and contour plots, respectively, of MAIL from gold particles in the prepolymer resin excited by 890 light with approximately 6 mW of excitation power at the sample. The corresponding SEM image of this region of the sample is shown in Figure 2.8c. The overlap of the MAIL and SEM images (Figure 2.9) shows once again that larger aggregates tend to have higher emission intensities.

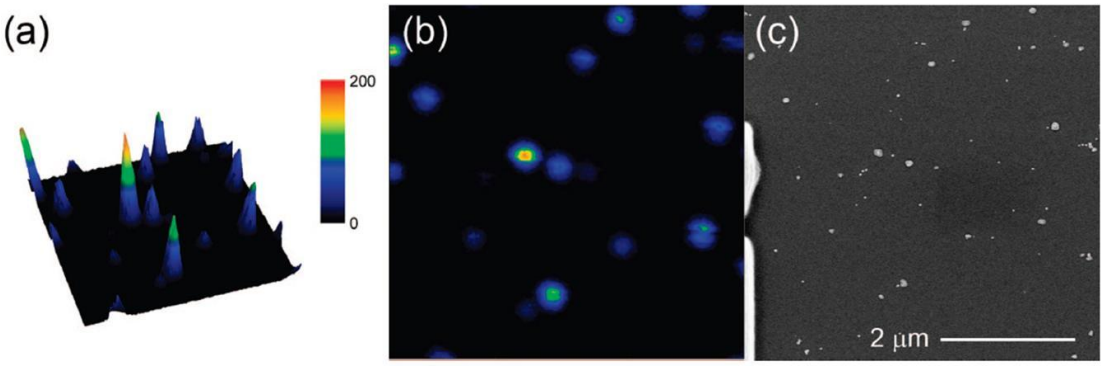

Figure 2.8. (a) 3D and (b) contour plots of MAIL from gold nanoparticles deposited on a glass substrate, immersed in prepolymer resin, and excited with 890 nm light. The intensity scale is the same for both images. (c) An SEM image of the same region of the sample.

Also shown in Figure 2.9 are close-up SEM images of different particles and aggregates. Aggregates A, B, and C all show strong MAIL emission and have polymerized shells around them. However, the particles and aggregates D, E, and F do not exhibit detectable MAIL emission at this excitation intensity and do not have

polymerized shells about them. Once again there is a direct correspondence between MAIL emission and MEMAP.

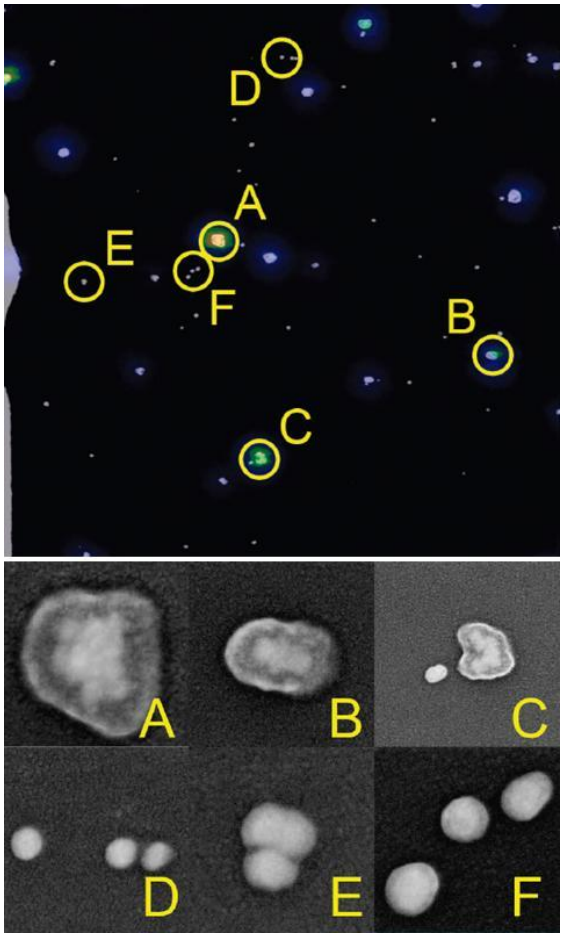

Figure 2.9. An overlay of the MAIL and SEM images from Figure 2.8 (top) and close-up SEM images of selected particles and aggregates with a polymer shell (middle) and without a polymer shell (bottom). The magnifications of the close-ups vary.

2.4 Discussion

The results presented here clarify a number of issues regarding field-enhanced

phenomena of gold nanoparticles. While our studies have focused on MAIL and MEMAP, what we have learned may have implications for other processes that depend on field enhancement as well.

Our first important observation is that efficient MAIL generally arises from aggregates rather than from single particles. This result is consistent with previous observations that aggregates of nanoparticles give considerably stronger SERS enhancements than do single particles.[11,19] Not all aggregates of the same size lead to MAIL emission, indicating that shape plays an important role in this process as well. For instance, we rarely observe strong MAIL signals from linear aggregates, even when they contain four or more particles. Additionally, the emission efficiency for different aggregates depends upon the excitation wavelength. Thus, high MAIL efficiency may in part result from having a plasmon band that is sufficiently red-shifted to overlap well with the excitation wavelength. However, our results suggest that the plasmon band is not the only important factor in MAIL.

The second important observation is that there is a strong correspondence between the particles and aggregates that exhibit strong MAIL and those that exhibit strong MEMAP. We can conclude from this result that MAIL and MEMAP both depend on field enhancement. However, as discussed above a number of facets of our results with 800 nm excitation call into question whether MEMAP occurs through field enhancement of the two-photon absorption of the photoinitiator molecules.

The third key observation is that MEMAP occurs with 890 nm laser pulses, even though two-photon excitation of the photoinitiator is not possible at this wavelength. The most likely explanation for this phenomenon is that three-photon

excitation of the nanoparticles leads to MAIL emission that in turn excites the photoinitiator. Thus, in our system MEMAP is likely to be a consequence of MAIL rather than a direct effect of field enhancement. It remains possible that field enhancement promotes three-photon excitation of the photoinitiator, but we view this explanation as unlikely for a number of reasons. First, even at very high excitation powers (on the order of 100 mW) it is not possible to excite the photoinitiator directly with three 890 nm photons. Second, as discussed above, the MEMAP process creates a polymer shell that extends over the entire nanoparticle or aggregate, and does not show any elongation along the direction of the laser polarization. A field-enhancement hot spot may drive emission anywhere within an aggregate, but is likely to have a considerably more localized effect on polymerization. MAIL emission is expected to be relatively isotropic, and so would lead to uniform polymer shells around luminescent regions of nanostructures. The bandwidth of our laser pulses is small enough (~10 nm) that we can also rule out two-photon excitation of the photoinitiator from photons at the blue tail of the laser spectrum when the center wavelength of the pulses is 890 nm.

As the results of our MEMAP experiments are similar for excitation wavelengths ranging from 725 to 890 nm, it appears likely that the mechanism is the same over this entire tuning range. It remains possible that enhanced two-photon absorption and excitation via MAIL emission both play a role in MEMAP at the shorter wavelengths, but as the qualitative features of MEMAP are independent of wavelength over the range studied, we believe that the latter mechanism dominates in all of our experiments.

It is natural to ask whether the mechanism that is responsible for MEMAP in our system was also operative in previous reports of this effect.[23,30-32] It is not possible to give a definitive answer for this question at present, as different nanostructures, photoinitiators, and polymer systems were used in the previous studies. MAIL emission was observed in gold nanobowties, and was strongest in the region in which MEMAP occurred.[23] However, MAIL in the bowtie system arose from two-photon absorption, and so the essential physics may be different from that of our nanoparticles and aggregates. It will be interesting to employ wavelength-dependent studies to investigate the mechanism for MEMAP in these other systems.

Finally, we should also consider whether MAIL plays a role in other field-enhanced effects of noble-metal nanostructures. For instance, SERS is known to be most efficient in dimers or other aggregates of nanoparticles.[11,19] However, calculations of the field enhancements available from such aggregates cannot account for the highest observed enhancements of Raman scattering. In a full quantum treatment of spontaneous Raman scattering, a vacuum field at the scattered frequency is involved.[39] Any process that increases the field at the scattered frequency above the vacuum level will act to increase the efficiency of the SERS process, and so it is possible that MAIL plays a role in this technique under some circumstances.

The studies reported here were performed with ultrafast lasers, and SERS is generally performed with CW lasers. MAIL with CW lasers would be expected to be a weak effect, but we should note that MEMAP has been reported with an incoherent light source.[31] Even a weak MAIL effect may have the potential to increase the efficiency of SERS measurably.

2.5 Conclusions

In this chapter we have explored the connection between two field-enhanced phenomena of noble-metal nanostructures, MAIL and MEMAP. Aggregation of nanoparticles increases the efficiency of both of these phenomena. We have found a strong correlation between particles and aggregates that exhibit MAIL and MEMAP. On the basis of wavelength-dependent studies, we believe that the predominant mechanism for MEMAP in the systems studied here is MAIL-mediated excitation of the photoinitiator rather than field-enhanced two-photon absorption. This mechanism may be relevant for other field-enhanced phenomena of noble metal nanoparticles as well.

References

(1) Kelly, K. L.; Coronado, E.; Zhao, L. L.; Schatz, G. C.: The optical properties of metal nanoparticles: The influence of size, shape, and dielectric environment. *J. Phys. Chem. B* **2003**, *107*, 668-677.

(2) Schwartzberg, A. M.; Zhang, J. Z.: Novel optical properties and emerging applications of metal nanostructures. *J. Phys. Chem. C* **2008**, *112*, 10323-10337.

(3) Yang, W. H.; Schatz, G. C.; Vanduyne, R. P.: Discrete dipole approximation for calculating extinction and Raman intensities for small particles with arbitrary shapes *J. Chem. Phys.* **1995**, *103*, 869-875.

(4) Bell, S. E. J.; Sirimuthu, N. M. S.: Quantitative surface-enhanced Raman spectroscopy. *Chem. Soc. Rev.* **2008**, *37*, 1012-1024.

(5) Tian, Z. Q.; Ren, B.; Wu, D. Y.: Surface-enhanced Raman scattering: From noble to transition metals and from rough surfaces to ordered nanostructures. *J. Phys. Chem. B* **2002**, *106*, 9463-9483.

(6) Kneipp, K.; Wang, Y.; Kneipp, H.; Perelman, L. T.; Itzkan, I.; Dasari, R.; Feld, M. S.: Single molecule detection using surface-enhanced Raman scattering (SERS). *Phys. Rev. Lett.* **1997**, *78*, 1667-1670.

(7) Nie, S. M.; Chiu, D. T.; Zare, R. N.: Probing individual molecules with confocal fluorescence microscopy. *Science* **1994**, *266*, 1018-1021.

(8) Qian, X. M.; Nie, S. M.: Single-molecule and single-nanoparticle SERS: from fundamental mechanisms to biomedical applications. *Chem. Soc. Rev.* **2008**, *37*, 912-920.

(9) Pieczonka, N. P. W.; Aroca, R. F.: Single molecule analysis by surfaced-enhanced Raman scattering. *Chem. Soc. Rev.* **2008**, *37*, 946-954.

(10) Kneipp, J.; Kneipp, H.; Kneipp, K.: SERS - a single-molecule and nanoscale tool for bioanalytics. *Chem. Soc. Rev.* **2008**, *37*, 1052-1060.

(11) Camden, J. P.; Dieringer, J. A.; Wang, Y.; Masiello, D. J.; Marks, L. D.; Schatz, G. C.; Van Duyne, R. P.: Probing the structure of single-molecule surface-enhanced Raman scattering hot spots. *J. Am. Chem. Soc.* **2008**, *130*, 12616-12617.

(12) Lal, S.; Grady, N. K.; Kundu, J.; Levin, C. S.; Lassiter, J. B.; Halas, N. J.: Tailoring plasmonic substrates for surface enhanced spectroscopies. *Chem. Soc. Rev.* **2008**, *37*, 898-911.

(13) Goutev, N.; Futamata, M.: Attenuated total reflection surface-enhanced infrared absorption spectroscopy of carboxyl terminated self-assembled monolayers on gold. *Appl. Spectrosc.* **2003**, *57*, 506-513.

(14) Osawa, M.: Surface-enhanced infrared absorption. In near-field optics and surface plasmon polaritons. Springer: New York, 2001; Vol. 81; pp 163.

(15) Cai, W. B.; Amano, T.; Osawa, M.: A comparison of surface-enhanced infrared and surface-enhanced Raman spectra of pyrazine adsorbed on polycrystalline gold electrodes. *J. Electroanal. Chem.* **2001**, *500*, 147-155.

(16) Osawa, M.; Ataka, K.; Yoshii, K.; Nishikawa, Y.: Surface-enhanced infrared-spectroscopy - The origin of the absorption enhancement and band selection rule in the infrared-spectra of molecules adsorbed on fine metal particles. *Appl. Spectrosc.* **1993**, *47*, 1497-1502.

(17) Xu, H. X.; Aizpurua, J.; Kall, M.; Apell, P.: Electromagnetic

contributions to single-molecule sensitivity in surface-enhanced Raman scattering. *Phys. Rev. E* **2000**, *62*, 4318-4324.

(18) GarciaVidal, F. J.; Pendry, J. B.: Collective theory for surface enhanced Raman scattering. *Phys. Rev. Lett.* **1996**, *77*, 1163-1166.

(19) Michaels, A. M.; Jiang, J.; Brus, L.: Ag nanocrystal junctions as the site for surface-enhanced Raman scattering of single Rhodamine 6G molecules. *J. Phys. Chem. B* **2000**, *104*, 11965-11971.

(20) Michaels, A. M.; Nirmal, M.; Brus, L. E.: Surface enhanced Raman spectroscopy of individual rhodamine 6G molecules on large Ag nanocrystals. *J. Am. Chem. Soc.* **1999**, *121*, 9932-9939.

(21) Beversluis, M. R.; Bouhelier, A.; Novotny, L.: Continuum generation from single gold nanostructures through near-field mediated intraband transitions. *Phys. Rev. B* **2003**, *68*, 115433.

(22) Durr, N. J.; Larson, T.; Smith, D. K.; Korgel, B. A.; Sokolov, K.; Ben-Yakar, A.: Two-photon luminescence imaging of cancer cells using molecularly targeted gold nanorods. *Nano Lett.* **2007**, *7*, 941-945.

(23) Sundaramurthy, A.; Schuck, P. J.; Conley, N. R.; Fromm, D. P.; Kino, G. S.; Moerner, W. E.: Toward nanometer-scale optical photolithography: Utilizing the near-field of bowtie optical nanoantennas. *Nano Lett.* **2006**, *6*, 355-360.

(24) Eichelbaum, M.; Kneipp, J.; Schmidt, B. E.; Panne, U.; Rademann, K.: SERS and multiphoton-induced luminescence of gold micro- and nanostructures fabricated by NIR femtosecond-laser irradiation. *Chemphyschem* **2008**, *9*, 2163-2167.

(25) Farrer, R. A.; Butterfield, F. L.; Chen, V. W.; Fourkas, J. T.: Highly

efficient multiphoton-absorption-induced luminescence from gold nanoparticles. *Nano Lett.* **2005**, *5*, 1139-1142.

(26) Kempa, T.; Farrer, R. A.; Giersig, M.; Fourkas, J. T.: Photochemical synthesis and multiphoton luminescence of monodisperse silver nanocrystals. *Plasmonics* **2006**, *1*, 45-51.

(27) LaFratta, C. N.; Fourkas, J. T.; Baldacchini, T.; Farrer, R. A.: Multiphoton fabrication. *Angew. Chem. Int. Ed.* **2007**, *46*, 6238-6258.

(28) Maruo, S.; Fourkas, J. T.: Recent progress in multiphoton microfabrication. *Laser Photon. Rev.* **2008**, *2*, 100-111.

(29) Rumi, M. B., S.; Wang, J.; Perry, J. W.; Marder, S. R. : *Two-photon absorbing materials and two-photon-induced chemistry. In photoresponsive polymers I*. Springer: Berlin, 2008; Vol. 213; pp 1.

(30) Postnikova, B. J.; Currie, J.; Doyle, T.; Hanes, R. E.; Anslyn, E. V.; Shear, J. B.; Vanden Bout, D. E.: Towards nanoscale three-dimensional fabrication using two-photon initiated polymerization and near-field excitation. *Microelectron. Eng.* **2003**, *69*, 459-465.

(31) Ueno, K.; Juodkazis, S.; Shibuya, T.; Yokota, Y.; Mizeikis, V.; Sasaki, K.; Misawa, H.: Nanoparticle plasmon-assisted two-photon polymerization induced by incoherent excitation source. *J. Am. Chem. Soc.* **2008**, *130*, 6928-6929.

(32) Yin, X. F., Nicholas; Zhang, Xiang; Martini, Ignacio B.; Schwartz, Benjamin J.: Near-field multiphoton nanolithography using an apertureless optical probe. *In nonlinear optical transmission and multiphoton processes in organics.* ; Yeates, A. T., Belfield, K. D., Kajzar, F., Lawson, C. M., Ed., 2003; Vol. 5211; pp

96-103

(33) Jang, S. M.; Park, J. S.; Shin, S. M.; Yoon, C. J.; Choi, B. K.; Gong, M. S.; Joo, S. W.: Adsorption of 4-biphenylmethanethiolate on different-sized gold nanoparticle surfaces. *Langmuir* **2004**, *20*, 1922-1927.

(34) Garcia-Santamaria, F.; Salgueirino-Maceira, V.; Lopez, C.; Liz-Marzan, L. M.: Synthetic opals based on silica-coated gold nanoparticles. *Langmuir* **2002**, *18*, 4519-4522.

(35) Liz-Marzan, L. M.; Giersig, M.; Mulvaney, P.: Synthesis of nanosized gold-silica core-shell particles. *Langmuir* **1996**, *12*, 4329-4335.

(36) Baldacchini, T.; LaFratta, C. N.; Farrer, R. A.; Teich, M. C.; Saleh, B. E. A.; Naughton, M. J.; Fourkas, J. T.: Acrylic-based resin with favorable properties for three-dimensional two-photon polymerization. *J. Appl. Phys.* **2004**, *95*, 6072-6076.

(37) Kim, H.; Xiang, C.; Guell, A. G.; Penner, R. M.; Potma, E. O.: Tunable two-photon excited luminescence in single gold nanowires fabricated by lithographically patterned nanowire electrodeposition. *J. Phys. Chem. C* **2008**, *112*, 12721-12727.

(38) Su, X.; Li, M.; Zhou, Z.; Zhai, Y.; Fu, Q.; Huang, C.; Song, H.; Hao, Z.: Microstructure and multiphoton luminescence of Au nanocrystals prepared by using glancing deposition method. *J. Lumin.* **2008**, *128*, 642-646.

(39) Louden, R.: *The quantum theory of light*. 2nd ed.; Oxford University Press: New York, 1983.

Chapter 3: Polymerization induced by nonlinear luminescence of gold nanowires*

3.1 Introduction

Field enhancement[1,2] by metal nanostructures has played a pivotal role in optical measurements beyond the diffraction limit.[3,4] Optical studies of metal nanomaterials have been performed using surface-enhanced Raman scattering (SERS),[5] surface-enhanced infrared absorption (SEIRA),[6] multiphoton-absorption-induced luminescence (MAIL),[7,8] and metal-enhanced multiphoton absorption polymerization (MEMAP).[7,9] In order to develop a better understanding of the field enhancement of plasmonic nanostructures, correlations among different optical phenomena in a single sample have been studied. For example, the relationship between the efficiencies of MAIL and MEMAP in gold nanoparticle clusters was discussed in the last Chapter. The efficiencies of MEMAP and SERS have also been examined on silver nanostructures.[10]

Luminescence of metal nanomaterials induced by a multiphoton absorption process was discovered more than 20 years ago.[11] Since then, MAIL has been observed from a variety of plasmonic nanostructures, including gold nanoparticles,[7] nanorods,[8] nanowires,[12,13] nanoshells,[14] nanoplates,[15] and nanobowties.[9] The emission spectrum of MAIL in most cases spans the visible region and extends into

* Reproduced with permission from [Nah et al., *J. Phys. Chem. C*, **2010**, *114* (17), pp 7774–7779. Publication Date (Web): March 10, 2010 DOI: 10.1021/jp100387k] Copyright © 2009 American Chemical Society.

the ultraviolet and near-infrared regions of the spectrum. As discussed in Chapter 2, the broadband emission of MAIL was recently used as the predominant source of polymerization of gold nanoparticles.[7]

In the presence of metal nanostructures, it is possible that MEMAP can be initiated with excitation intensities below the typical threshold of the photoresist due to field enhancement. MEMAP has been investigated for a wide range of metal nanostructures such as nanoparticle aggregates,[7] nanorods,[16] nanobowties,[9] and sharp metallic tips.[17] Originally, it was thought that when ultrafast near-infrared pulses excite metal nanostructures in a prepolymer resin, the photoinitiator molecules near the nanostructures can be excited by two-photon absorption and induce polymerization.[16] However, study in Chapter 2 demonstrated that for nanoparticle aggregates, MEMAP could be driven equally efficiently even at wavelengths for which two-photon excitation of the photoinitiator was not possible.[7] This result strongly suggests that MAIL from the nanostructure can drive the transition of the photoinitiator by single photon absorption of broadband luminescence from gold nanoparticles.[7]

In order to explore the dominant mechanism of MEMAP and its correlation to MAIL in greater detail, we used gold nanowires because their uniform geometry. By maintaining good control of the morphology, we can rule out the effects from aggregates and defects. Different types of photoinitiators and photoresists were employed to observe the MEMAP process in order to generalize these results. In this Chapter, the strong correlation between MAIL and MEMAP from gold nanowires will be discussed. We will demonstrate based on wavelength-dependent studies that

the dominant mechanism of MEMAP is the single-photon excitation of the photoinitiator driven by MAIL.[7]

3.2 Experimental Section

3.2.1 Sample preparation

To promote adhesion[18] of polymeric structures created with multiphoton absorption polymerization (MAP), glass coverslips were pretreated by immersion in a solution of 93 vol% ethanol, 5 vol% distilled water and 2 vol% (3-acryloxypropyl) trimethoxysilane (95 %, Gelest, Inc.) for 12 h. The coverslips were then rinsed in ethanol for 1 hour and dried in an oven at 95 ℃ for 1 hour.

In order to facilitate the identification of specific nanowires with scanning electron microscopy (SEM) imaging after MAIL and MEMAP experiments, MAP[19-21] was used to write lines forming a 75 μm × 75 μm grid divided into 36 squares on the substrate. An acrylic resin composed of 54 wt% tris(2- hydroxyethyl) isocyanurate triacrylate (SR 399, Sartomer), 43 wt% dipentaerythritol pentaacrylate esters (SR 368, Sartomer), and 3 wt% Lucirin TPO-L (BASF) was used to fabricate the patterns.

MAP was performed using the same laser and microscope system used for MAIL excitation and imaging described in Chapter 2. Using a tunable femtosecond Ti:sapphire oscillator (Coherent Mira 900-F) and an oil-immersion objective (Zeiss R Plan-FLUAR) on an inverted microscope (Zeiss Axiovert 100), polymer features were fabricated at a stage velocity of 20 μm/sec. After fabrication, the unexposed

resin was rinsed in dimethylformamide two times for 3 min each, following by two rinses in ethanol for 3 min each.

Once patterned substrates had been prepared, one drop of a gold nanowire suspension was placed on the coverslip in the region with the pattern. The synthesis of gold nanowires has been described previously.[22,23] The gold nanowire suspension was prepared by mixing approximately 200 μg of dried gold nanowires with 200 μL of distilled water. Sonication for 30 min dispersed the gold nanowires thoroughly in the distilled water, and a light pink suspension was obtained. To deposit the gold nanowires on the patterned substrates, the distilled water was evaporated in an oven at 95 ℃ for 3 min.

3.2.2 Acrylic photoresists for MEMAP

The acrylic photoresist was composed of 55 wt% SR 399, 44 wt% SR 368, and 1 wt% of a radical photoinitiator. We tested two different radical photoinitiators, 2-benzyl-2-dimethylamino-1-(4-morpholinophenyl)-butanone-1 (Irgacure 369, Ciba) and 1-hydroxy cyclohexylphenylketone (Irgacure 184, Ciba). After thorough mixing, one drop of a prepolymer photoresist was placed on a substrate with gold nanowires. The sample was then covered with a coverslip using a layer of Scotch tape as a spacer.

For development after MEMAP experiments, samples were immersed in dimethylformamide for 3 min twice and then in ethanol for 3 min twice to remove any unpolymerized resin. After drying, samples were sputter-coated with 10 nm of Pt/Pd for SEM imaging.

3.2.3 SU8 photoresists for MEMAP

Commercial SU8 2000 Series resists (MicroChem) are composed of 23−96 wt% of cyclopentanone, 0.3−5 wt% of triarylsulfonium hexafluoroantimonate salts in propylene carbonate, and 3−75 wt% of epoxy resin. The structure of SU8 is shown in Figure 3.1. SU8 undergoes cationic polymerization rather than radical polymerization, and so uses a photoacid generator (PAG) rather than a radical photoinitiator.

SU8 with a low concentration of PAG was prepared as follows. Triarylsulfonium hexafluoroantimonate salts in propylene carbonate (0.006 g; 50 %, Aldrich) was mixed with 1.5 g of cyclopentanone (99 %, Fluka). The mixture was then further diluted to 0.01 wt% of PAG in cyclopentanone. EPON Resin SU8 (EPIKOTE^{TM} 157, Hexion) was ground into fine powder and blended with the mixture in a 1:1 weight ratio so that the final SU8 photoresist would contain 0.01 wt% PAG.

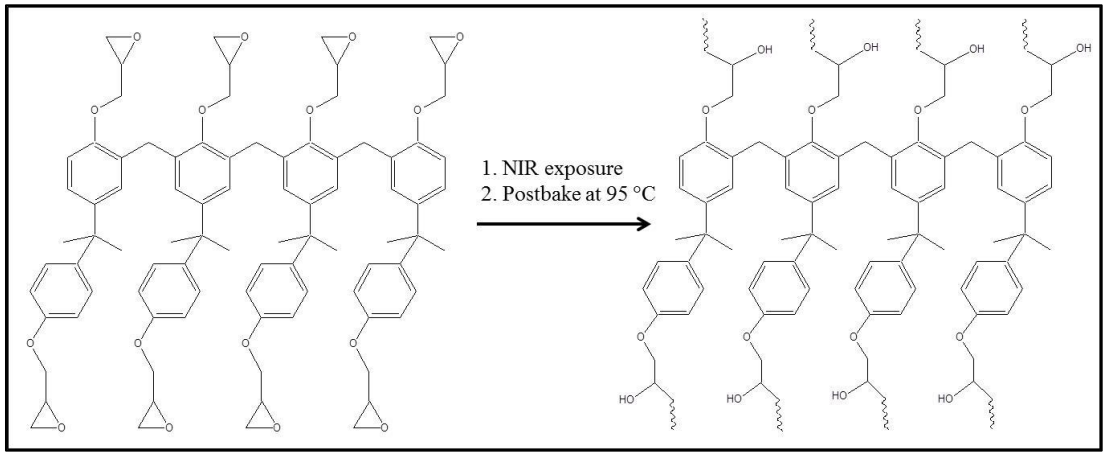

Figure 3.1. Chemical structure of SU8 (left hand side). During the postbake at 95 °C after the NIR exposure, the oxygen of the epoxy group forms hydroxyl group by combining with the photoacid (H^+), and SU 8 monomers start to be cross-linked and become polymers (right

hand side).

The mixture was dissolved completely after 4 h and was filtered twice through 200-nm pores. To render the SU8 photoresist viscous enough to be spread out as a film, the solution was heated in an oven at 95 ℃ for 5 min and then at 110 ℃ for 2 min. After repeating this evaporation process until three-fourths of the original volume remained, the sample was cooled to room temperature.

One drop of SU8 photoresist was placed on a substrate with gold nanowires. Spinning at 4000 rpm for 1 min formed a 20-μm-thick film. The SU8 film was then placed in an oven to bake at 65 ℃ for 2 min, at 95 ℃ for 20 min, and then at 65 ℃ for 5 min. After this prebake, the sample was cooled to room temperature.

After MEMAP exposure, the SU8 film was postbaked by placing it in an oven at 65 ℃ for 2 min, at 95 ℃ for 20 min, and then 65 ℃ for 5 min. During the postbake, the generated acid diffuses and leads to the crosslinking among monomers. After the sample was cooled to room temperature, it was rinsed in SU-8 Developer (MicroChem) for 6 min two times, following by an isopropanol rinse for 3 min. After drying, the sample was sputter-coated with 10 nm of Pt/Pd for SEM imaging.

3.2.4 MAIL imaging and MEMAP

The laser described above was employed for the MAIL and MEMAP studies. The laser was tuned from 724 nm to 930 nm to cover the wavelength range used in the experiments. The objective and microscope are the same ones described above. Samples were mounted on a three-dimensional (3D) piezoelectric stage (P-562 PIMars^{TM} XYZ Piezo System, Physik Instrumente) for fine sample positioning in all

dimensions. The piezo stage was attached to a motor-driven stage (Bioprecision, Ludl Electronic Products) for coarse sample positioning.

To capture the MAIL images, the beam was scanned over a sample using galvanometric mirrors. All luminescence signals were detected by a single-photon-counting avalanche photodiode (EG&G) and transferred to a computer. Scanning of the sample and imaging of luminescence were performed using programs written in LabView (National Instruments).

In typical MAIL and MEMAP experiments, the beam scanned an area of about 2.5 μm^2 containing a single gold nanowire for 2 s with 88 × 88 pixel resolution. The scanning was repeated three times, and the MAIL signals were averaged. For samples with photoresists, MAIL and MEMAP were typically performed simultaneously. For samples without a photoresist, immersion oil (Immersol 518 F fluorescence free, Zeiss) was placed on the substrate to facilitate the identification of single gold nanowires for MAIL studies.

3.3 Results

The linear absorption spectra of thin films of the photoresists used in this study are shown in Figure 3.2, denoted by the relevant photoinitiator. The linear absorption of Irgacure 369 and the PAG cuts off before 450 nm, and the absorption of Irgacure 184 cuts off at about 375 nm. To determine the longest wavelength at which MAP was possible using two-photon absorption in the absence of metal nanowires, we performed wavelength-dependent studies up to the maximum laser power available

(~12 mW; all reported laser powers are at the sample). For Irgacure 369 and Irgacure 184, MAP was not observed at any intensity at wavelengths of 890 nm and longer. However, for commercial SU8 we observed MAP at low laser powers (1.3 mW) even with the laser tuned out to 930 nm. As can be seen from Figure 3.2, the linear absorption spectrum of the PAG used in SU8 has gone to baseline at wavelengths that are considerably less than 465 nm (which is half of 930 nm).

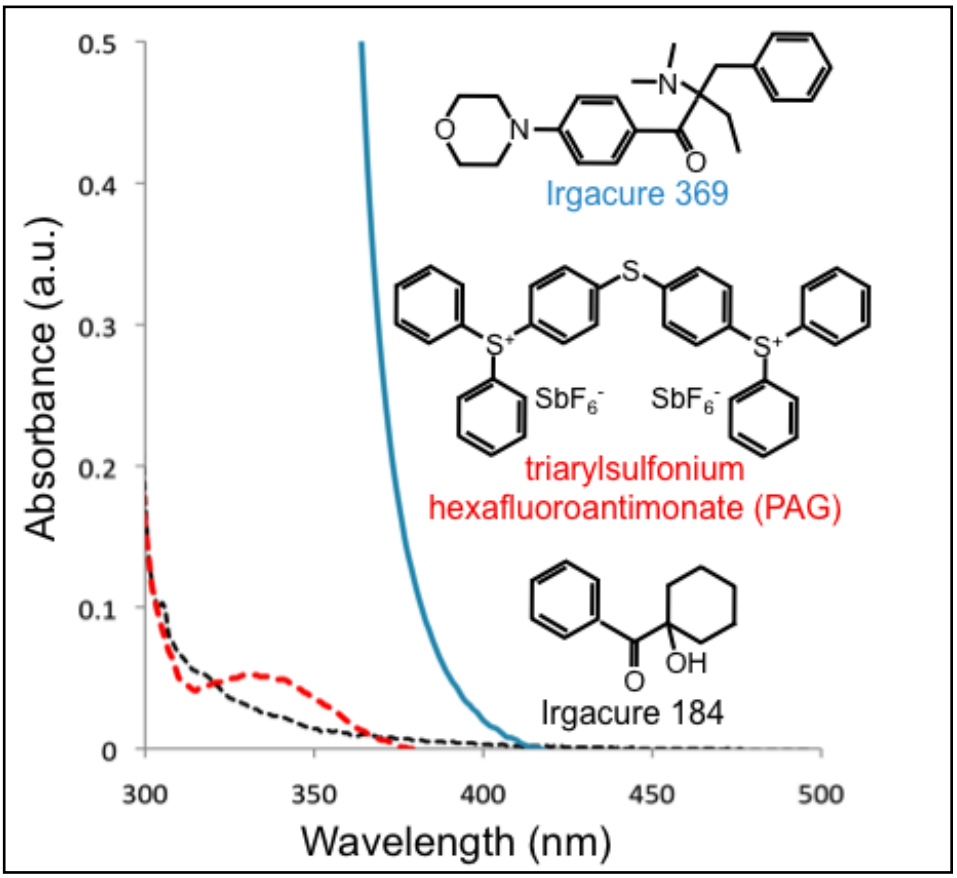

Figure 3.2. Linear absorption spectra of thin films of the photoresists used for MEMAP.

On the basis of the linear absorption spectrum of the PAG, it is surprising that MAP should be so efficient in SU8 at wavelengths as long as 930 nm. However, it

should be kept in mind that the concentration of the PAG in commercial SU8 photoresists is on the order of 1 wt%. While this is a typical concentration for photopolymerization, it is high enough that some degree of aggregation is possible. Furthermore, the PAG is actually a mixture of the structure shown in Figure 3.2 and one in which one end of the molecule terminates in a phenyl group rather than a triarylsulfonium group. Highly polar species of this type may have a propensity to form aggregates of antiparallel molecules. In these so-called H-aggregates, the linear absorption spectrum shifts to the blue.[24] However, for symmetry reasons the two-photon absorption spectrum of the aggregate can shift to the red.

To test whether aggregation is responsible for our ability to perform MAP in SU8 at long wavelengths, we prepared our own SU8 with a lower concentration of PAG, as described above. With only 0.01 wt% of the PAG, we are unable to perform MAP at wavelengths longer than 800 nm. However, at high powers, we do observe laser-induced damage in the photoresist.

We next consider the wavelength dependence of MAIL for these nanowires. Shown in Figure 3.3A is an SEM image of a typical gold nanowire along with normalized MAIL excitation images (i.e., each image was scaled by its maximum intensity) obtained at different laser wavelengths at a constant excitation power of 0.83 mW in Figure 3.3B. At shorter wavelengths, MAIL can be excited anywhere along the length of the wire. However, as the wavelength increases, MAIL excitation is efficient only at the ends of the nanowire. Furthermore, as shown in the unnormalized MAIL excitation images (i.e., no scaling was performed) in Figure 3.3C, the MAIL excitation efficiency is strongest at the shortest and longest

wavelengths, and decreases in between. This phenomenon may reflect stronger coupling into transverse plasmons at shorter wavelengths and into longitudinal plasmons at longer wavelengths. We have observed similar behavior for all isolated nanowires that we have studied.

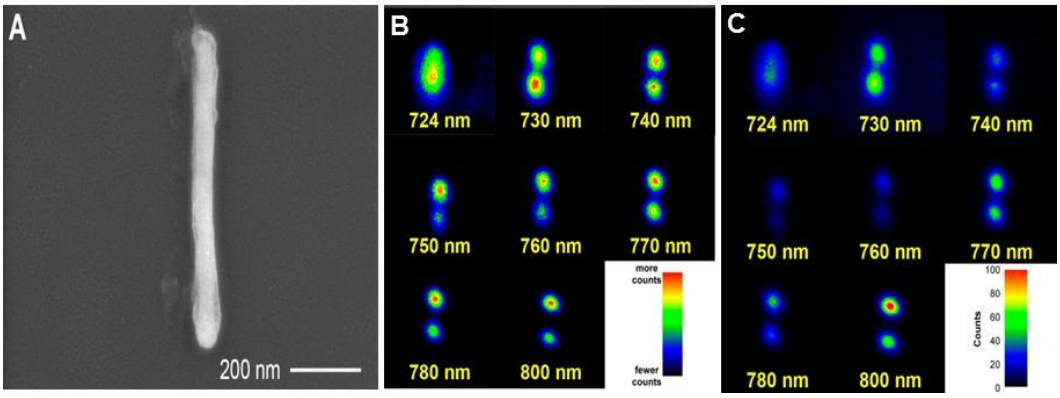

Figure 3.3. (A) SEM of a gold nanowire used for MAIL imaging. The thin coating at the ends of the wire arises from a photochemical reaction of the immersion oil used. (B) Normalized MAIL excitation images of this nanowire obtained at different laser wavelengths. (C) Unnormalized MAIL excitation images corresponding to the normalized MAIL excitation images in (B). The excitation power at each wavelength was 0.83 mW at the sample.

We next consider the correlation between MAIL and MEMAP. Shown in Figure 3.4 are MAIL excitation images of two nanowires in an acrylic photoresist with Irgacure 184 as the photoinitiator. The first nanowire (Figure 3.4A) was excited at 730 nm, and shows efficient excitation along its entire length. The second nanowire (Figure 3.4C) was excited at 740 nm, and the areas of efficient excitation are biased towards the ends of the nanowire. The accompanying SEM images of the nanowires after MEMAP show that the areas of polymerization are strongly

correlated with the areas of efficient MAIL excitation. Similar behavior was observed for all nanowires studied, indicating that there is a strong correlation between MAIL and MEMAP.

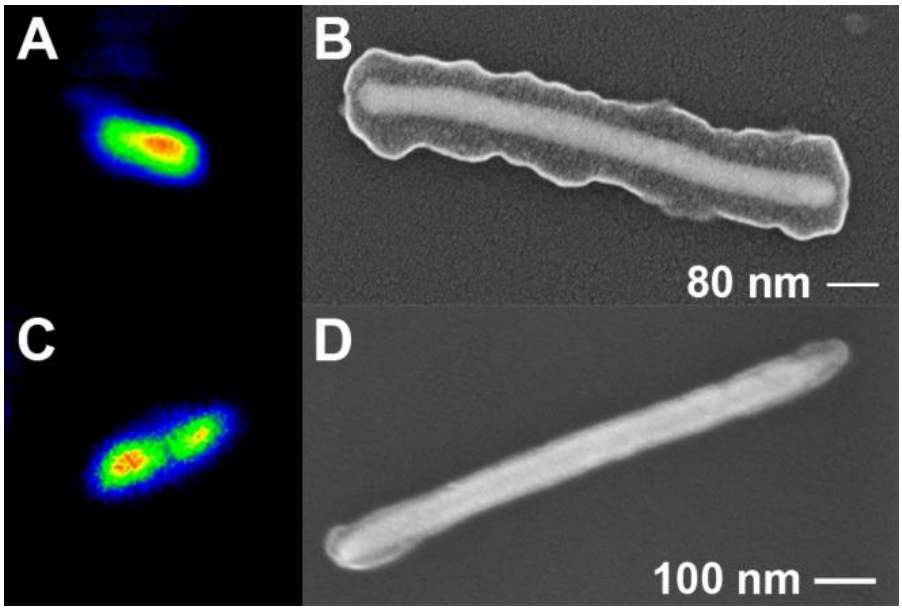

Figure 3.4. (A) MAIL excitation image of a nanowire excited with 730 nm light in an acrylic resin containing 1 wt% Irgacure 184. (B) SEM image of the nanowire from (A) after development. (C) MAIL excitation image of a nanowire excited with 740 nm light in an acrylic resin containing 1 wt% Irgacure 184. (D) SEM image of the nanowire from (C) after development.

To investigate the mechanism of MEMAP, we performed experiments with an excitation wavelength of 890 nm. Even at the highest powers available, MAP was not possible at this wavelength with any of the photoresists used here. It is therefore unlikely that MAP can be driven by two-photon absorption for any of these photoresists at 890 nm. However, MAIL in gold nanostructures can readily be driven

by absorption of three or more 890-nm photons,[7,25] leading to MAIL emission that extends into the UV region of the spectrum. Thus, if MEMAP occurs in these photoresists with 890-nm excitation, it is a strong indication that this process occurs not through enhanced two-photon excitation of the photoinitiator, but rather through single-photon excitation of the photoinitiator by MAIL emission.

Shown in Figure 3.5A is an SEM image of a gold nanowire that was scanned with 890-nm pulses at an average power of 4.1 mW while in an acrylic photoresist with Irgacure 369 as the photoinitiator. The MAIL excitation image obtained during exposure is shown in Figure 3.5B, along with a superimposed SEM image of the nanowire. The polymer coating is seen predominantly at the ends of the nanowire, and is strongly spatially correlated with the MAIL excitation image.

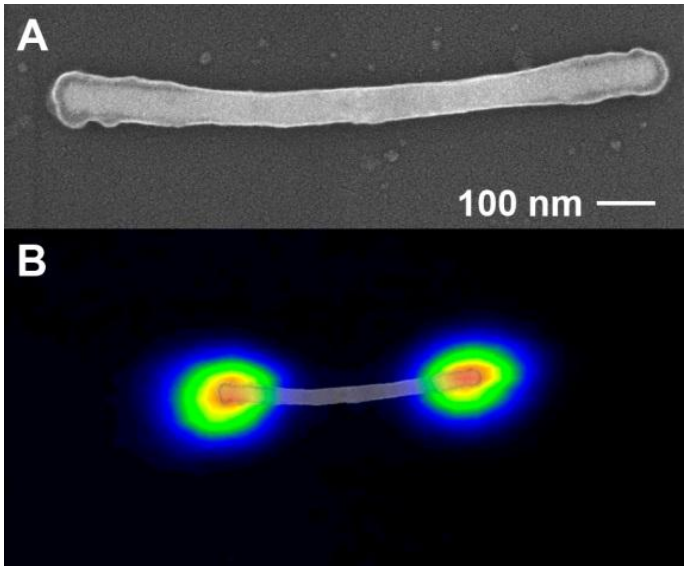

Figure 3.5. (A) SEM image of a nanowire that has undergone MEMAP in an acrylic resin with 1 wt% Irgacure 369 at an excitation wavelength of 890 nm. (B) MAIL excitation image of the nanowire from (A) obtained during the MEMAP exposure. An SEM image of the nanowire has been overlaid on the MAIL image.

In Figure 3.6A we show an SEM image of a gold nanowire that was exposed to 890-nm pulses at an average power of 2.5 mW while in an acrylic photoresist with Irgacure 184 as the photoinitiator. Again, a polymer coating is observed at the ends of the nanowire. This coating is less prominent than for Irgacure 369, presumably because the MAIL emission of the nanowire has less overlap with the linear absorption spectrum of Irgacure 184 (see Figure 3.2). As can be seen in Figure 3.6B, again there is a strong correlation between the location of the polymer coating and the bright regions in the MAIL excitation image.

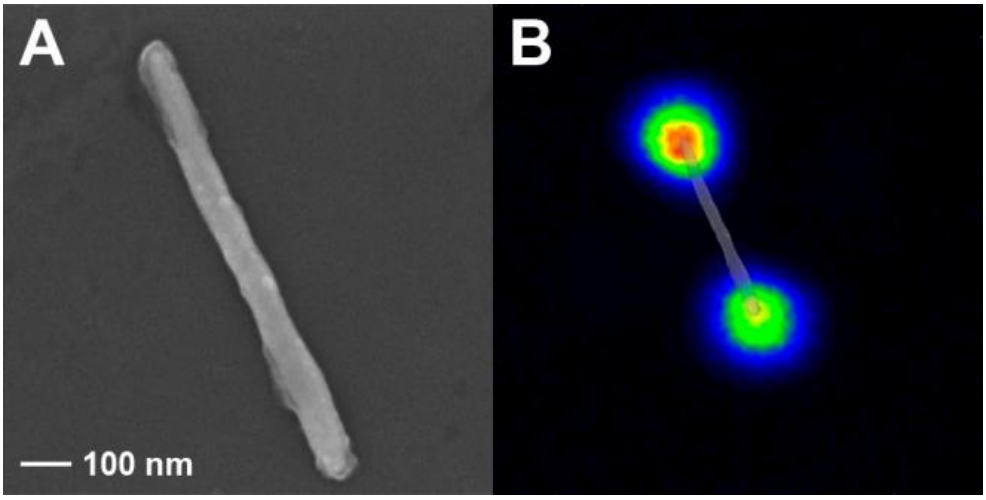

Figure 3.6. (A) SEM image of a nanowire that has undergone MEMAP in an acrylic resin with 1 wt% Irgacure 184 at an excitation wavelength of 890 nm. (B) MAIL excitation image of the nanowire from (A) obtained during the MEMAP exposure. An SEM image of the nanowire has been overlaid on the MAIL image.

A gold nanowire that was exposed to 890 nm pulses at an average power of 3.3 mW while in SU8 with 0.01 wt% PAG is shown in Figure 3.7A. Once again the polymerization is highly localized to the ends of the wire. In SU8 the polymerized

regions extend farther away from the wire than was the case for acrylic photoresists, which may result from diffusion of the acid generated during exposure in combination with local heating due to excitation of the nanowire. As can be seen from the MAIL excitation image in Figure 3.7B, there is once again a strong correlation between the spatial locations of MAIL and MEMAP.

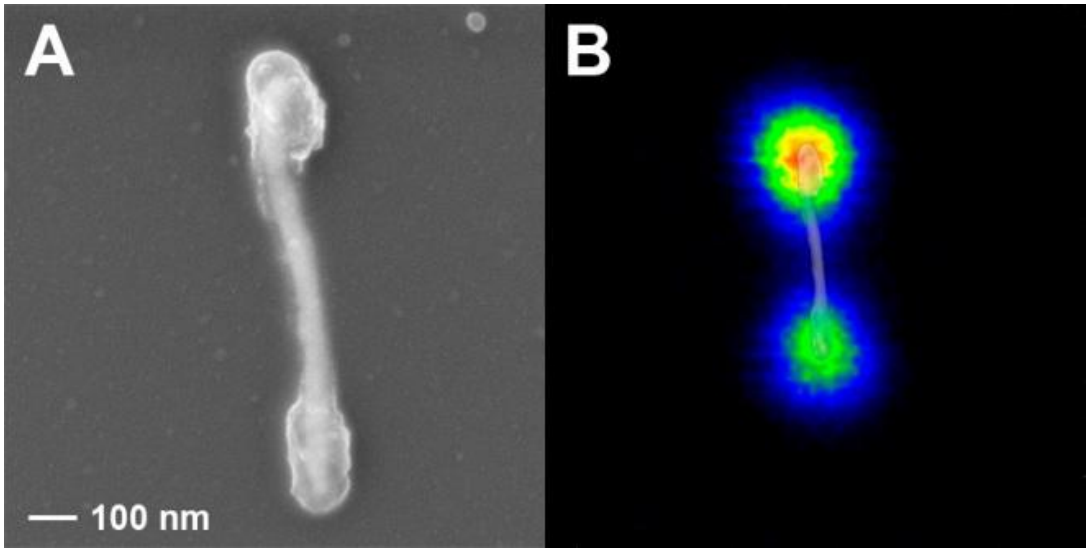

Figure 3.7. (A) SEM image of a nanowire that has undergone MEMAP in SU8 with 0.01 wt% PAG at an excitation wavelength of 890 nm. (B) MAIL excitation image of the nanowire from (A) obtained during the MEMAP exposure. An SEM image of the nanowire has been overlaid on the MAIL image.

3.5 Discussion

The relationship between MAIL and MEMAP using clusters of gold nanoparticles demonstrated that linear absorption of MAIL emission was the

predominant mechanism of MEMAP[7]. However, not all aggregates exhibited efficient MAIL and MEMAP from the study using gold clusters.[7] The gold nanowires we studied are much more uniform than the gold nanoparticle aggregates. These MEMAP results of nanowires in different photoresists demonstrate that MEMAP is driven by the linear absorption of MAIL emission.

MAP cannot be driven by two-photon excitation at 890 nm in any of the photoresists studied here. In fact, for SU8 the threshold for laser-induced damage at this wavelength is lower than the threshold for MAP. However, in all cases MEMAP occurs efficiently at this wavelength and has a strong spatial correlation with MAIL excitation. This result indicates that at long wavelengths, the dominant mechanism for MEMAP is linear absorption of MAIL emission. As there is no significant qualitative change in MEMAP behavior in moving to the shorter excitation wavelengths studied here, it appears likely that the dominant mechanism for MEMAP remains the same over the entire range of wavelengths.

The fact that MEMAP appears to be driven predominantly by MAIL emission for every photoinitiator that we have studied suggests that this is a highly general mechanism. Indeed, Diebold, Peng and Mazur have also suggested that this mechanism holds in their experiments on a positive-tone photoresist on rough silver surfaces.[10] It will be interesting to investigate whether MAIL plays a role in other processes that depend upon field enhancement at noble-metal nanostructures. For instance, processes that involve emission, such as SERS, have maximum efficiencies that have not yet been able to be described adequately by theory. On the other hand, for processes that depend only on absorption, such as SEIRA, the observed

enhancement matches well with theoretical predictions.

3.6 Conclusions

We have demonstrated that there is a strong spatial correlation between MAIL and MEMAP for gold nanowires excited at wavelengths ranging from 730 nm to 890 nm. Experiments performed at long wavelengths indicate that for all of the photoresists studied here, MEMAP is driven predominantly by linear absorption of MAIL emission. Our data also suggest that the same mechanism dominates at shorter wavelengths. Experiments on other types of noble-metal nanostructures can explore the generality of this mechanism for MEMAP.

References

(1) Kelly, K. L.; Coronado, E.; Zhao, L. L.; Schatz, G. C.: The optical properties of metal nanoparticles: The influence of size, shape, and dielectric environment. *J. Phys. Chem. B* **2003**, *107*, 668-677.

(2) Schwartzberg, A. M.; Zhang, J. Z.: Novel optical properties and emerging applications of metal nanostructures. *J. Phys. Chem. C* **2008**, *112*, 10323-10337.

(3) Gramotnev, D. K.; Bozhevolnyi, S. I.: Plasmonics beyond the diffraction limit. *Nature Photon.* **2010**, *4*, 83-91.

(4) Kawata, S.; Inouye, Y.; Verma, P.: Plasmonics for near-field nano-imaging and superlensing. *Nature Photon.* **2009**, *3*, 388-394.

(5) Willets, K. A.; Van Duyne, R. P.: Localized surface plasmon resonance spectroscopy and sensing. *Annu. Rev. Phys. Chem.* **2007**, *58*, 267-297.

(6) Lal, S.; Grady, N. K.; Kundu, J.; Levin, C. S.; Lassiter, J. B.; Halas, N. J.: Tailoring plasmonic substrates for surface enhanced spectroscopies. *Chem. Soc. Rev.* **2008**, *37*, 898-911.

(7) Nah, S.; Li, L.; Fourkas, J. T.: Field-enhanced phenomena of gold nanoparticles. *J. Phys. Chem. A* **2009**, *113*, 4416-4422.

(8) Muhlschlegel, P.; Eisler, H. J.; Martin, O. J. F.; Hecht, B.; Pohl, D. W.: Resonant optical antennas. *Science* **2005**, *308*, 1607-1609.

(9) Sundaramurthy, A.; Schuck, P. J.; Conley, N. R.; Fromm, D. P.; Kino, G. S.; Moerner, W. E.: Toward nanometer-scale optical photolithography: Utilizing the near-field of bowtie optical nanoantennas. *Nano Lett.* **2006**, *6*, 355-360.

(10) Diebold, E. D.; Peng, P.; Mazur, E.: Isolating surface-enhanced Raman scattering hot spots using multiphoton lithography. *J. Am. Chem. Soc.* **2009**, *131*, 16356-16357.

(11) Boyd, G. T.; Yu, Z. H.; Shen, Y. R.: Photoinduced luminescence from the noble-metals and its enhancement on roughened surfaces. *Phys. Rev. B* **1986**, *33*, 7923-7936.

(12) Biagioni, P.; Celebrano, M.; Savoini, M.; Grancini, G.; Brida, D.; Matefi-Tempfli, S.; Matefi-Tempfli, M.; Duo, L.; Hecht, B.; Cerullo, G.; Finazzi, M.: Dependence of the two-photon photoluminescence yield of gold nanostructures on the laser pulse duration. *Phys. Rev. B* **2009**, *80*, 045411.

(13) Gong, H. M.; Zhou, Z. K.; Xiao, S.; Su, X. R.; Wang, Q. Q.: Strong near-infrared avalanche photoluminescence from Ag nanowire arrays. *Plasmonics* **2008**, *3*, 59-64.

(14) Park, J.; Estrada, A.; Sharp, K.; Sang, K.; Schwartz, J. A.; Smith, D. K.; Coleman, C.; Payne, J. D.; Korgel, B. A.; Dunn, A. K.; Tunnell, J. W.: Two-photon-induced photoluminescence imaging of tumors using near-infrared excited gold nanoshells. *Opt. Express* **2008**, *16*, 1590-1599.

(15) Imura, K.; Nagahara, T.; Okamoto, H.: Photoluminescence from gold nanoplates induced by near-field two-photon absorption. *Appl. Phys. Lett.* **2006**, *88*, 023104.

(16) Murazawa, N.; Ueno, K.; Mizeikis, V.; Juodkazis, S.; Misawa, H.: Spatially selective nonlinear photopolymerization induced by the near-field of surface

plasmons localized on rectangular gold nanorods. *J. Phys. Chem. C* **2009**, *113*, 1147-1149.

(17) Yin, X. F., Nicholas; Zhang, Xiang; Martini, Ignacio B.; Schwartz, Benjamin J.: Near-field multiphoton nanolithography using an apertureless optical probe. In *nonlinear optical transmission and multiphoton processes in organics.* ; Yeates, A. T., Belfield, K. D., Kajzar, F., Lawson, C. M., Ed., 2003; Vol. 5211; pp 96-103

(18) Baldacchini, T.; LaFratta, C. N.; Farrer, R. A.; Teich, M. C.; Saleh, B. E. A.; Naughton, M. J.; Fourkas, J. T.: Acrylic-based resin with favorable properties for three-dimensional two-photon polymerization. *J. Appl. Phys.* **2004**, *95*, 6072-6076.

(19) LaFratta, C. N.; Fourkas, J. T.; Baldacchini, T.; Farrer, R. A.: Multiphoton fabrication. *Angew. Chem. Int. Ed.* **2007**, *46*, 6238-6258.

(20) Maruo, S.; Fourkas, J. T.: Recent progress in multiphoton microfabrication. *Laser Photon. Rev.* **2008**, *2*, 100-111.

(21) Rumi, M. B., S.; Wang, J.; Perry, J. W.; Marder, S. R. : *Two-photon absorbing materials and two-photon-induced chemistry. In photoresponsive polymers I.* Springer: Berlin, 2008; Vol. 213; pp 1.

(22) Liu, R.; Lee, S. B.: MnO2/Poly(3,4-ethylenedioxythiophene) coaxial nanowires by one-step coelectrodeposition for electrochemical energy storage. *J. Am. Chem. Soc.* **2008**, *130*, 2942-2943.

(23) Xiao, R.; Il Cho, S.; Liu, R.; Lee, S. B.: Controlled electrochemical synthesis of conductive polymer nanotube structures. *J. Am. Chem. Soc.* **2007**, *129*, 4483-4489.

(24) Xue, P.; Lu, R.; Yang, X.; Zhao, L.; Xu, D.; Liu, Y.; Zhang, H.; Nomoto, H.; Takafuji, M.; Ihara, H.: Self-assembly of a chiral lipid gelator controlled by solvent and speed of gelation. *Chem.-Eur. J.* **2009**, *15*, 9824-9835.

(25) Farrer, R. A.; Butterfield, F. L.; Chen, V. W.; Fourkas, J. T.: Highly efficient multiphoton-absorption-induced luminescence from gold nanoparticles. *Nano Lett.* **2005**, *5*, 1139-1142.

Chapter 4: Observation of field-enhanced areas of plasmonic gold nanoplates

4.1 Introduction

Gold nanostructures display surface plasmon (SP) associated field enhancement of optical signals. This phenomenon is typically observed at localized areas of the nanostructures, such as sharp tips[1] or edges.[2] The different shapes of the tips or edges lead to the different intensity patterns of plasmonic optical signals. When detecting the electric fields as associated with scattering,[3] absorption,[4] and luminescence[5] from plasmonic nanostructures, the resulting spectra can be enhanced and shifted to different regions of the spectrum depending upon the local geometry of the nanostructures. Among the variety of gold nanostructures available, gold nanoplates,[6,7] planar nanostructures that are several micrometers in length and up to hundreds nanometers in thickness, have been used to study the electric field-enhancement of the scattering[8-12] and fluorescence[13-15] signals and to examine chemical reactions on planar surfaces[16] because they can be used as substrates for the fabrication of single crystalline nanostructures[11] and the placement of other nanostructures.[10]

Recent work[3] has shown that when white light excites nanoplate dimers, a three orders of magnitude enhancement of the scattering intensity can be observed as the gap between the dimers is decreased down to 10 nm. As the nanoplates are placed closer, the scattering spectrum is also red-shifted because the repulsive force

of the surface charge in the individual nanoplates induced by the irradiation of light becomes weak when another nanoplate is nearby.[3,17] In addition, a gold nanoplate was used as a field-enhancing substrate to measure fluorescence from a dye attached on a gold nanoparticle that was placed on the top of the nanoplate.[10] The nanoplate provided additional localized SP resonances between the two gold nanostructures, which resulted in a 43-fold increase in the fluorescence.[10] Scattering and fluorescence using gold nanoplates have been studied primarily with visible light excitation. There are only a few studies[6,18] regarding the direct observation of luminescence from metal nanoplates due to the requirement of an ultraviolet excitation source.

Here we present a photoluminescence study from individual gold nanoplates driven by nonlinear absorption of near-infrared (NIR) light, a technique used previously with gold nanoparticles[19] and gold nanowires[20], as discussed in previous Chapters. The luminescence we observed was localized at the edges of each nanoplate, in contrast with a previous report[18] in which the luminescence was observed on the flat surface of the nanoplates. The luminescent regions of the nanoplate were changed depending on the polarization axis of linearly polarized NIR light. Polymer features created by multiphoton-absorption-induced luminescence (MAIL) helped to visualize the localized field-enhanced luminescent areas on the nanoplates.

4.2 Experimental section

In order to measure nonlinear luminescence from single nanoplates, the sample was prepared by placing 2 μL of a gold nanoplate aqueous suspension on a polymer-patterned glass coverslip and drying the solution at 25 ℃ for 5 min. The procedures of the fabrication of polymer patterns by multiphoton absorption polymerization (MAP), the treatment of the glass coverslip with an acrylate solution, and optical measurement of MAIL were the same as those described in the experimental section in Chapter 2.

For MAIL observation, non-fluorescent immersion oil was placed on top of the nanoplates to satisfy the refractive index-matching condition. The matched refractive indices significantly reduced scattering from the sample surfaces. After MAIL signals were measured, the immersion oil was removed by rinsing the sample in hexane for 3 min and in ethanol for 5 min. To observe wavelength-dependent MAIL signals, excitation wavelengths ranging from 714 to 880 nm were employed.

In the metal-enhanced MAP (MEMAP) process, 5 μL of an acrylate prepolymer resin composed of 55 wt% dipentaerythritol pentaacrylate (SR 399, Sartomer), 44 wt% tris (2-hydroxy ethyl) isocyanurate triacrylate (SR 368, Sartomer), and 1 wt% of 1-hydroxy cyclohexylphenylketone (Irgacure 184, Ciba) was added on the top of the dried nanoplates. After the MEMAP experiment, unpolymerized resin was removed by rinsing the sample in dimethylformamide for 3 min twice and in ethanol for 3 min two times. When the sample was completely dried at room temperature, it was sputter-coated with 10 nm Pt/Pd for SEM imaging.

4.3 Results and discussion

4.3.1 MAIL of single nanoplates

Figure 4.1a shows a typical MAIL image of a hexagonal nanoplate, which was obtained by scanning the entire nanoplate with 800 nm light. Due to the localized SPs and the "lightning rod" nanoantenna effect,[2,21,22] nonlinear absorption of NIR photons becomes more efficient at the edges. As a result, the MAIL intensities are much brighter at the circumference of the nanoplate than in the flat middle area. While MAIL is localized at the circumference, scattering measured by the irradiation with 800 nm continuous wave (CW) is observed in the middle part of the nanoplate as shown in Figure 4.1b. The proper depth of focus was determined by the MAIL signals while adjusting the focal point in the z-axis. MAIL images were then collected and averaged over three scans. At the same position on the z-axis, the light was changed from mode-locked pulses to CW, and scattering was measured from the same nanoplate.

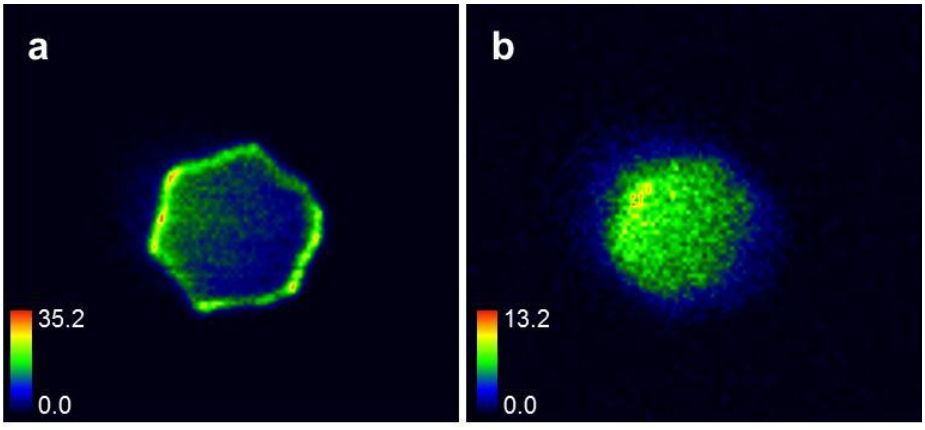

Figure 4.1. (a) MAIL excitation image of a nanoplate excited with 800 nm light. (b) Scattering image of the same nanoplate irradiated with CW 800 nm light.

Nanoplates are likely to overlap with each other due to van der Waals interaction.[23] Figure 4.2a shows a MAIL image measured from overlaid triangular and hexagonal nanoplates. The triangular nanoplate, which was placed inside the circumference of the hexagonal nanoplate, showed stronger MAIL intensities at the corners than at the circumference of the hexagonal nanoplate. When the color bar shows the low range of the MAIL intensity, the weak MAIL intensity from the hexagonal nanoplate is seen clearly in Figure 4.2b. Figure 4.2c shows scattering from the overlapping nanoplates with CW irradiation. The scattering is brighter in the region where two nanoplates are overlaid than in the exposed region of the hexagonal nanoplate.

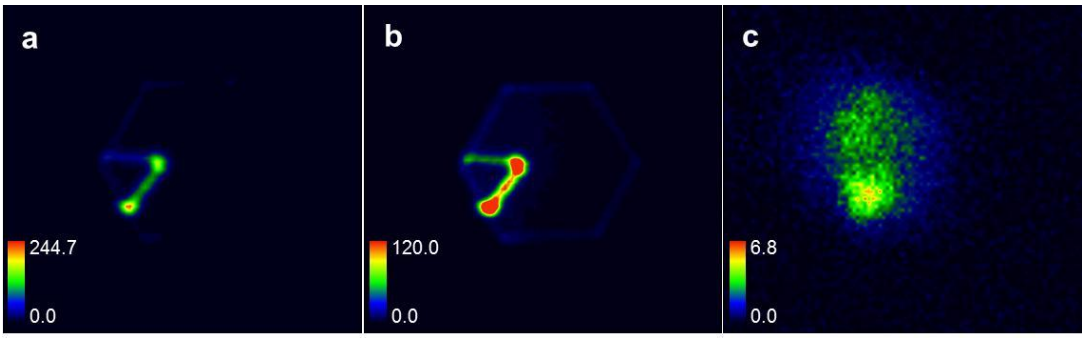

Figure 4.2. (a) MAIL excitation image of overlaid two nanoplates excited with 800 nm light. (b) MAIL excitation image of (a) with a color bar showing the low range of the MAIL intensity. (c) Scattering image of the same nanoplates excited with CW 800 nm light.

We observed the polarization dependence of MAIL signals from a single nanoplate using $\lambda/2$ wave plate to rotate the excitation polarization. When the polarization of the 800 nm light was parallel to the long axis of the nanoplate, the MAIL intensities were the strongest, especially at the edges that were also parallel to

the long axis of the nanoplate. Figure 4.3 shows MAIL images with corresponding polarization directions indicated by red arrows. As the polarization was changed, the brightest MAIL signals were detected at different regions of the circumference of the nanoplate.

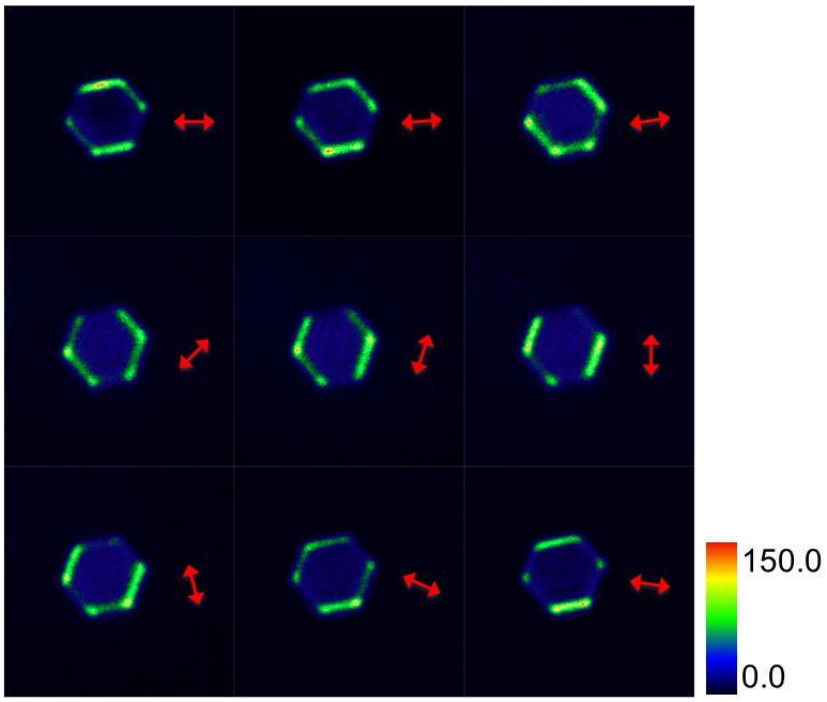

Figure 4.3. MAIL excitation images of a hexagonal nanoplate with different polarizations of light. The red arrows indicate the corresponding polarizations for each nanoplate. The 800 nm excitation power at the nanoplate was 2 mW.

Because the MAIL signals are localized at the edges of the nanoplates, we can predict the MAIL patterns when different shapes of the nanoplates are employed. For instance, when focused ion beam milling is performed on a nanoplate,[24] a variety of shapes of single crystalline gold nanoplates can be fabricated. The resulting MAIL patterns can be predicted and controlled by applying different polarizations.

4.3.2. MEMAP of single nanoplates

We next used MEMAP to observe MAIL-induced polymerization reactions on single nanoplates. In the presence of an acrylate prepolymer resin on the top of the nanoplates, raster scanning of NIR light induced selective polymerization. Figure 4.4a shows the MAIL signals localized at three corners of a triangular nanoplate when scanning with 1.7 mW of 800 nm excitation. Figure 4.4b shows a corresponding SEM image taken from the same nanoplate. As seen in the close-up SEM images in Figure 4.4c, 4.4d, and 4.4e, thin polymer features were created at the three corners of the nanoplate where MAIL signals were observed.

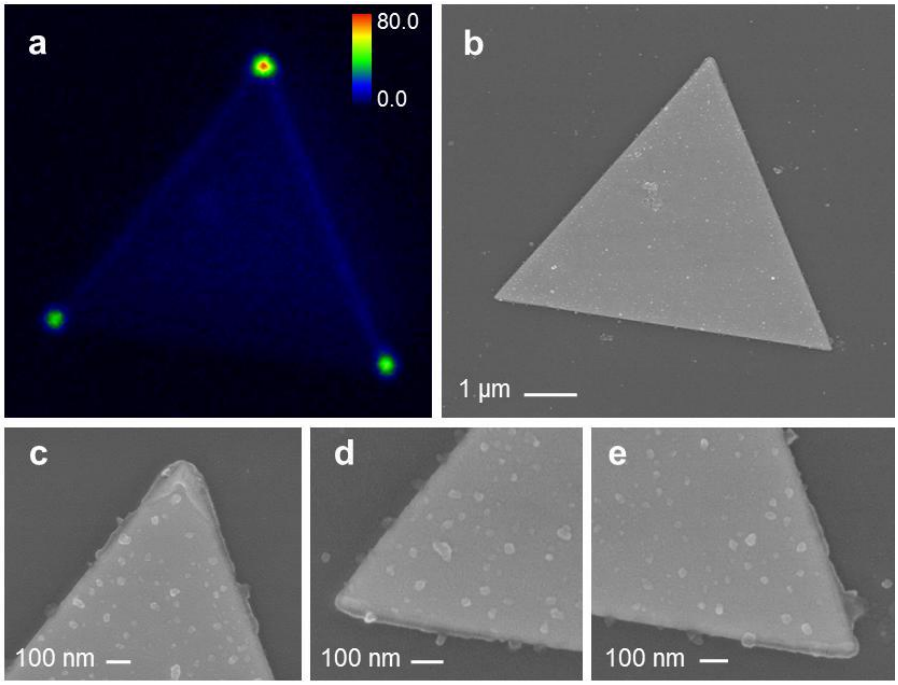

Figure 4.4. (a) MAIL excitation image of a triangular nanoplate excited with 800 nm light. (b) SEM image of the nanoplate from (a). (c) Close-up SEM image of the top tip of the nanoplate. (d) Close-up SEM image of the left hand tip of the nanoplate. (e) Close-up SEM image of the right hand tip of the nanoplate.

Scanning of NIR pulses on one portion of a hexagonal nanoplate induced localized MAIL signals at the edges of the nanoplate, as shown in Figure 4.5a. Figure 4.5b shows a corresponding SEM image from the same nanoplate, and close-up SEM images are shown in Figure 4.5c and 4.5d. Again polymer features were created from the areas where MAIL signals were observed. None of the SEM images we measured from many single nanoplate experiments showed any detectable polymer in the middle part of the nanoplates. This observation indicates that photopolymerization is not driven by scattered light.

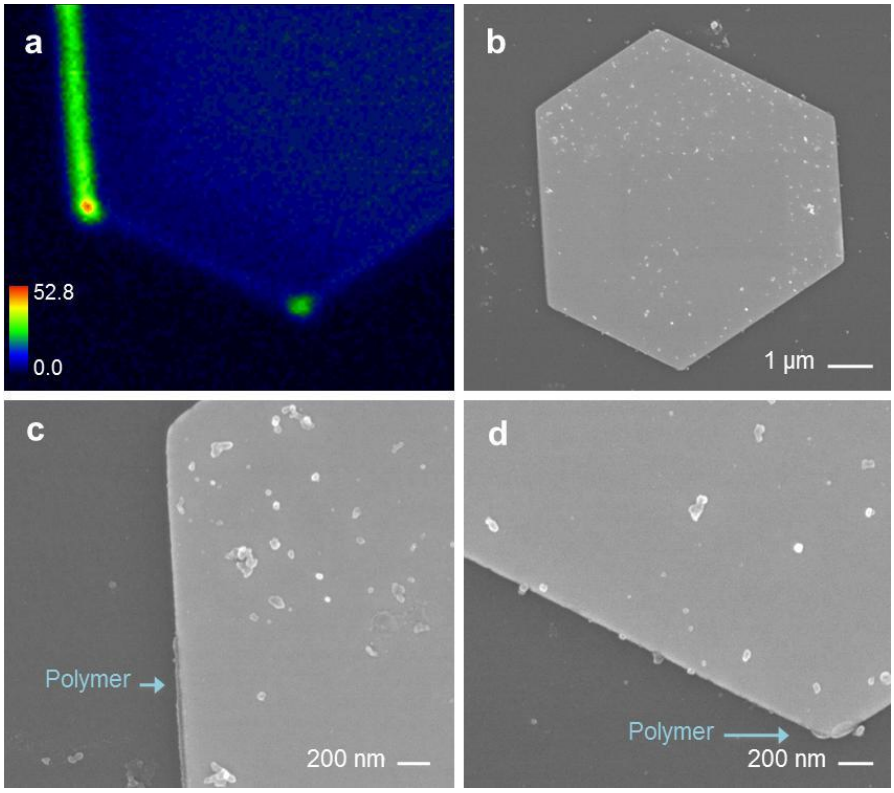

Figure 4.5. (a) MAIL excitation image of one portion of a hexagonal nanoplate excited with 800 nm light. (b) SEM image of the nanoplate from (a). (c) Close-up SEM image of the left hand edge of the nanoplate. (d) Close-up SEM image of the bottom tip of the nanoplate.

The correlation of MAIL to MEMAP on single nanoplates was also examined at different wavelengths. Figure 4.6a shows localized MAIL signals measured by locally exciting at the top portion of a truncated triangular nanoplate with 714 nm light. The nonlinear luminescence measured from gold nanoplates spans the near-ultraviolet region to NIR region of the spectrum[14], which can in turn excite a photoinitiator to induce polymerization. Although the MAIL signals were clearly observed with a 0.83 mW excitation power, the polymerization was not induced at the nanoplate, as shown in Figure 4.6b. A close-up SEM image in Figure 4.6c also did not show any polymer features. A further investigation in different conditions such as applying higher excitation power and employing longer laser exposure time than those used in this initial experiment is necessary because polymerization of gold nanowires was observed with 724 nm excitation.[13]

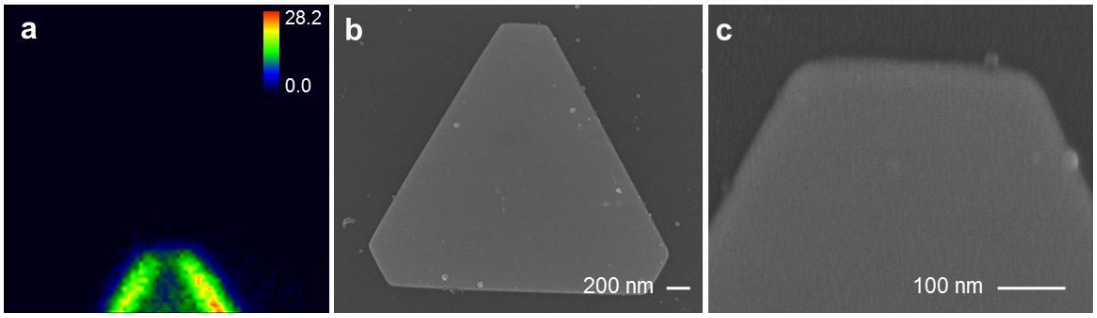

Figure 4.6. (a) MAIL excitation image of the top portion of a triangular nanoplate excited with 714 nm light. (b) SEM image of the nanoplate from (a). (c) Close-up SEM image of the top tip of the nanoplate.

Excitation with 2.5 mW of 880 nm light on a truncated triangular nanoplate did induce polymerization. As shown in Figure 4.7a, the MAIL signals are observed

again at the edges of the nanoplate. Figure 4.7b shows a corresponding SEM image of the same nanoplate used in MAIL imaging. The thin polymer features were created by the MAIL excitation as shown in a close-up SEM image of the bottom edge of the nanoplate in Figure 4.7c. The efficiency of MAIL-induced polymerization of each nanoplate can be different because plasmonic optical properties of each nanoplate are different depending upon the nanoplate length, nanoplate thickness, and nanoplate-tip truncation.[25]

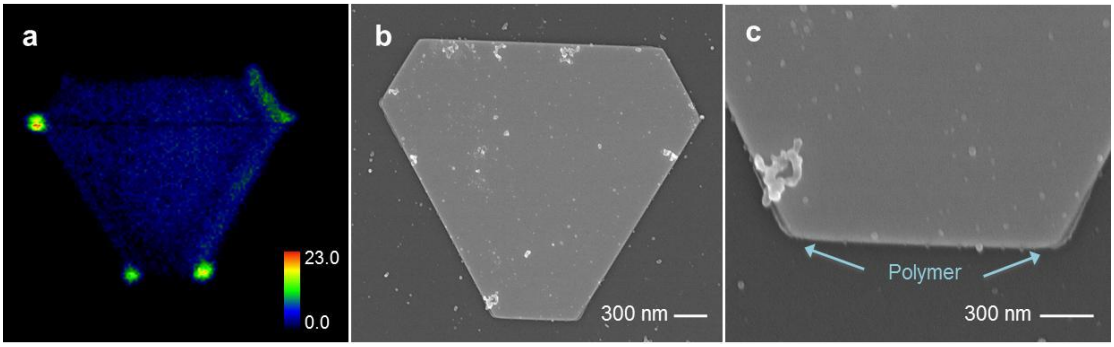

Figure 4.7. (a) MAIL excitation image of a truncated triangular nanoplate excited with 880 nm light. (b) SEM image of the nanoplate from (a). (c) Close-up SEM image of the bottom edge of the nanoplate.

The MAIL-induced polymerization at localized regions of the nanoplates can be useful in designing nanostructure assemblies. For example, QDs could be placed on the edges of a nanoplate with MEMAP. Different polarization of incident light could change the orientation of QDs arrays attached on the nanoplate. When the QDs absorb MAIL from the nanoplates, they can generate bright visible emission, due to the high fluorescence quantum yield. The conversion of NIR light to visible emission in nanocomposites could be used to fabricate frequency switching systems.

4.4. Conclusions

We observed nonlinear luminescence directly from single gold nanoplates using NIR light. The MAIL signals are localized at the tips and edges of the nanoplates where electric fields are crowded and enhanced by SPs. The MAIL intensities were changed in different regions of the nanoplates by changing the polarization direction of NIR light. In the presence of a prepolymer resin, MAIL induced polymerization at the tips and edges of single nanoplates. The thin polymer features created were localized at the regions where MAIL signals were observed, which showed a strong correlation between MAIL and MEMAP on single nanoplates. The MAIL-driven polymerization could be applied to fabricate nanostructure assemblies with NIR excitation. If gold nanoplates are attached in a microfluidic channel and a solution of nanoparticles such as gold, gold-silica core-shell, and silver nanoparticles is added into the channel, NIR excitation could create nanoparticle-nanoplate assemblies, which could be used as surface-enhanced Raman scattering-active substrates. If QDs are immobilized on a nanoplate, NIR excitation on the nanoplate generates broadband of MAIL, which could excite the QDs and generate visible light.

References

(1) Nelayah, J.; Kociak, M.; Stephan, O.; Garcia de Abajo, F. J.; Tence, M.; Henrard, L.; Taverna, D.; Pastoriza-Santos, I.; Liz-Marzan, L. M.; Colliex, C.: Mapping surface plasmons on a single metallic nanoparticle. *Nature Phys.* **2007**, *3*, 348-353.

(2) Muhlschlegel, P.; Eisler, H. J.; Martin, O. J. F.; Hecht, B.; Pohl, D. W.: Resonant optical antennas. *Science* **2005**, *308*, 1607-1609.

(3) Zijlstra, P.; Chon, J. W. M.; Gu, M.: Five-dimensional optical recording mediated by surface plasmons in gold nanorods. *Nature* **2009**, *459*, 410-413.

(4) Lal, S.; Grady, N. K.; Kundu, J.; Levin, C. S.; Lassiter, J. B.; Halas, N. J.: Tailoring plasmonic substrates for surface enhanced spectroscopies. *Chem. Soc. Rev.* **2008**, *37*, 898-911.

(5) Bouhelier, A.; Bachelot, R.; Lerondel, G.; Kostcheev, S.; Royer, P.; Wiederrecht, G. P.: Surface plasmon characteristics of tunable photoluminescence in single gold nanorods. *Phys. Rev. Lett.* **2005**, *95*, 267405.

(6) Millstone, J. E.; Hurst, S. J.; Metraux, G. S.; Cutler, J. I.; Mirkin, C. A.: Colloidal gold and silver triangular nanoprisms. *Small* **2009**, *5*, 646-664.

(7) Yu, P.; Huang, J.; Tang, J.: Observation of coalescence process of silver nanospheres during shape transformation to nanoprisms. *Nanoscale Res. Lett.* **2011**, *6*, 46.

(8) Walker, D. A.; Browne, K. P.; Kowalczyk, B.; Grzybowski, B. A.: Self-assembly of nanotriangle super lattices facilitated by repulsive electrostatic interactions. *Angew. Chem. Int. Ed.* **2010**, *49*, 6760-6763.

(9) Wang, Y.; Zou, X.; Ren, W.; Wang, W.; Wang, E.: Effect of silver nanoplates on Raman spectra of p-aminothiophenol assembled on smooth macroscopic gold and silver surface. *J. Phys. Chem. C* **2007**, *111*, 3259-3265.

(10) Juluri, B. K.; Chaturvedi, N.; Hao, Q.; Lu, M.; Velegol, D.; Jensen, L.; Huang, T. J.: Scalable manufacturing of plasmonic nanodisk dimers and Cusp nanostructures using salting-out quenching method and colloidal lithography. *Acs Nano* **2011**, *5*, 5838-5847.

(11) Baigorri, R.; Garcia-Mina, J. M.; Aroca, R. F.; Alvarez-Puebla, R. A.: Optical enhancing properties of anisotropic gold nanoplates prepared with different fractions of a natural humic substance. *Chem. Mater.* **2008**, *20*, 1516-1521.

(12) Zou, X.; Dong, S.: Surface-enhanced Raman scattering studies on aggregated silver nanoplates in aqueous solution. *J. Phys. Chem. B* **2006**, *110*, 21545-21550.

(13) Kravets, V. G.; Zoriniants, G.; Burrows, C. P.; Schedin, F.; Geim, A. K.; Barnes, W. L.; Grigorenko, A. N.: Composite Au nanostructures for fluorescence studies in visible light. *Nano Lett.* **2010**, *10*, 874-879.

(14) Huang, J.-S.; Callegari, V.; Geisler, P.; Bruening, C.; Kern, J.; Prangsma, J. C.; Wu, X.; Feichtner, T.; Ziegler, J.; Weinmann, P.; Kamp, M.; Forchel, A.; Biagioni, P.; Sennhauser, U.; Hecht, B.: Atomically flat single-crystalline gold nanostructures for plasmonic nanocircuitry. *Nature Comm.* **2010**, *1*:150.

(15) Pompa, P. P.; Martiradonna, L.; Della Torre, A.; Della Sala, F.; Manna, L.; De Vittorio, M.; Calabi, F.; Cingolani, R.; Rinaldi, R.: Metal-enhanced

fluorescence of colloidal nanocrystals with nanoscale control. *Nature Nanotech.* **2006**, *1*, 126-130.

(16) Zheng, Y. B.; Yang, Y.-W.; Jensen, L.; Fang, L.; Juluri, B. K.; Flood, A. H.; Weiss, P. S.; Stoddart, J. F.; Huang, T. J.: Active molecular plasmonics: Controlling plasmon resonances with molecular switches. *Nano Lett.* **2009**, *9*, 819-825.

(17) Rechberger, W.; Hohenau, A.; Leitner, A.; Krenn, J. R.; Lamprecht, B.; Aussenegg, F. R.: Optical properties of two interacting gold nanoparticles. *Opt. Comm.* **2003**, *220*, 137-141.

(18) Imura, K.; Nagahara, T.; Okamoto, H.: Photoluminescence from gold nanoplates induced by near-field two-photon absorption. *Appl. Phys. Lett.* **2006**, *88*, 023104.

(19) Nah, S.; Li, L.; Fourkas, J. T.: Field-enhanced phenomena of gold nanoparticles. *J. Phys. Chem. A* **2009**, *113*, 4416-4422.

(20) Nah, S.; Li, L.; Liu, R.; Hao, J.; Lee, S. B.; Fourkas, J. T.: Metal-enhanced multiphoton absorption polymerization with gold nanowires. *J. Phys. Chem. C* **2010**, *114*, 7774-7779.

(21) Schumacher, T.; Kratzer, K.; Molnar, D.; Hentschel, M.; Giessen, H.; Lippitz, M.: Nanoantenna-enhanced ultrafast nonlinear spectroscopy of a single gold nanoparticle. *Nature Comm.* **2011**, *2*:333.

(22) Novotny, L.; Beversluis, M. R.; Youngworth, K. S.; Brown, T. G.: Longitudinal field modes probed by single molecules. *Phys. Rev. Lett.* **2001**, *86*, 5251-5254.

(23) Jones, M. R.; Macfarlane, R. J.; Lee, B.; Zhang, J.; Young, K. L.; Senesi, A. J.; Mirkin, C. A.: DNA-nanoparticle superlattices formed from anisotropic building blocks. *Nature Mater.* **2010**, *9*, 913-917.

(24) Ah, C. S.; Yun, Y. J.; Park, H. J.; Kim, W. J.; Ha, D. H.; Yun, W. S.: Size-controlled synthesis of machinable single crystalline gold nanoplates. *Chem. Mater.* **2005**, *17*, 5558-5561.

(25) Millstone, J. E.; Park, S.; Shuford, K. L.; Qin, L. D.; Schatz, G. C.; Mirkin, C. A.: Observation of a quadrupole plasmon mode for a colloidal solution of gold nanoprisms. *J. Am. Chem. Soc.* **2005**, *127*, 5312-5313.

Chapter 5: Remote polymerization with guided luminescence in silver nanowires

5.1 Introduction

Noble-metal nanowires can guide and propagate light efficiently even though the nanowire diameter is typically considerably smaller than the free-space wavelength of the light.[1-5] This tight optical confinement has generated considerable interest for applications[6-11] in areas such as light harvesting, nanoscale imaging, and spectroscopy. Many of these applications require the ability to integrate noble-metal nanowires with other nanostructures, such as quantum dots (QDs) or dielectric nanoparticles, to create active devices.[9] On-demand fabrication of integrated nanosystems composed of nanowires, dielectric elements and active nanoemitters remains a challenging problem. The most common strategies for creating such devices to date have relied on bottom-up approaches such as random assembly[12,13] or self-assembly,[14] but these methods suffer from low device yield. Furthermore, the yield typically drops off exponentially with the number of components, and becomes prohibitively small when attempting to integrate even a small number of elements. Reliable assembly of large numbers of elements requires a top-down approach in which preselected nanostructures are placed controllably at predetermined locations on a metal nanowire. A top-down approach to nanoassembly could open up the possibility for development of complex, multi-element nanosystems with a broad range of new device applications.

In addition to the overcoming inherent difficulty of high-yield assembly of nanowire-based devices, it is also essential to be able to couple light into and out of such devices. In metallic nanowires, momentum-matching constraints only allow for efficient far-field coupling of light that propagates nearly parallel to the wire axis, a condition that is often difficult to achieve in practice (and particularly so over a broad wavelength range). One way to circumvent this problem is to use a near-field scanning probe, but this approach works best for coupling to one device at a time. Contacting metal nanowires with other nanostructures that act in essence as far-field to near-field converters has also been pursued,[15] but this approach generally relies on random assembly of the nanowires and nanostructures, again leading to a low device yield.

Here we demonstrate that, via nonlinear light/matter interactions, metal nanowires can act effectively as their own far-field to near-field optical converters. Specifically, irradiating an end of a silver nanowire (AgNW) with ultrafast pulses of near-infrared (NIR) light leads to the efficient generation of broadband visible radiation through multiphoton-absorption-induced luminescence (MAIL).[16] Because this luminescence is generated within the AgNW, a large portion of the light is inherently momentum matched and can propagate down the wire. Waveguiding of this broadband luminescence further allows localized, nanoscale photochemistry to be driven at the far end of the nanowire or at any location along the nanowire that is in contact with another nanoscale object. By using this method in concert with the fluid-based nanomanipulation of individual nanoparticles,[17] we demonstrate the on-demand, high-precision fabrication of nanophotonic devices based on AgNWs.

5.2 Experimental methods

AgNWs were synthesized using a reported procedure.[18] In a typical method, 5 mL of ethylene glycol (Fisher Scientific) was heated to 160 ℃ in a round-bottom flask equipped with a condenser, a thermometer, and a magnetic stirring bar. The ethylene glycol was used as a reducing agent and a solvent. To prepare Pt seeds, 0.5 mL of $PtCl_2$ (Aldrich, 98 %, 1.5×10^{-4} M in ethylene glycol) was added into the hot ethylene glycol solution in the flask. After 4 min of thorough stirring of the solution, 2.5 mL of $AgNO_3$ (Sigma-Aldrich, 99+ %, 0.12 M in ethylene glycol) and 5 mL of poly (vinyl pyrrolidone) (PVP, City Chemical, MW 40000, 0.36 M in ethylene glycol) were simultaneously added for 6 min. At the beginning of blending, the transparent solution turned to dark yellow as Ag atoms were reduced on the Pt seeds and changed to turbid grey as Ag nanowires were formed within 15 min. The solution was held at 160 ℃ for 60 min to allow $AgNO_3$ to be reduced completely and was stirred thoroughly during the reaction. The nanowire solution was cooled to room temperature. To separate Ag nanowires from Ag nanoparticles, the solution was diluted with ethanol of 5 times volume of the solution and centrifuged for 20 min at 2000 rpm at 20 ℃. After the centrifugation, the supernatant was removed and ethanol was added into the solution. After repeating the centrifugation until the supernatant become clear, the final solution was kept in ethanol or deionized water at 4 ℃.

The substrates used were microscope glass coverslips functionalized with acrylate groups to promote polymer adhesion.[19] In the polymerization process, a water-based acrylic photoresist composed of 50 wt% ethoxylated-15

trimethylolpropane triacrylate (SR 9035, Sartomer), 49 wt% distilled water, and 1 wt% sodium 4-[2-(4-morpholino)benzoyl-2-dimethylamino]butylbenzenesulfonate (MBS)[20] was used. For the AgNW junction experiments, an acrylic photoresist composed of 54 wt% dipentaerythritol pentaacrylate esters (SR 399, Sartomer), 43 wt% tris (2-hydroxyethyl) isocyanurate triacrylate (SR 368, Sartomer), and 1 wt% 1-hydroxy cyclohexylphenylketone (Irgacure 184, Ciba) as a photoinitiator was used.[21]

The laser and microscope system used for MAIL excitation and imaging are described in previous Chapters. Light at wavelengths longer than 690 nm was filtered out before the single-photon-counting avalanche photodiode detector and the spectrometer (Acton SP2300i, Princeton Instruments) coupled with an optical fiber (BFB-455-7, Princeton Instruments) to prevent detection of scattered excitation pulses.

An electroosmotic flow control (EOFC) system described previously[17,22] was used to position nanoparticles in solution. The associated water-based photoresist was composed of 40 vol% SR 9035, 1.35 wt% Acrysol RM-825 rheology modifier (Rohm and Haas), 1 wt% MBS, 0.3 wt% erucyl dimethyl amidopropyl betaine as a surfactant, and 200 pM QTracker PEG CdSe/ZnS 655nm QDs (Invitrogen) in deionized water. The dye-infused nanobeads (DINs) were 1.4×10^{-11} % (w/v) carboxylic acid-functionalized Fluorescent Microspheres Polystyrene (Phosphorex, Inc.).

5.3 Results and discussion

The majority of work on the plasmonic properties of metal nanowires has focused on their linear optical behavior. However, the nonlinear optical (NLO) properties of nanowires are beginning to attract interest.[21,23,24] Chapter 3 demonstrated the connection between two NLO effects, MAIL and metal-enhanced multiphoton absorption polymerization (MEMAP) in gold nanowires.[21] In MAIL,[16] field enhancement by a nanowire leads to the efficient multiphoton absorption of ultrafast pulses of NIR light, producing broadband visible luminescence. The "lightning-rod" effect[25,26] makes excitation especially efficient at the ends of nanowires. In MEMAP,[27] a noble-metal nanostructure enhances the efficiency of multiphoton exposure of a negative-tone photoresist. Polymeric features can be created at the ends of a noble-metal nanowire at a laser fluence (integrated exposure) considerably lower than that needed in the bulk photoresist.[21] We have demonstrated in previous chapters that MEMAP occurs through a two-stage process in which light is first converted efficiently from NIR to visible wavelengths by MAIL, and the visible light then exposes photoresist in close proximity to the luminescent region of the nanostructure via linear excitation.[21]

As shown in Figure 5.1, AgNWs exhibit MAIL when excited with NIR, ultrafast pulses. The spot size of the linearly polarized excitation beam used here was about 350 nm, which is much smaller than the length of the nanowire. In the luminescence excitation map in Figure 5.1a, the luminescence emanating from one end of an AgNW was collected by a single-photon-counting avalanche photodiode, while all other luminescence was blocked. To create the map, the luminescence

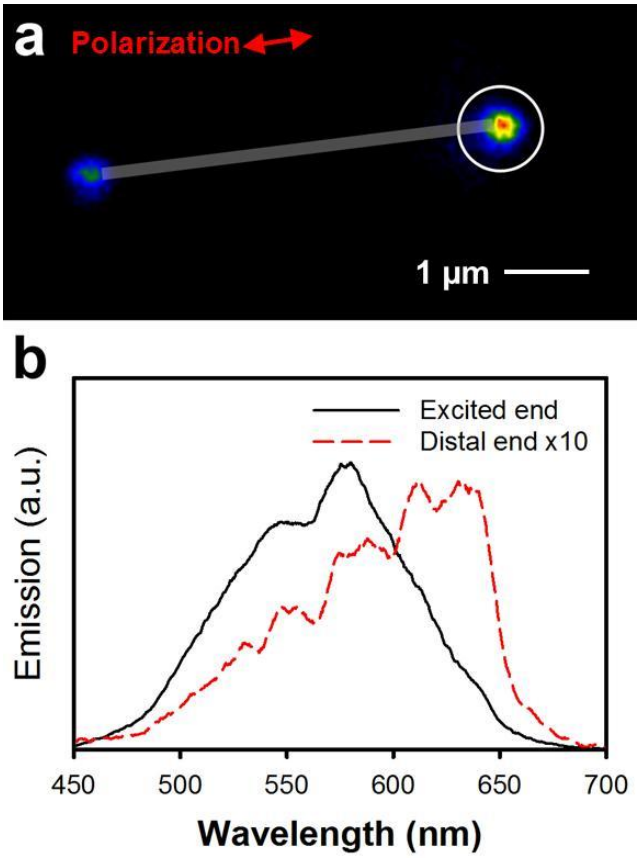

Figure 5.1. AgNW luminescence excitation map and luminescence spectra for pulsed 800-nm excitation. (a) Map of the luminescence intensity from the circled region of the AgNW as a function of the position irradiated with an 800-nm excitation beam focused to a diameter of about 350 nm. The gray bar indicates the approximate location of the AgNW. Red represents the highest luminescence intensity. (b) Representative luminescence spectra from the excited and distal ends of an AgNW. The long-wavelength portion of each spectrum is attenuated by a filter that was used to block scattered excitation light.

intensity from this region was then measured as a function of the position of the excitation spot. The most efficient luminescence is observed when the polarization is parallel to the axis of the nanowire. While the observed luminescence is brightest from the end that is excited, a substantial luminescence signal is also observed at this

same position when the opposite end of the wire is illuminated. Luminescence spectra collected from this region of the AgNW span most of the visible region of the electromagnetic spectrum, regardless of which end of the wire is excited (Figure 5.1b). The shapes of the luminescence spectra at the excited and distal ends do not depend on excitation intensity for all excitation intensities for which luminescence can be observed.

There are two possible mechanisms for broadband luminescence from the distal end of an irradiated nanowire. One possibility is that the luminescence from the excited end propagates to the distal end, where it is emitted. The other possibility is that the excitation pulse itself propagates along the nanowire and generates MAIL at the distal end. A number of lines of evidence support the first mechanism. First, because MAIL is generated within the wire, a significant portion of the luminescence is inherently momentum matched and should propagate efficiently to the distal end. Second, attenuation of the excitation pulse due to propagation down a nanowire should decrease the efficiency of the nonlinear excitation process to a significant extent. Third, the luminescence spectrum from the distal end differs from that at the excited end, as seen in Figure 5.1b. Guided luminescence would be expected to exhibit frequency-dependent attenuation in the nanowire, whereas luminescence generated at the distal end by a guided excitation pulse should have the same spectrum as the luminescence at the excited end.

As an additional test that distal emission arises from guided luminescence, we generated MAIL excitation maps using beams with spatially non-uniform polarization states, azimuthally polarized and radially polarized beams. The azimuthally polarized

beam has a transverse field intensity distribution while the radially polarized beam has a longitudinal field intensity distribution.[30-33] The excitation map for radially polarized light is shown in Figure 5.2a and the excitation map for azimuthally polarized light is shown in Figure 5.2b. In both cases emission is observed from the distal end of the wire only when the portion of the beam that is polarized parallel to the AgNW overlaps with the excited end of the wire. For both of these polarizations, two excitation lobes appear at each end of the AgNW, corresponding to the positions in the excitation beam in which the light is polarized parallel to the nanowire.

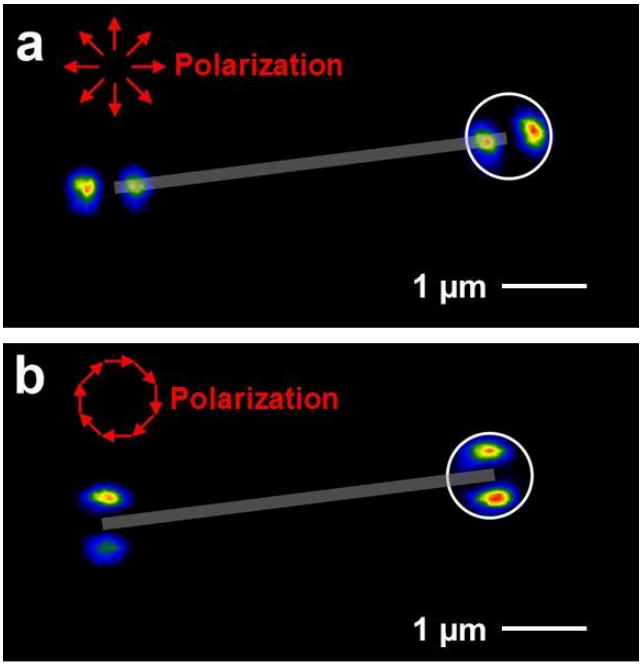

Figure 5.2. AgNW luminescence excitation maps using pulsed 800-nm excitation with different spatially-nonuniform polarizations. (a) Luminescence from the same AgNW shown in Figure 5.1 but using radially polarized excitation. The spatial dependence of the polarization in a transverse plane in the focal region is shown schematically with the red arrows. (b) Same as (a), but with azimuthally polarized excitation.

In order for the excitation pulse to propagate along the nanowire it must be momentum-matched, which means that the propagation vector must have a significant, positive projection along the vector leading from the excited end of the wire to the distal end. In the case of radially polarized light only one of these lobes (the one that overlaps with the wire in Figure 5.2a) can satisfy momentum matching for the fundamental field. In the case of azimuthally polarized light, the lobes are on either side of the wire, and so neither lobe can satisfy momentum matching for the fundamental field. These images provide strong evidence that the observed distal emission arises from guided, nonlinearly generated luminescence as opposed to luminescence generated at the distal end by guided excitation pulses. We therefore use the term guided multiphoton-absorption-induced luminescence (GMAIL) to describe the process through which excitation of one end of an AgNW leads to luminescence at the opposite end.

GMAIL offers the opportunity to deliver broadband, visible radiation to perform photochemistry in a nanoscale spatial region that is distant from the site of excitation. Because MAIL can be excited efficiently and selectively at the end of an AgNW, photochemistry can be localized at the ends of an AgNW without being driven in the surrounding bulk medium. To illustrate the use of GMAIL to perform localized photochemistry at a distance, we show in Figure 5.3a an SEM image of an AgNW that was immersed in a liquid, negative-tone photoresist. One end of the AgNW was irradiated with 800-nm pulses at a fluence too low to expose the bulk photoresist.

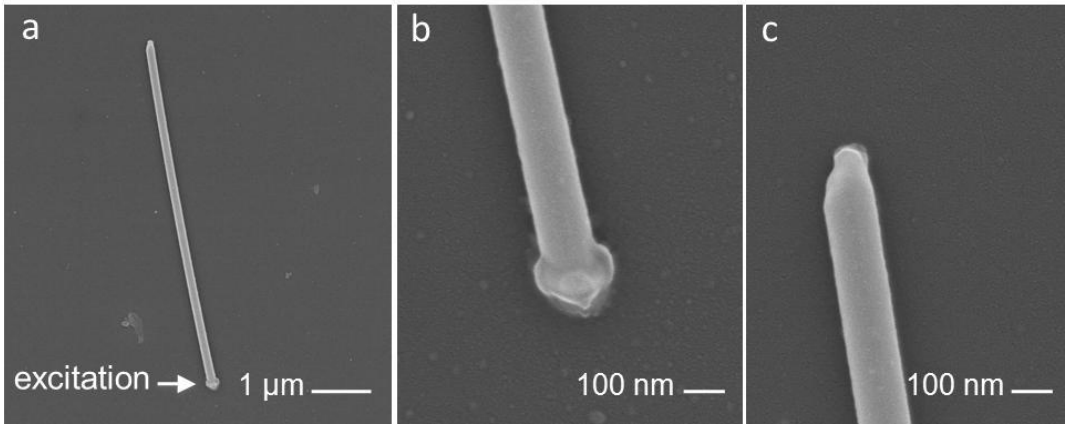

Figure 5.3. Remote, localized photochemistry driven by GMAIL. (a) SEM of an AgNW on a glass substrate. The AgNW was immersed in a negative-tone photoresist and was excited with 800-nm pulses at the location indicated in the image. (b) SEM of the end of the AgNW that was excited. (c) SEM of the distal end of the AgNW.

Exposed photoresist is observed at both ends of the AgNW (Figures. 5.3b and 5.3c). The polymerized region at the distal end is significantly smaller than the region at the excited end, and has a diameter that is smaller than that of the AgNW. Due to the need to satisfy momentum matching, guided luminescence will be emitted from the distal end with a strong forward directional preference, whereas luminescence generated at the distal end by waveguided fundamental radiation will be emitted in all directions (as is the MAIL generated at the end of the AgNW that is excited). Thus, the small diameter of the polymerized region at the distal end of the AgNW further supports guided luminescence as the source of distal emission.

Another possible source of apparent emission (and potentially photopolymerization) at the distal end of an AgNW is scattered MAIL from the excited end of the wire. To test whether scattering is responsible for the distal

emission observed, we studied groups of AgNWs for which scattering is incident on nanowires near one that is excited. An example of one such study is shown in Figure 5.4. We chose two nearly parallel AgNWs, and excited the end of one that was near the end of another (Figures 5.4a-5.4c). Luminescence was observed at the proximal

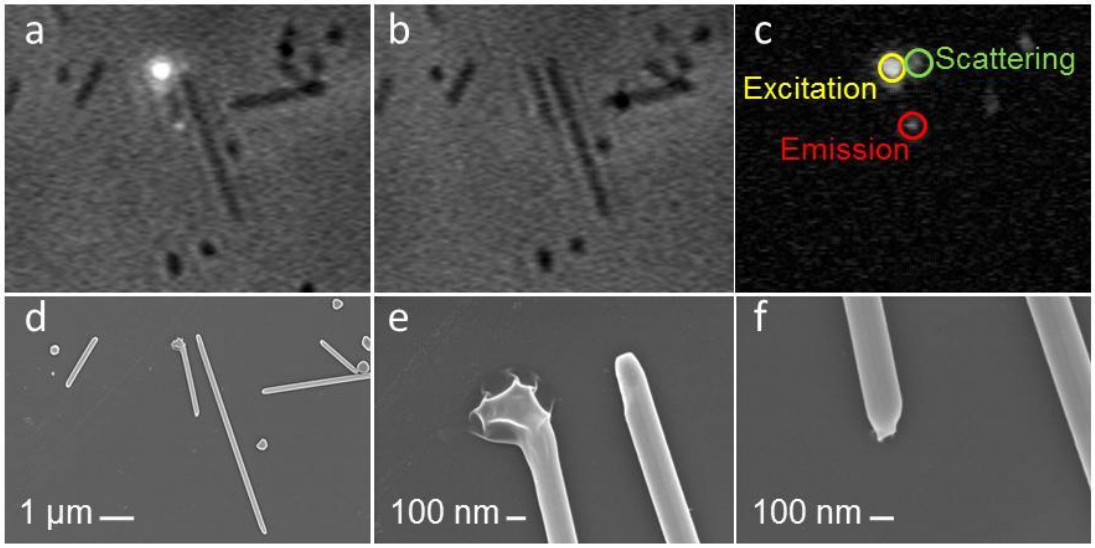

Figure 5.4. Comparison of scattering and guided emission. (a) Optical image of AgNWs in a photoresist. (b) The same nanowires when the top of the left hand AgNW is excited with ultrafast, 800-nm pulses. (c) Subtraction of image (a) from image (b). (d) SEM of the nanowires after development of the photoresist. (e) Close-up of the excited nanowire and the end of its neighbor. (f) Close-up of the distal end of the excited nanowire.

end of the excited AgNW, and scattering was observed from the end of the nearby AgNW. The distal end of the AgNW that was excited also exhibited emission. To test whether the distal emission arose from guided emission or from scattering of light, these experiments were performed in a photoresist, and the AgNWs were imaged using scanning electron microscopy after the resist was developed. As seen

in Figures 5.4d−5.4f, polymer is observed at both the excited end and the distal end of the first nanowire. However, the end of the neighboring nanowire shows no polymerization. Thus, scattering is not sufficiently intense to cause polymerization, and we can conclude that the polymer at the distal end of the excited nanowire is the result of GMAIL. We can therefore rule out scattering as the source of distal photopolymerization.

When another nanostructure comes into contact with an AgNW, the waveguide becomes leaky at the junction,[1,28] providing an opportunity to drive localized photochemistry. Figure 5.5a is an SEM of two AgNWs in a T geometry. The nanowires were immersed in an acrylic photoresist, and one end of the "crossbar" AgNW was excited. Photoresist exposure in the junction region is visible in Figure 5.5b. Thus, contact with another nanostructure can cause sufficient leakage of GMAIL to drive localized photochemistry.

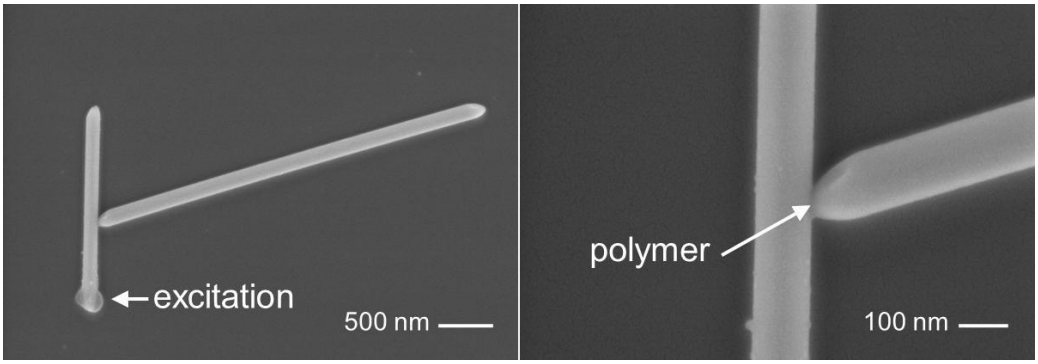

Figure 5.5. "Spot-welding" of AgNWs using GMAIL. (a) SEM of two AgNWs in a T configuration on a glass substrate. The AgNWs were immersed in a negative-tone photoresist, and the region indicated was irradiated with pulses of 800-nm light. (b) Close-up of the contact region of the two AgNWs. A thin layer of exposed photoresist is visible at the intersection of the wires.

Light emitted from a radiative object that is in the near field of an AgNW can couple into the nanowire's SPP modes.[12,13] This phenomenon is attractive for use in nanophotonic devices. However, nanophotonic devices that employ AgNWs are generally created via uncontrolled deposition of one or more nanoparticle emitters, leading to a low device yield.[29] GMAIL provides a means for high-precision fabrication of such devices with preselected nanowires. This process begins with the immersion of a substrate with AgNWs in a liquid photoresist containing nanostructures such as dye- DINs or QDs. Nanostructures are immobilized on a selected nanowire by irradiating one of its ends. Immobilization of a nanostructure occurs only when sufficient optical coupling exists between the nanostructure and the AgNW to drive "spot welding." This optical coupling is also the condition desired for the fabrication of nanophotonic devices.

To demonstrate this principle, a microfluidic system was used to flow a suspension of DINs over AgNWs in a water-based photoresist while selected nanowires were irradiated at one end. As shown in Figure 5.6a, DINs were immobilized on irradiated nanowires. Control nanowires that were not irradiated had few or no attached DINs (Figure 5.6b).

To fabricate nanophotonic devices with predetermined geometry using GMAIL, EOFC was used to manipulate CdSe QDs in a microfluidic system fabricated using a polydimethyl siloxane mold placed on a glass coverslip. An individual QD in a water-based photoresist was delivered to a selected position on an AgNW. When the QD was in the desired position, the end of the AgNW was irradiated with ultrafast pulses, spot-welding the QD to the nanowire. Immobilized

QDs exhibit strong optical coupling to the nanowires, as can be seen in Figure 5.7 from the synchronized blinking of the QD and the ends of the nanowire.

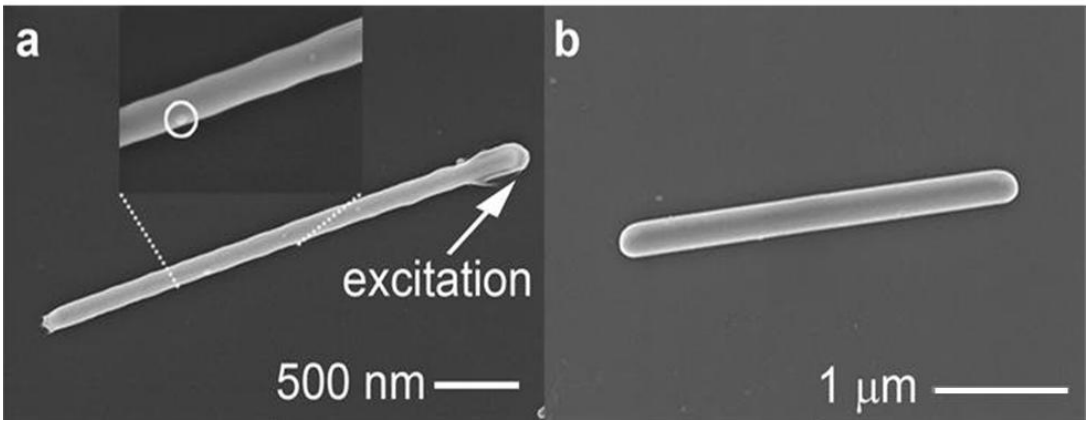

Figure 5.6 Immobilization of nanoparticles on AgNWs using GMAIL. (a) SEM of an AgNW that was irradiated at one end with pulses of 800-nm light while a suspension of DINs was flowed over it. A DIN immobilized on the AgNW is circled in the inset. (b) SEM of an AgNW that was not irradiated while a suspension of DINs was flowed over it. No DINs were immobilized on this nanowire.

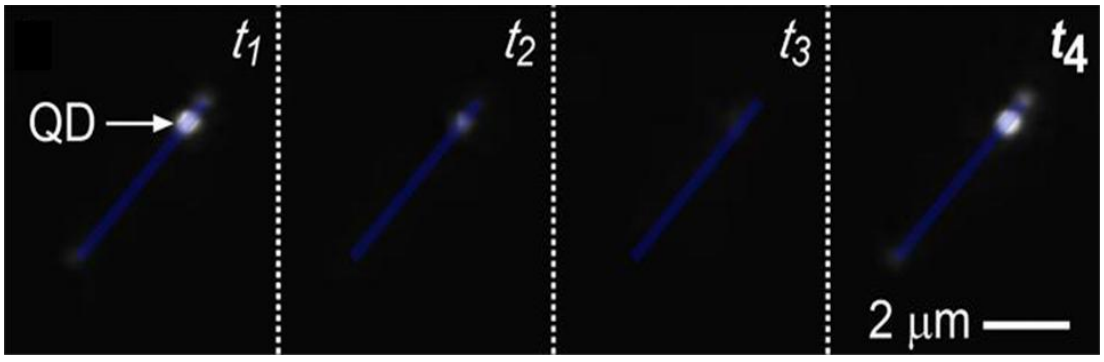

Figure 5.7 Series of luminescence images, at four different times (t_1 to t_4), of a QD that was immobilized to an AgNW using GMAIL. The blue bar shows the approximate location of the AgNW. The correlation between the intensities of the QD and the ends of the AgNW at any given time (which is most easily seen at the end of the AgNW closest to the QD)

indicates that there is strong optical coupling between the two structures.

Figure 5.8 shows frames from a video of a typical immobilization experiment. EOFC is used to bring a selected QD into proximity of an AgNW. When the QD is in optical coupling range, emission from the QD can be observed at the ends of the AgNW. One end of the AgNW is irradiated with ultrafast, 800-nm pulses with a power of about 0.75 mW at the nanowire, immobilizing the QD. Even at high flow velocities, the QD remains tethered to the AgNW.

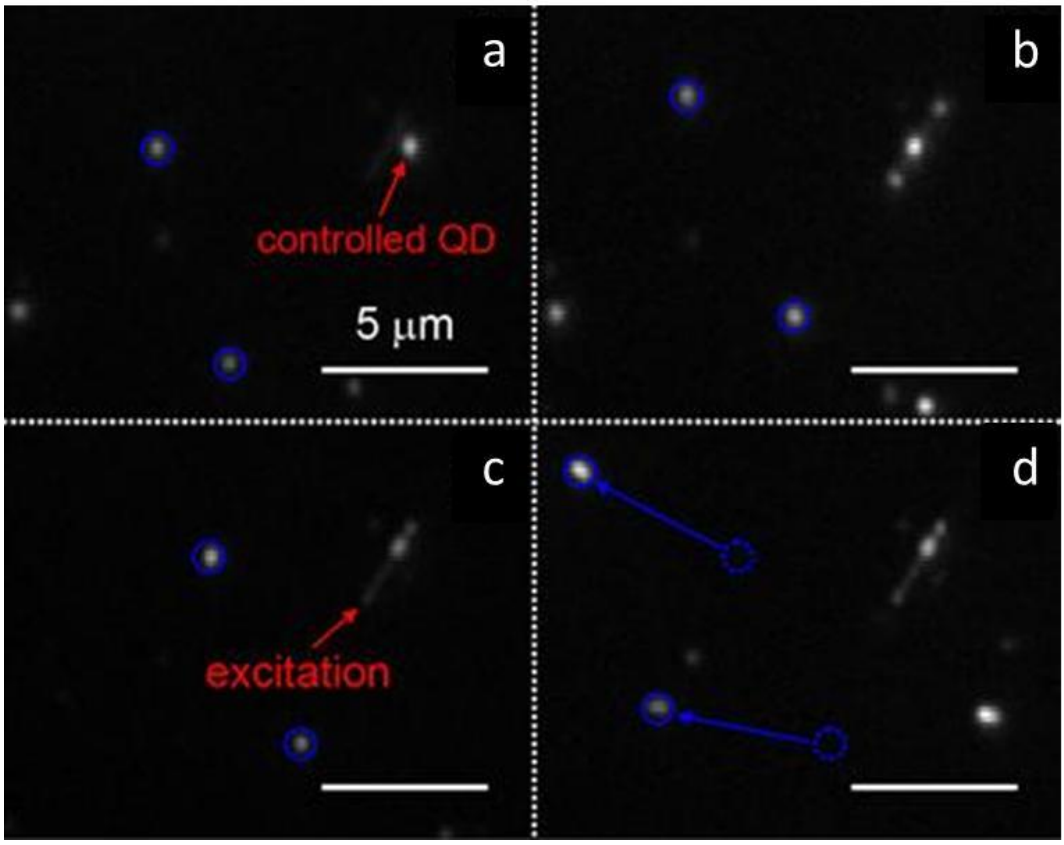

Figure 5.8. Immobilization of a QD on an AgNW. (a) A number of QDs are visible in the EOFC microfluidic system. The control algorithm was used to position the QD nearest the AgNW in this image. Two other QDs are circled in blue for reference. (b) The selected QD

is brought into optical contact with the AgNW using EOFC. Note that the other two QDs have also moved during this process. (c) The selected QD is "spot-welded" to the AgNW using GMAIL. (d) To demonstrate immobilization, the flow in the microfluidic channel is increased. While the immobilized QD remains stationary on the AgNW, the other QDs have moved many micrometers away from their previous positions.

We have also demonstrated the immobilization of two QDs on a single nanowire. The method described in the above section can be used to position and immobilize multiple QDs on a single AgNW. Each time a QD is brought to its desired position on an AgNW, the end of the AgNW is irradiated with ultrafast pulses at 800 nm to perform immobilization using GMAIL. A representative AgNW that has two QDs attached to it separated by a distance of 2.5±0.1 μm is shown in Figure 5.9.

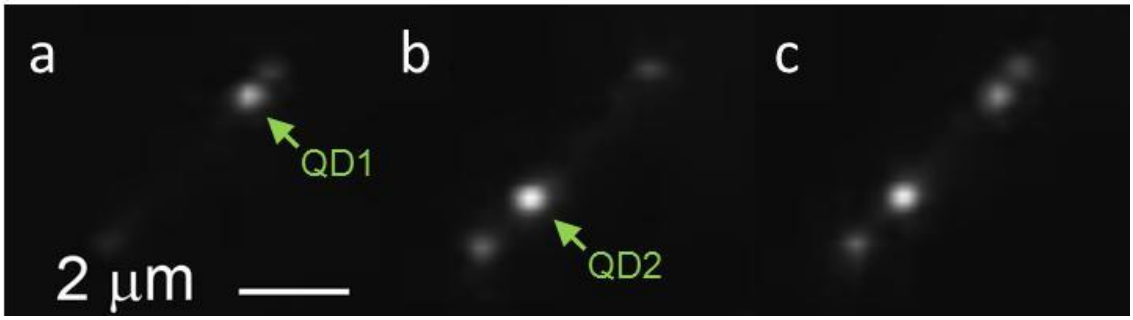

Figure 5.9. Immobilization of two QDs on an AgNW. (a) The upper QD is in a luminescent state and can be seen to be optically coupled to the AgNW; the lower QD is in a dark state at this time. (b) The lower QD is in a luminescent state and can be seen to be optically coupled to the AgNW; the upper QD is in a dark state at this time. (c) Both QDs were in a luminescent state when this image was obtained.

To demonstrate the correlation between the blinking of a QD immobilized on a nanowire and emission from the nanowire ends, we analyzed video of an AgNW with two immobilized QDs (the system shown in Figure 5.9). The two QDs were near opposite ends of the AgNW. As shown in Figure 5.10, the emission from each

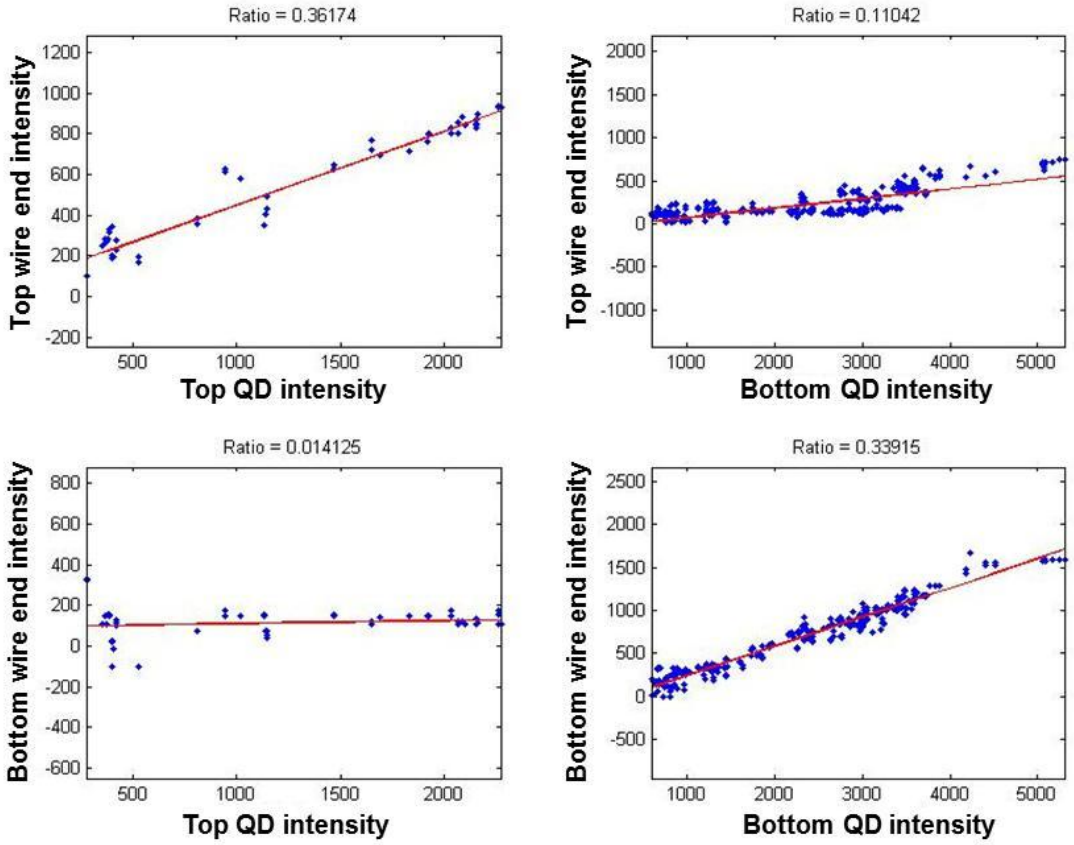

Figure 5.10. Correlation of QD blinking and AgNW end emission. Shown here are plots of the relative emission intensity for each QD and each end of the AgNW shown in Figure 5.9.

end of the nanowire is strongly correlated with (but less intense than) the emission of the QD closest to it. There is also a correlation between the blinking of a QD and emission from the far end of the AgNW, but in this case the emission from the

AgNW is far weaker than the emission from the QD (as is expected based on guiding losses). While we sometimes observed QD emission without observing emission from the more distant end of the AgNW, we never observed AgNW emission that was stronger than the emission of either QD.

5.4 Conclusions

The efficient generation of MAIL at the end of an AgNW allows the nanowire to act as its own far-field to near-field converter. Far-field illumination in the NIR generates broadband visible luminescence at the end of an AgNW. The luminescence is in the near-field of the nanowire, and so can couple into the SPP mode effectively and thereby propagate for many micrometers to the opposite end of the nanowire. The guided luminescence is then emitted at the distal end, where it can drive localized photochemistry. Leakage from the waveguide can also lead to localized photochemistry wherever another nanostructure contacts the AgNW. We have demonstrated the use of this technique for the on-demand, precision fabrication of nanophotonic devices based on AgNWs.

Although our focus here has been on photopolymerization, GMAIL can be used to drive virtually any photochemical or photophysical process without direct laser irradiation of the region of interest. This capability offers great potential for applications such as biological studies involving localized photouncaging or fluorescence excitation, materials imaging, and photolithography. Additionally, because the nanowires act as their own far-field to near-field converters, it is possible

to use this method to couple light efficiently into a large number of nanowire-based devices simultaneously without physically contacting any of them.

References

(1) Sanders, A. W.; Routenberg, D. A.; Wiley, B. J.; Xia, Y.; Dufresne, E. R.; Reed, M. A.: Observation of plasmon propagation, redirection, and fan-out in silver nanowires. *Nano Lett.* **2006**, *6*, 1822-1826.

(2) Nelayah, J.; Gu, J.; Sigle, W.; Koch, C. T.; Pastoriza-Santos, I.; Liz-Marzan, L. M.; van Aken, P. A.: Direct imaging of surface plasmon resonances on single triangular silver nanoprisms at optical wavelength using low-loss EFTEM imaging. *Opt. Lett.* **2009**, *34*, 1003-1005.

(3) Ditlbacher, H.; Hohenau, A.; Wagner, D.; Kreibig, U.; Rogers, M.; Hofer, F.; Aussenegg, F. R.; Krenn, J. R.: Silver nanowires as surface plasmon resonators. *Phys. Rev. Lett.* **2005**, *95*, 257403.

(4) Dickson, R. M.; Lyon, L. A.: Unidirectional plasmon propagation in metallic nanowires. *J. Phys. Chem. B* **2000**, *104*, 6095-6098.

(5) Takahara, J.; Yamagishi, S.; Taki, H.; Morimoto, A.; Kobayashi, T.: Guiding of a one-dimensional optical beam with nanometer diameter. *Opt. Lett.* **1997**, *22*, 475-477.

(6) Brongersma, M. L.; Kik, P. G.: *Surface plasmon nanophotonics*; Springer: Dordrecht, 2007.

(7) Shalaev, V. M.; Kawata, S.: *Nanophotonics with surface plasmons*; Elsevier: Amsterdam, 2007.

(8) Maier, S. A.: *Plasmonics: Fundamentals and applications*; Springer: New York, 2007.

(9) Engheta, N.: Circuits with light at nanoscales: optical nanocircuits

inspired by metamaterials. *Science* **2007**, *317*, 1698-1702.

(10) Fang, Y.; Wei, H.; Hao, F.; Nordlander, P.; Xu, H.: Remote-excitation surface-enhanced Raman scattering using propagating Ag nanowire plasmons. *Nano Lett.* **2009**, *9*, 2049-2053.

(11) Hutchison, J. A.; Centeno, S. P.; Odaka, H.; Fukumura, H.; Hofkens, J.; Uji-i, H.: Subdiffraction limited, remote excitation of surface enhanced Raman scattering. *Nano Lett.* **2009**, *9*, 995-1001.

(12) Knight, M. W.; Grady, N. K.; Bardhan, R.; Hao, F.; Nordlander, P.; Halas, N. J.: Nanoparticle-mediated coupling of light into a nanowire. *Nano Lett.* **2007**, *7*, 2346-2350.

(13) Akimov, A. V.; Mukherjee, A.; Yu, C. L.; Chang, D. E.; Zibrov, A. S.; Hemmer, P. R.; Park, H.; Lukin, M. D.: Generation of single optical plasmons in metallic nanowires coupled to quantum dots. *Nature* **2007**, *450*, 402-406.

(14) Curto, A. G.; Volpe, G.; Taminiau, T. H.; Kreuzer, M. P.; Quidant, R.; van Hulst, N. F.: Unidirectional emission of a quantum dot coupled to a nanoantenna. *Science* **2010**, *329*, 930-933.

(15) Yan, R.; Pausauskie, P.; Huang, J.; Yang, P.: Direct photonic–plasmonic coupling and routing in single nanowires. *Proc. Nat. Acad. Sci. U.S.A.* **2009**, *106*, 21045-21050.

(16) Farrer, R. A.; Butterfield, F. L.; Chen, V. W.; Fourkas, J. T.: Highly efficient multiphoton-absorption-induced luminescence from gold nanoparticles. *Nano Lett.* **2005**, *5*, 1139-1142.

(17) Ropp, C.; Probst, R.; Cummins, Z.; Kumar, R.; Berglund, A. J.;

Raghavan, S. R.; Waks, E.; Shapiro, B.: Manipulating quantum dots to nanometer precision by control of flow. *Nano Lett.* **2010**, *10*, 2525-2530.

(18) Sun, Y. G.; Yin, Y. D.; Mayers, B. T.; Herricks, T.; Xia, Y. N.: Uniform silver nanowires synthesis by reducing $AgNO_3$ with ethylene glycol in the presence of seeds and poly(vinyl pyrrolidone). *Chem. Mater.* **2002**, *14*, 4736-4745.

(19) Baldacchini, T.; LaFratta, C.; Farrer, R. A.; Teich, M. C.; Saleh, B. E. A.; Naughton, M. J.; Fourkas, J. T.: Acrylic-based resin with favorable properties for three-dimensional two-photon polymerization. *J. Appl. Phys.* **2004**, *95*, 6072-6076.

(20) Kojima, K.; Ito, M.; Morishita, H.; Hayashi, N.: A novel water-soluble photoinitiator for the acrylic photopolymerization type resist system. *Chem. Mater.* **1998**, *10*, 3429-3433.

(21) Nah, S.; Li, L.; Liu, R.; Hao, J.; Lee, S. B.; Fourkas, J. T.: Metal-enhanced multiphoton absorption polymerization with gold nanowires. *J. Phys. Chem. C* **2010**, *114*, 7774-7779.

(22) Ropp, C.; Cummins, Z.; Probst, R.; Qin, S.; Fourkas, J. T.; Shapiro, B.; Waks, E.: Positioning and immobilization of individual quantum dots with nanoscale precision. *Nano Lett.* **2010**, *10*, 4673–4679.

(23) Han, Y.; Sun, J.; Ye, H.; Wu, W.; Shi, G.: Nonlinear refraction of silver nanowires from nanosecond to femtosecond laser excitation. *Appl. Phys. B: Lasers and Optics* **2009**, *94*, 233-237.

(24) Schuller, J. A.; Barnard, E. S.; Cai, W.; Jun, Y. C.; White, J. S.; Brongersma, M. L.: Plasmonics for extreme light concentration and manipulation. *Nature Mater.* **2010**, *9*, 193-204.

(25) Muhlschlegel, P.; Eisler, H. J.; Martin, O. J. F.; Hecht, B.; Pohl, D. W.: Resonant optical antennas. *Science* **2005**, *308*, 1607-1609.

(26) Tao, A. R.; Yang, P.: Polarized surface-enhanced Raman spectroscopy on coupled metallic nanowires. *J. Phys. Chem. B* **2005**, *109*, 15687-15690.

(27) Sundaramurthy, A.; Schuck, P. J.; Conley, N. R.; Fromm, D. P.; Kino, G. S.; Moerner, W. E.: Toward nanometer-scale optical photolithography: Utilizing the near-field of bowtie optical nanoantennas. *Nano Lett.* **2006**, *6*, 355-360.

(28) Fang, Y. R.; Li, Z. P.; Huang, Y. Z.; Zhang, S. P.; Nordlander, P.; Halas, N. J.; Xu, H. X.: Branched silver nanowires as controllable plasmon routers. *Nano Lett.* **2010**, *10*, 1950-1954.

(29) Pyayt, A. L.; Wiley, B.; Xia, Y. N.; Chen, A.; Dalton, L.: Integration of photonic and silver nanowire plasmonic waveguides. *Nature Nanotech.* **2008**, *3*, 660-665.

Chapter 6: Nonlinear optical properties of carbon nanostructures

6.1 Introduction

Carbon nanotubes (CNTs) are composed of hexagonal honeycomb carbon lattices and are nearly one-dimensional, with diameters of 0.7 to 3 nm and lengths up to centimetres.[1] Because of the unique geometry, their electronic and optical properties have led to advances in a variety of applications. For example, strong electron-electron interactions of CNTs lead to efficient electron transport ideal for making chemical sensors[2] and field-effect transistors.[3] In addition, optoelectronic devices have been fabricated that exploit the fact that electronic excitation on CNTs can generate optical emission[4-6] and optical excitation on CNTs can generate electrical signals.[7,8]

When a CNT is composed of a single rolled sheet of monolayer graphene,[9] it is known as a single-walled carbon nanotube (SWCNT). When the cylinder shape of a SWCNT is formed, the orientation of the carbon lattice with respect to the CNT axis influences the optical and electrical properties.[1] Each carbon lattice point (n,m) is commonly indexed from a graphene sheet using unit vectors, a_1 and a_2, as shown in Figure 6.1. For example, the roll-up vector is pointing at lattice index (1,3) in this figure.

CNTs are semiconducting or metallic depending on the lattice point (n,m) in contact with the (0,0) point after rolling.[9] When the carbon n and m lattice indices satisfy the condition of $n - m = 3j$, where $j=0, 1, 2, 3\ldots$, CNTs adapt an armchair or

zigzag configuration and are metallic, as shown by the grey arrows in Figure 6.1.[9] When the n and m carbon lattices of the CNTs satisfy n – m ≠ 3j, where j=1, 2, 3…, the CNTs are semiconducting and are referred to as chiral nanotubes.[9] The chiral angle (θ) (Figure 6.1) is the angle between the arm chair and the zigzag axis, and ranges between 0 and 30 °. The chiral angle can also be used to assign the CNTs as semiconducting or metallic.[9] For example, CNTs are metallic if the chiral angle equals to 0 or 30 °.

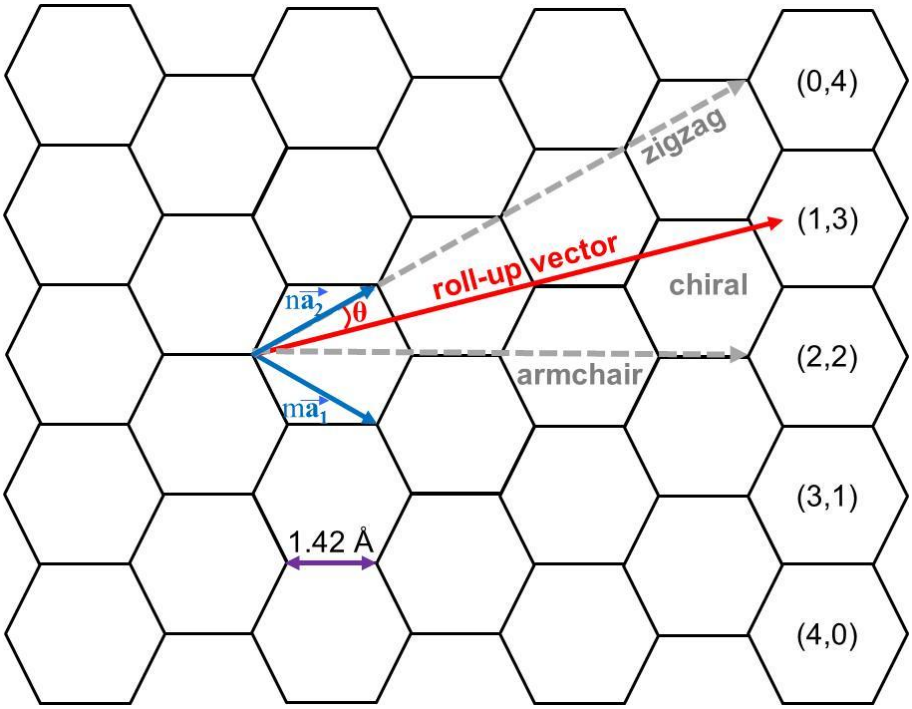

Figure 6.1. A graphene sheet with carbon lattices indexed with unit vectors, a_1 and a_2. When the sheet is rolled up from (0,0) to (n,m), the CNT lattice forms shapes such as zigzag, armchair, and chiral. The zigzag and armchair types of CNTs are metallic, otherwise CNTs are semiconducting.

The optical properties of CNTs are typically studied using semiconducting CNTs because metallic CNTs are not luminescent or show very weak emission.[9] When light excites semiconducting CNTs, optical signals such as absorption and luminescence emission can be detected in different regions of the spectrum due to their different interband transition mechanisms. The interband transition mechanisms of electrons are different depending on the diameters of the CNTs. For example, as the diameter of the semiconducting CNT becomes smaller, the band gap, which involves the states responsible for the transition, increases.[10] An increase in band gap leads to generation of optical signals at shorter wavelengths.

There are several challenges inherent to study the optical properties of CNTs because synthesis tends to form bundled structures owing to the van der Waals forces involved.[11] The optical signals of CNTs are dramatically quenched when the CNTs are aggregated by bundling.[10] In addition, it is difficult to separate CNTs with different diameters, leading to a size dispersion in solution.

Despite the expected difficulties of optical detection, absorption and photoluminescence have been observed from SWCNTs.[9,10,12-14] These transitions arise because SWCNTs have a series of electron-confined maxima in their density of states, called van Hove singularities (VHS).[10] Figure 6.2 shows a schematic of the density of electronic states for a SWCNT. The sharp VHS energies are mainly dependent upon the diameters of the SWCNTs.[10] The interband transition of the optical absorption E_{22} (V_2 to C_2) and luminescence emission E_{11} (C_1 to V_1) in SWCNTs is illustrated with solid arrows in the Figure 6.2.[9] The dashed arrows

indicate the nonradiative relaxation of the excited electron (in the conduction band) and hole (in the valence band).[9]

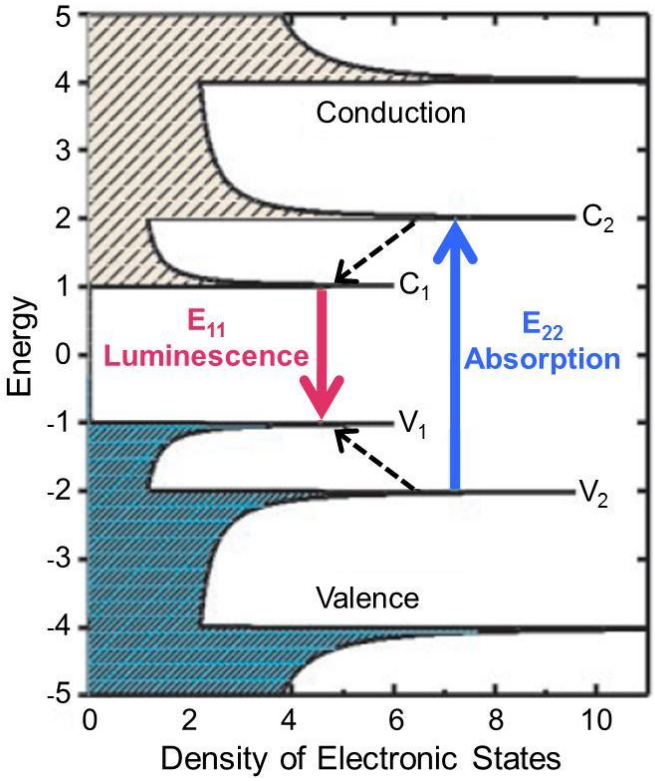

Figure 6.2. Schematic for the density of electronic states of a single CNT. The solid blue line indicates the absorption process from V_2 in the valence band to C_2 in the conduction band. The solid red line indicates the luminescence process from C1 to V1 after the excited electrons relax to the lower electronic level (reproduced from reference [9]).

An absorption spectrum obtained by O'Connell and coworkers includes a series of interband transitions from SWCNTs that were prepared with a surfactant-coating to prevent CNT aggregation.[10] The absorption from semiconducting CNTs was detected from 550 to 1600 nm, and the metallic CNTs absorbed between ~400

and 600 nm.[10] Photoluminescence of the surfactant-coated SWCNTs was observed at similar spectral ranges to the absorbance using excitation wavelengths from 300 nm to 930 nm.[10] The discrete peaks observed in the luminescence from each CNT appeared at different energies because each CNT has a different diameter, and thus different interband transition energy.[9] CNTs with 33 different carbon lattice indices were identified using luminescence spectral analysis.[9]

Luminescence from SWCNTs was also observed with near-infrared (NIR) excitation by nonlinear absorption process.[12,14,15] For example, a surfactant-coated SWCNT solution was excited with NIR light ranging from 1210 to 1970 nm, and two-photon absorption-induced luminescence was observed from 850 to 1070 nm.[12] As in the case of luminescence induced by single-photon absorption, the discrete luminescence peaks induced by the nonlinear absorption process appear at different wavelengths depending upon the diameters of the CNTs.[12] Nonlinear luminescence at similar wavelengths was measured from dried SWCNTs on a polymer matrix with visible-NIR excitation ranging from 620 to 1033 nm.[14]

The range of the broadband luminescence observed when excited electrons relax to holes from a series of exciton states is determined by the exciton binding energy, i.e., the Coulomb interaction between excited electron and hole.[12,14] Because the exciton binding energy is dependent on the SWCNT diameter, as the diameter is decreased, luminescence observed at shorter wavelengths is due to the increased exciton binding energy.[12,14] In addition to the Coulomb interaction, which is enhanced at smaller diameters, excitonic effects can be strongly increased by decreased dielectric screening.[14] Because of the one-dimensional geometry of

SWCNTs, the electric field lines of excited electron/hole pairs travel largely outside of the SWCNT.[14]

Multiwalled carbon nanotubes (MWCNTs) are composed of two or more layers of rolled graphene sheets forming concentric tubes. MWCNTs are coupled by van der Waals interactions.[16] When a semiconducting CNT is located within a metallic CNT, the semiconducting CNT is assumed to exhibit nonradiative decay of excitations through the fast relaxation in vibrational manifolds[17] of adjacent metallic CNTs.[16] In this case, the nonradiative decay between the energy states exceeds the rates of radiative emission. In addition, the outermost CNT, which has a small band gap due to the large diameter, is not expected to show luminescence due to vibrational relaxation reducing the optical emission.[16]

However, luminescence from a MWCNT solution has been observed with NIR excitation by a multiphoton absorption process.[16] A solution of polymer-coated MWCNTs was excited by 1064 nm light, and the observed luminescence ranged from the visible to NIR regions of the spectrum.[16] When the NIR light excites the MWCNTs, it is possible for three photons to be absorbed due to presence of the VHS, promoting electrons to the excited state[16]. When the electrons relax to lower-energy excited states, they can experience the high density of states again.[16] In this case, the probability of radiative relaxation becomes much larger than that of nonradiative decay, which is induced by the coupling of multiple CNTs and the small band gap.[16,18,19] As a result, luminescence can be observed. This mechanism, along with the Coulomb interaction between the excited electron and hole, was proposed for luminescence observed from CNTs.

To date, photoluminescence from single CNTs has been observed from purified CNT solutions[9,10,12] and from randomly dispersed SWCNTs on a polymer substrate.[14] In case of MWCNT solutions, the surfactant-coating method has so far achieved a purity of 91 % of single MWCNTs.[20] The consequent optical signals from the solution still contain spectral features from aggregated MWCNTs. Here we present the observation of luminescence from single MWCNTs following the nonlinear absorption of NIR light. Luminescence-driven polymerization of MWCNTs is also demonstrated. The nonlinear optical signals and polymerization of SWCNTs are also presented. In addition, the nonlinear optical properties of layered graphene sheets are also studied. Current-induced luminescence has been observed previously in these materials.[6]

6.2 Experimental section

Each aqueous solution of carbon nanostructures (2 μL) was dried on a glass coverslip at room temperature. The glass coverslip was functionalized with an acrylate solution to promote the adhesion of polymer structures. On the acrylate-modified glass coverslip, 6 × 6 grid polymer patterns were fabricated by multiphoton absorption polymerization (MAP) to facilitate of imaging the carbon nanostructures with SEM. The methods for the surface-functionalization of the glass coverslips and fabrication of polymer patterns were described in the experimental section in Chapter 2. To observe MAIL from each nanostructure, the methods of the sample preparation and optical measurement were performed as described in Chapter 2 as well.

For MAIL experiments, one drop of immersion oil was placed on the dried carbon nanostructures in order to satisfy the refractive index-matching condition of the objective. This condition minimized the scattering from the sample surfaces. As the NIR light was scanned over the nanostructures, the consequent MAIL excitation image was simultaneously observed using a single-photon-counting avalanche photodiode. MAIL emission spectra were also collected through an optical fiber (BFB-455-7, Princeton Instruments) and detected using a spectrometer (Acton SP2300i, Princeton Instruments) connected to a computer. After excitation, the sample was rinsed in hexane for 3 min and in ethanol for 5 min to remove the oil residue and then was dried at room temperature.

To investigate luminescence-induced polymerization, dried carbon nanostructures on an acrylate-functionalized glass coverslip were covered with one drop of an acrylate prepolymer resin. The resin was composed of 40 wt% ethoxylated-15 trimethylolpropane triacrylate (SR 9035, Sartomer), 59 wt% deionized water, and 1 wt% of a photoinitiator, sodium 4-[2-(4-Morpholino) benzoyl-2-dimethylamino] butylbenzenesulfonate (MBS, Sundia MediTech Company Ltd.). After raster scanning the NIR light over the nanostructures, the sample was rinsed in ethanol for 3 min twice to remove any unpolymerized resin. The sample was dried at room temperature, and then was sputter-coated with 10 nm Pt/Pd for SEM imaging.

6.3 Results and discussion

6.3.1 Nonlinear luminescence and polymerization of single MWCNTs

Single MWCNTs first were found by CCD camera imaging through a 100×, oil-immersion objective. Ultrafast NIR light was focused on each single MWCNT and scanned over the entire MWCNT for 3 s using scanning mirrors. The resulting MAIL signals were averaged three times. A typical MAIL contour plot from a MWCNT is shown in Figure 6.3. As 0.52 mW (measured at the sample stage) of 890 nm light scanned the 2.55 μm-long MWCNT, luminescence was simultaneously observed from the entire length of the MWCNT.

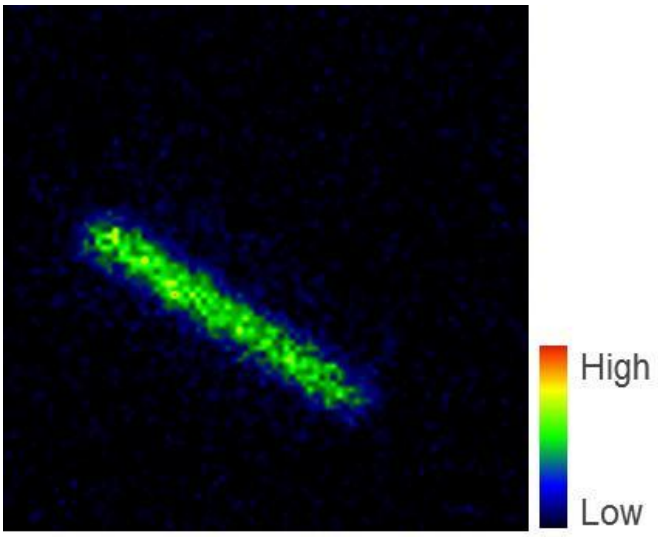

Figure 6.3. MAIL excitation image of a MWCNT with 890 nm light. The luminescence is observed from the entire length of the single MWCNT.

The bright, reproducible luminescence was then used to drive polymerization using single MWCNTs in a prepolymer resin. About 2 μL of a MWCNT solution was dried on a glass coverslip and covered with the water-soluble acrylate

prepolymer resin. As 890 nm light was scanned over a 1.65 µm-long MWCNT, MAIL was simultaneously observed from the entire length of the CNT as shown in Figure 6.4a. After the MAIL observation, a corresponding SEM image was obtained

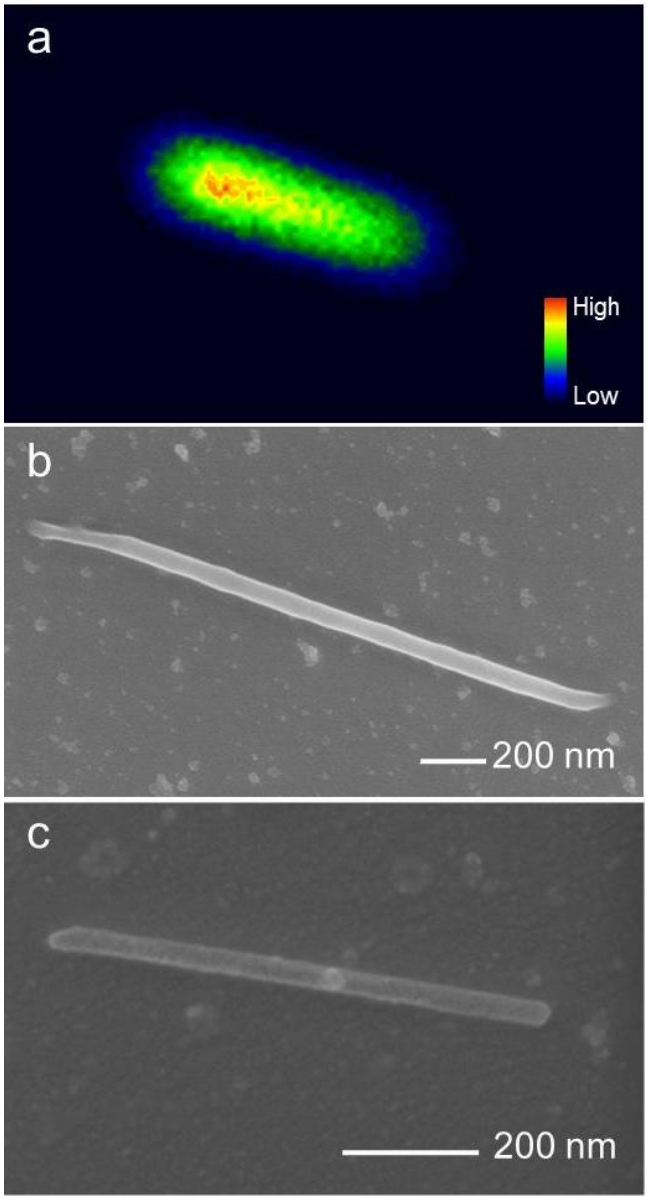

Figure 6.4. (a) MAIL excitation image of a MWCNT. MWCNTs were prepared in a prepolymer resin and excited with 890 nm light. (b) SEM image of the MWCNT from (a). (c) SEM image of a MWCNT that was not excited.

for the same CNT. As shown in the SEM image in Figure 6.4b, the entire CNT was covered with a thin polymer coating. Two ends of the MWCNT became elongated compared to the control MWCNT, which was not excited (Figure 6.4c). Polymerization was observed from all single MWCNTs scanned with NIR light at both 800 and 890 nm.

When one end of a 3.12 µm-long MWCNT was irradiated with 890 nm light, luminescence was simultaneously observed from the excited area. The MAIL intensity shown in Figure 6.5a was approximately equal to that obtained from

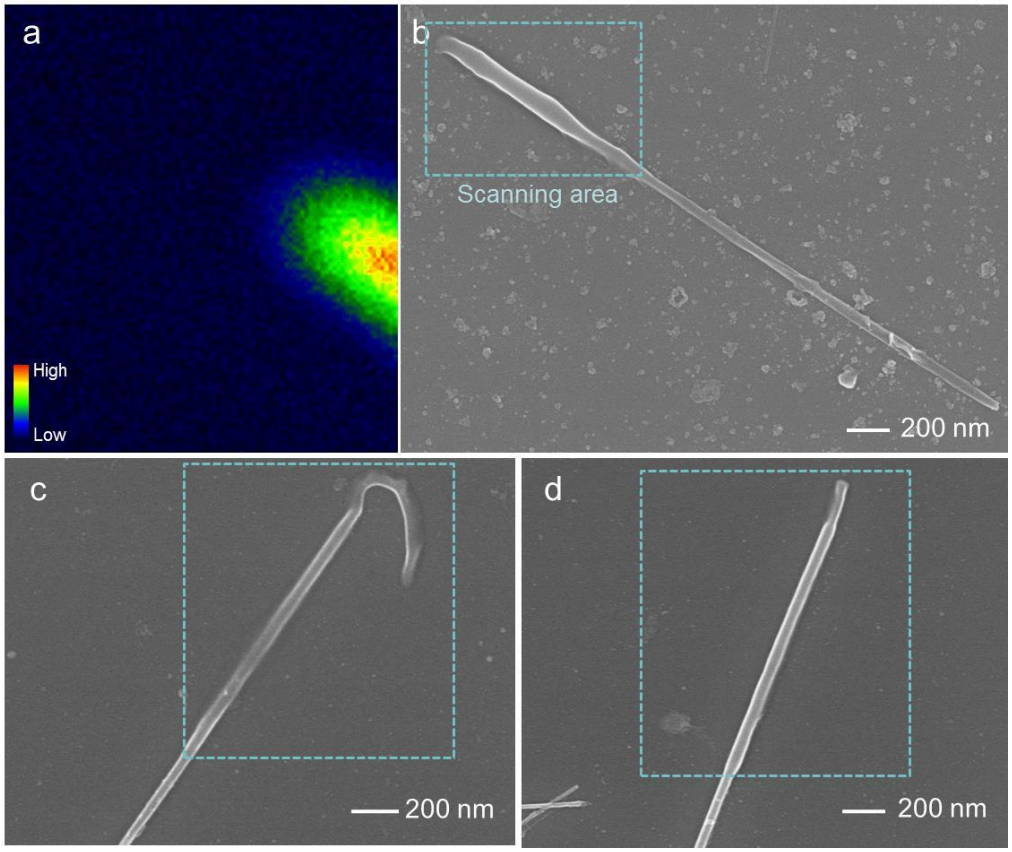

Figure 6.5. (a) MAIL excitation image from one end of a MWCNT scanned with 890 nm. (b) SEM image of the corresponding MWCNT. (c), (d) SEM images of a MWCNT irradiated on one end.

irradiating the entire MWCNT. A corresponding SEM image obtained for the same CNT is shown in Figure 6.5b. The area of the CNT in which bright luminescence was observed was covered with polymer. The polymer was thickest in the scanning region. This phenomenon was observable on several MWCNTs that were partially illuminated. Interestingly, inner CNTs protruding from the ends were also polymerized as they were scanned (Figure 6.5c and 6.5d). This result implies that MAIL leads to polymerization on single MWCNTs, although it is not clear if the protruding inner CNTs produce significant luminescence intensity which can cause polymerization.

To study the polymerization mechanism of MWCNTs, luminescence emission spectra were measured from single MWCNTs with 60 s exposure of 800 nm light. The linear absorption spectrum of the photoinitiator, MBS, was measured using a UV/visible spectrometer. The black solid line in Figure 6.6 shows the smoothed (10-point) MAIL spectrum measured from a MWCNT.

The linear absorption band of MBS is shown in green in Figure 6.6. The MAIL emission ranges from 500 to 690 nm, although emission from 690 nm to the NIR region is attenuated due to three shortpass filters used to remove residual 800 nm light. It should also be noted that the spectrum from 690 to 720 nm was observed from a glass surface without MWCNTs as well. The MAIL spectrum we observed was the same as that measured from a MWCNT solution reported previously.[16]

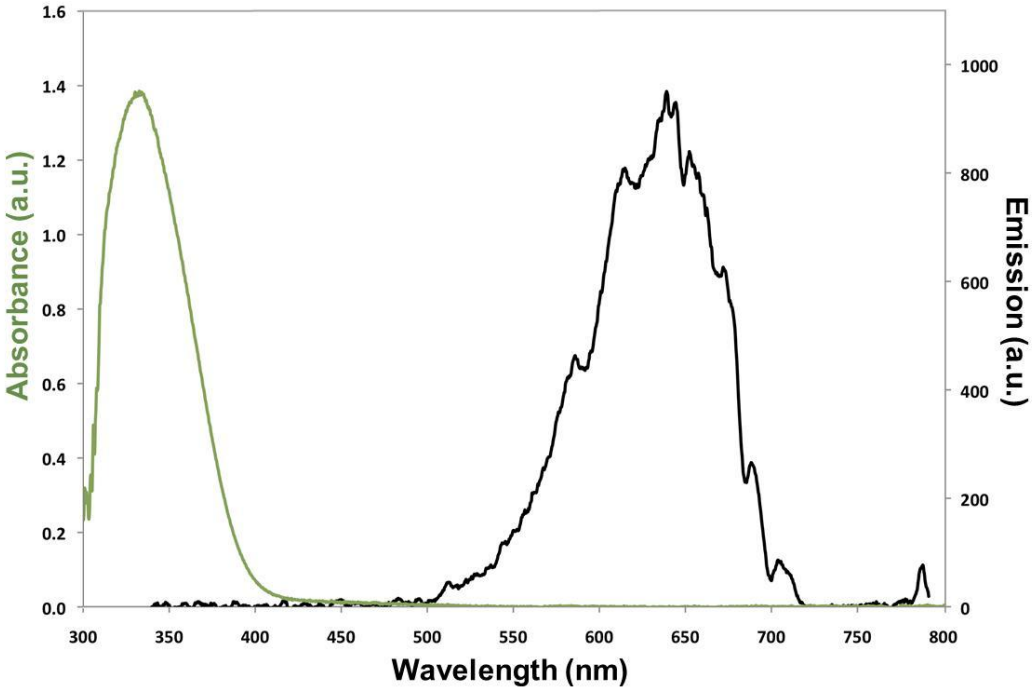

Figure 6.6. Absorption spectrum of MBS (green) and a typical MAIL excitation spectrum from a MWCNT (black).

As seen in Figure 6.6, the MAIL spectral region overlaps slightly with the linear absorption band of MBS at wavelengths around 480 nm. Although the MAIL intensity and the absorption cross section of MBS are weak in this spectral region, the MAIL-driven excitation of the MBS can occur with efficiency capable of inducing polymerization. Consequently, the raster scanning of NIR excitation caused the polymerization only at the MWCNT surfaces where MAIL signals were observed as seen from the previous figures. To study the MAIL-associated polymerization mechanism in greater detail, we used the same prepolymer resin without MBS.

Figure 6.7a shows a MAIL image from 890 nm excitation observed from a MWCNT immersed in the prepolymer resin without MBS. A corresponding SEM image measured from the same MWCNT is shown in Figure 6.7b. The MWCNT in

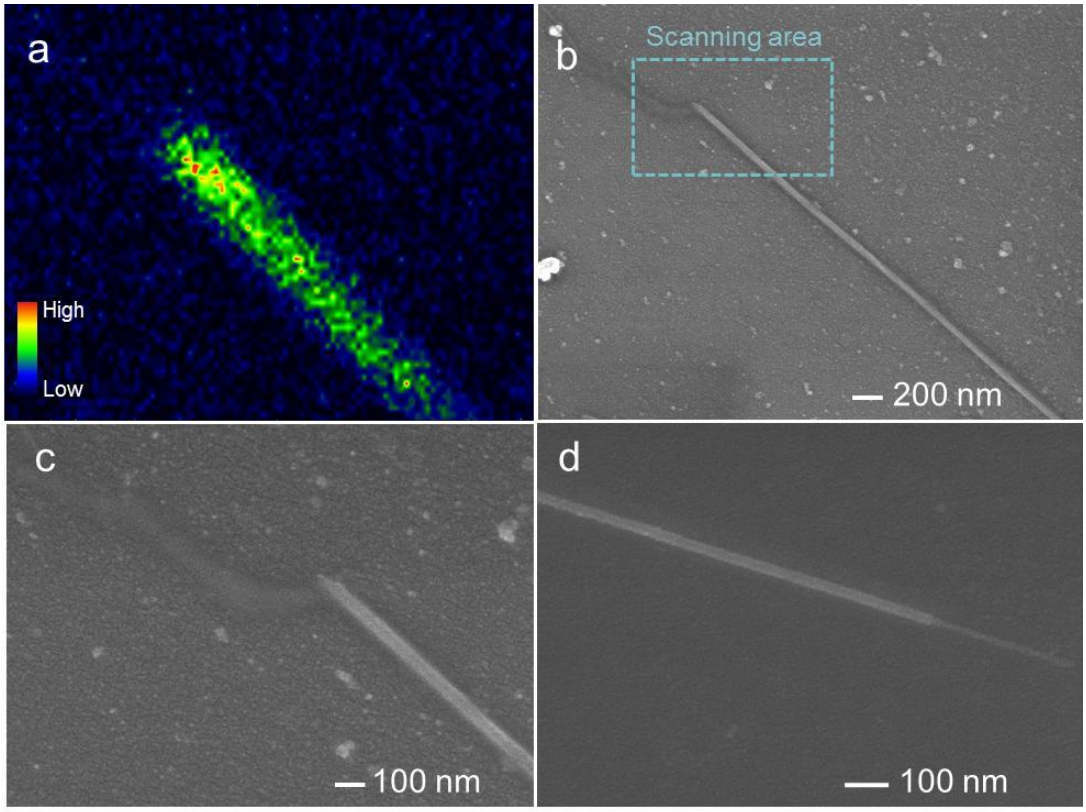

Figure 6.7. (a) MAIL excitation image from one end of a MWCNT using 890 nm excitation. The MWCNT sample was prepared in a prepolymer resin without MBS. (b) SEM image of the corresponding MWCNT. The blue-dashed square indicates the area excited with 890 nm light. (c) Close-up SEM image of one end of the MWCNT. (d) SEM image of a typical MWCNT. CNT with a smaller diameters is apparent on the right hand side of the MWCNT.

the SEM image did not show any surface difference, as opposed to the case of MWCNTs immersed in a prepolymer resin including MBS. The thickness of the entire nanotube is the same, and a close-up SEM image in Figure 6.7c shows no polymer features. One MWCNT end shows a thin nanostructure in a dark color. This structure could be inner CNTs that were bent due to the light excitation because the inner CNTs can be found in control MWCNTs that were not excited, as shown in

Figure 6.7d. It should be noted that polymerization of MWCNTs was not observed with CW excitation at 405 nm, 532 nm, 800 nm, and 890 nm without MBS in the resin. In addition, MAIL from MWCNTs was not observed using CW excitation at any wavelength.

In order to study the coupling between aggregated MWCNTs, several regions in which two MWCNTs crossed were illuminated in the presence of the prepolymer solution. Polymerization was observed at the crossed MWCNTs when 890 and 800 nm light was used. Figure 6.8a shows an SEM image of the polymerization at the junction of two single MWCNTs following 890 nm excitation. The close-up SEM image in Figure 6.8b clearly shows the polymer features fabricated between two CNTs. Excitation at 800 nm also induced polymerization between two MWCNTs as seen in Figure 6.8c, and the two MWCNTs are linked together by this process (Figure 6.8d). Because the polymer features can be strongly adhered on the acrylate-functionalized coverslip, sonication can remove all MWCNTs except the polymerized ones. By this method, fabrication of MWCNT patterns on a substrate can be performed in a controlled manner once a desired configuration is observed.

In the case of crossed MWCNTs in a resin without the MBS, Figure 6.9a and 6.9b show SEM images measured after 890 nm excitation at the junction. Although the same intensities and exposure time of NIR excitation as those for the results in Figure 6.8 were used, no polymer features were created at the contact area of two CNTs, and no changes in the thickness of the CNTs were observed.

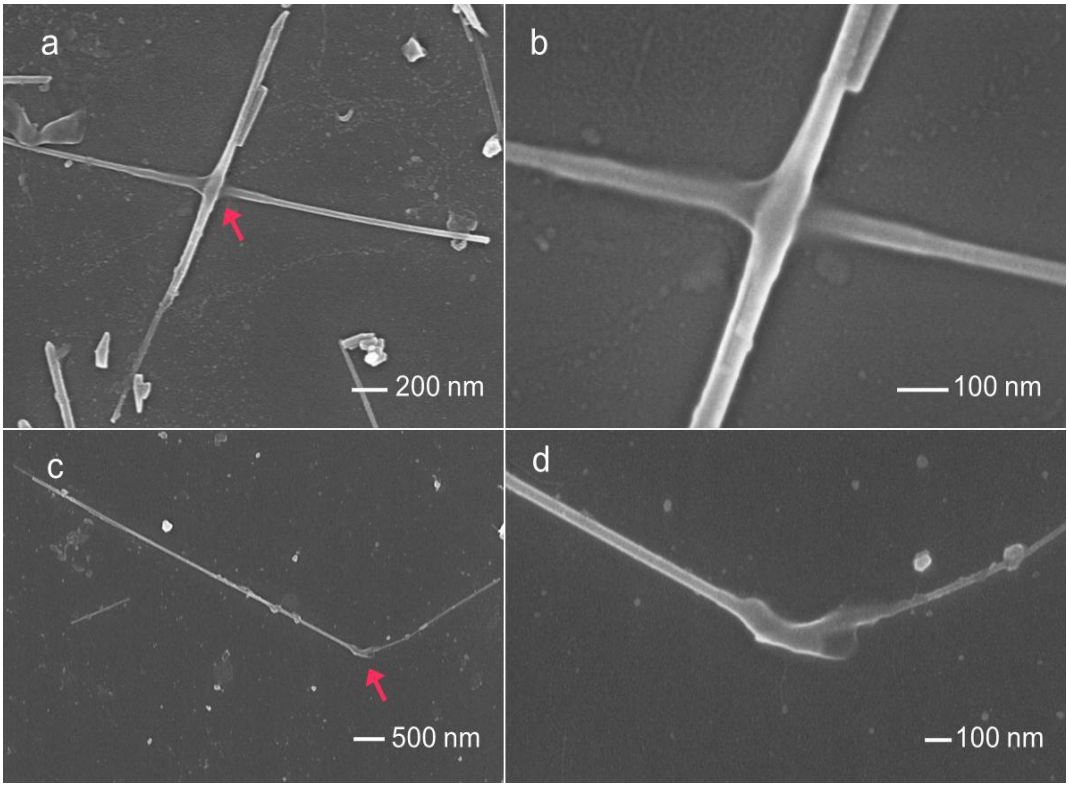

Figure 6.8. (a) SEM image of crossed MWCNTs that were excited with 890 nm light. The MWCNTs were prepared in a prepolymer resin. (b) Close-up SEM image of the crossed MWCNTs of (a). (c) SEM image of crossed MWCNTs that were excited with 800 nm light. (d) Close-up SEM image of the corresponding crossed MWCNTs.

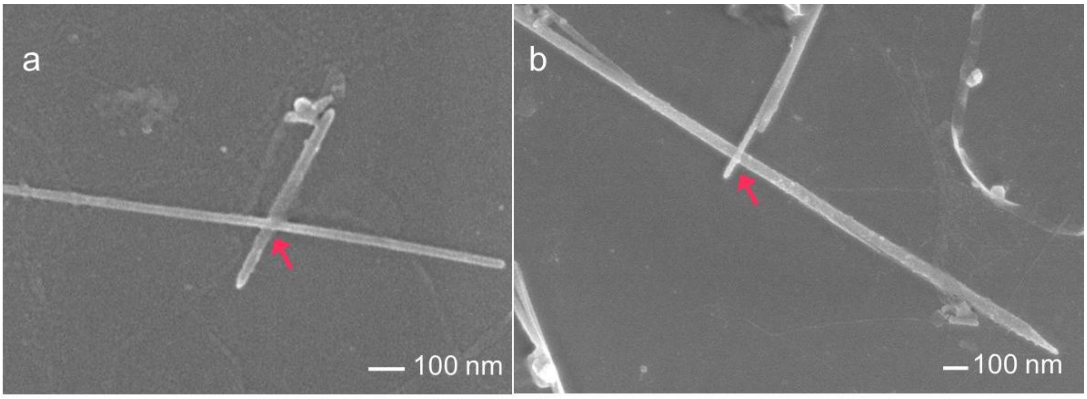

Figure 6.9. (a) SEM image of two MWCNTs crossed and excited at 890 nm light. The MWCNTs were prepared in a prepolymer resin without MBS. (b) SEM image of crossed

MWCNTs excited at 890 nm light. The red arrows indicate the area where the laser beam excited.

We have clearly observed nonlinear-absorption-induced luminescence from single MWCNTs. In the presence of a prepolymer resin, the luminescence excited the photoinitiator, MBS, and induced polymerization. To study the mechanism of the MAIL-driven polymerization in greater detail, single MWCNTs with different diameters and double-walled CNTs need to be employed. It has been noted that the MAIL spectra from each MWCNT can be different due to the diameter-dependent band gap, and the spectral overlap between the MAIL and the absorption band of MBS can be tuned.

6.3.2 Nonlinear luminescence and polymerization of SWCNTs

To study the nonlinear optical properties of SWCNTs, 2 μL a SWCNT aqueous solution was dried on a polymer-patterned glass coverslip at room temperature. Because SWCNTs are typically less than 3 nm in diameter, singe SWCNTs cannot be observed by optical imaging with the 100×, oil-immersion objective. Instead, we scanned 36 to 64 μm^2 areas with 800 nm excitation and used a single-photon-counting avalanche photodiode to observe luminescence signals from the SWCNTs.

Figure 6.10 shows typical luminescence images observed from SWCNTs with 2 mW of 800 nm excitation. The MAIL signals measured from the SWCNTs

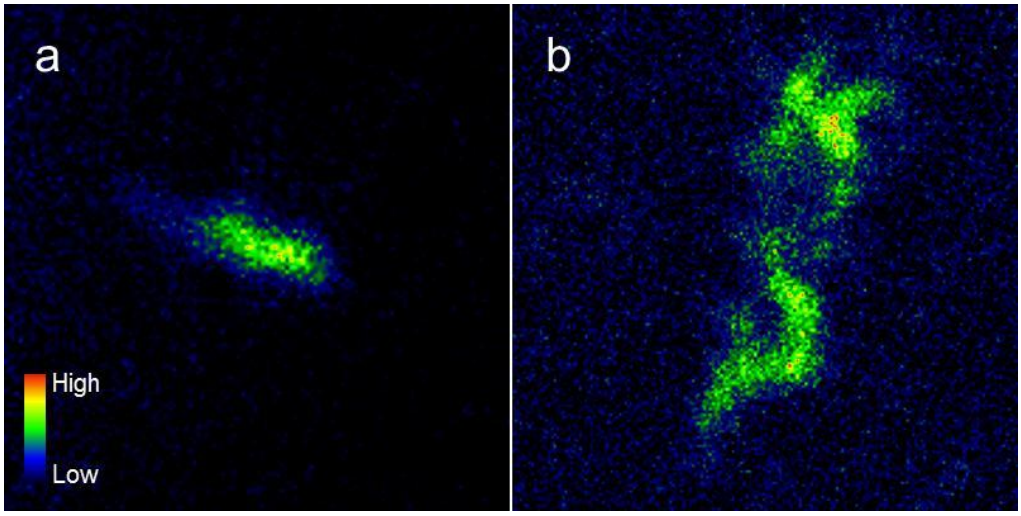

Figure 6.10. (a) MAIL excitation image of SWCNTs with 800 nm excitation. (b) MAIL excitation image of more aggregated SWCNTs than that of (a).

indicates that semiconducting SWCNTs were present. Due to the small diameters of the SWCNTs, the correlation between the luminescence patterns and orientations of SWCNTs was not clear. In addition, because of the limitation of the SEM resolution, the SWCNTs shown in SEM images could be either single SWCNTs or SWCNT bundles. While nonlinear absorption of NIR light resulted in MAIL emission from the SWCNTs, luminescence was not observed from the SWCNTs with CW NIR excitation.

In the presence of a prepolymer resin, SWCNT bundles were polymerized under an exposure of 2 mW of 800 nm light. As the light excited the CNTs, thick polymer features were created at the surfaces of the SWCNTs, as seen in Figure 6.11a. When aggregated SWCNTs were excited, thicker polymers were observed than in the case of single or smaller CNT bundles, as shown in Figure 6.11b. Figures 6.11c and 6.11d show SEM images of control SWCNTs that were not exposed to the light.

The polymerization of SWCNTs can be used to fabricate CNT patterns with nanometer-scale precision. When a monolayer of SWCNTs on a glass coverslip is prepared by spin-coating and excited with NIR light by a tightly focused beam, we can create thin polymers around the SWCNTs. Since the polymer-covered SWCNT bundles can remain on an acrylate-functionalized coverslip after sonication, we can selectively produce polymerized-SWCNTs on transparent substrates in desired patterns.

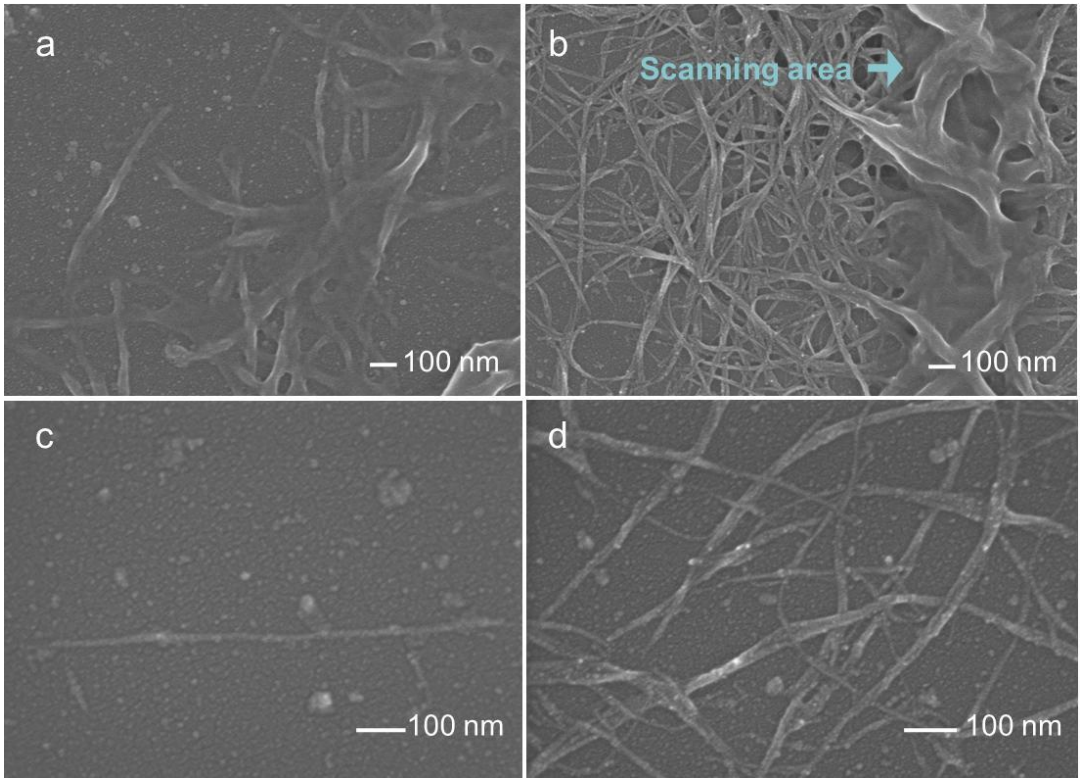

Figure 6.11. (a) SEM image of SWCNTs that were excited at 800 nm light. The SWCNTs were prepared in a prepolymer resin. (b) SEM image of SWCNTs that are more aggregated than in (a). The blue arrow indicates the areas exposed by 800 nm light. (c) SEM image of pristine SWCNTs. The CNTs were not exposed to the 800 nm light. (d) SEM image of other example of pristine SWCNTs.

6.3.3 Nonlinear luminescence and polymerization of graphene

To study the nonlinear optical properties of multiple sheets of graphene, 2 µL of a graphene aqueous solution was dried on a polymer-patterned glass coverslip. One drop of a prepolymer resin was placed on the top of the graphene. The layered sheets of graphene were easily observed using a CCD camera by imaging through a 100×, oil-immersion objective.

Figure 6.12a shows typical MAIL signals from graphene irradiated with 2 mW of 800 nm light. The corresponding SEM image is shown in Figure 6.12b. The four graphene structures shown in the SEM image were luminescent, although their size was not directly correlated to the MAIL intensities. When light excited the graphene, the geometry of the surfaces became smooth due to the creation of polymer films, as seen in Figure 6.13a and 6.13b. The surfaces of the unexposed graphene sheets retain a rough surface and show sharp edges (Figure 6.13c and 6.13d).

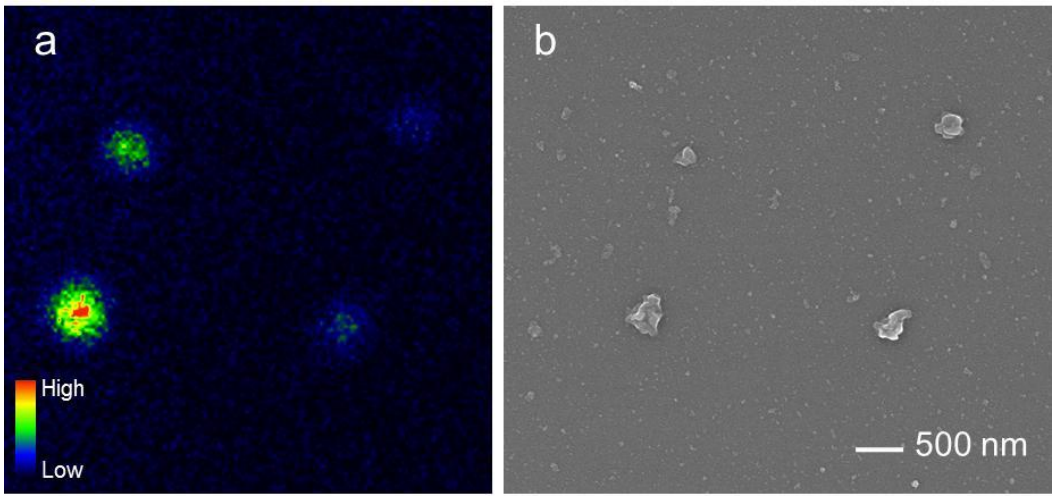

Figure 6.12. (a) MAIL excitation image of four layered graphene sheets excited at 800 nm. The graphene sheets were prepared in a prepolymer resin. (b) SEM image of the corresponding layered graphene sheets.

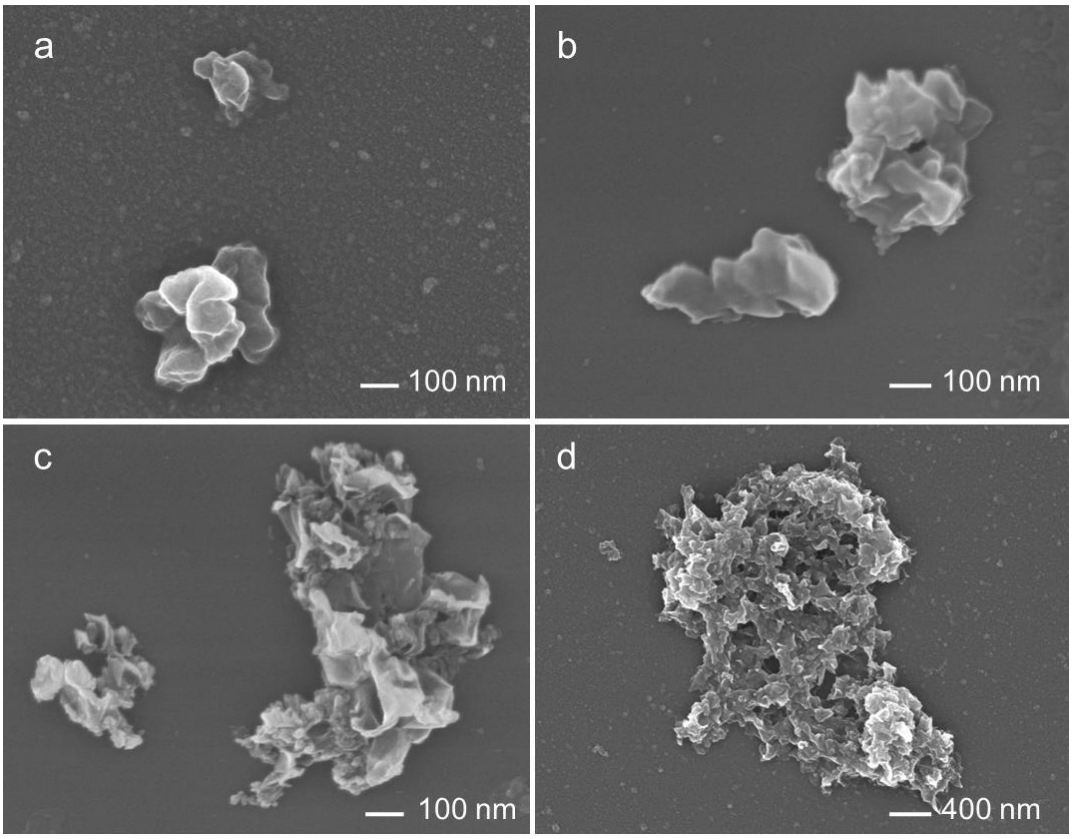

Figure 6.13. (a), (b) SEM images of layered graphene sheets that were prepared in a prepolymer resin and excited at 800 nm light. (c), (d) SEM images of pristine graphene sheets.

Interestingly, not all graphene sheets exhibited luminescence during irradiation. For example, the MAIL intensities shown in Figure 6.14a were measured from graphene sheets with 2 mW of 890 nm excitation. Although the corresponding SEM image in Figure 6.14b indicated that three graphene sheets were present within the scanning area, only two of them displayed luminescence. As seen from the close-up SEM image in Figure 6.14c, the luminescent graphene sheets were covered with thin polymer films while the non-luminescent sheets exhibited the rough geometry of

the unpolymerized surface. This result demonstrated the strong correlation between MAIL and polymerization of graphenes.

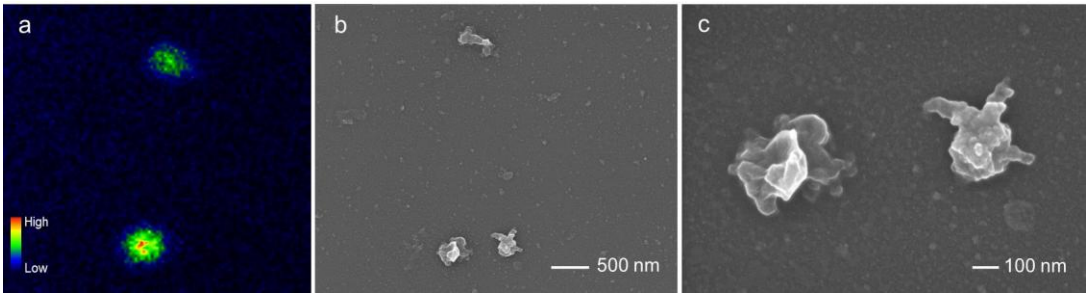

Figure 6.14. (a) MAIL excitation image of layered graphene sheets excited with 890 nm light. (b) SEM image of the corresponding graphene sheets. (c) Close-up SEM image of the two graphene sheets shown at the bottom of (b).

The nonlinear luminescence from the layered graphene sheets showed bright intensity that was able to induce polymerization. This optical property can be studied using double layers of graphene sheets, which can also be compared to the optical behavior of SWCNTs, because a SWCNT is a cylindrical form of one sheet of graphene.

6.4 Conclusions

We studied nonlinear optical properties of carbon nanostructures. By exciting single MWCNTs with NIR light, luminescence was observed from the scanned areas. In the presence of a prepolymer resin, MAIL led to the excitation of a photoinitiator, inducing polymerization. We showed that CW NIR excitation was not sufficient to

induce luminescence, and no polymerization was observed from the MWCNTs. We also examined polymerization in the absence of photoinitiator, and no polymerization was observed under pulsed or CW irradiation on the MWCNTs. These results indicated that MAIL excitation of the photoinitiator from the CNTs is the dominant source for the polymerization, not direct absorption of the NIR by the photoinitiator.

MAIL and its correlation to the polymerization were studied using SWCNTs and graphene sheets. Although the investigation of MAIL from single SWCNTs was difficult due to the small diameters of the structures, MAIL and the consequent polymerization were observed from SWCNT bundles using NIR excitation. MAIL from multiple sheets of graphenes was also detected, and its consequent polymer films were observed on the surfaces of the graphene sheets. The correlation between MAIL intensity and polymerization indicated that MAIL from the carbon nanomaterials was the dominant force to induce polymerization.

References

(1) Avouris, P.; Freitag, M.; Perebeinos, V.: Carbon-nanotube photonics and optoelectronics. *Nature Photon.* **2008**, *2*, 341-350.

(2) Snow, E. S.; Perkins, F. K.; Houser, E. J.; Badescu, S. C.; Reinecke, T. L.: Chemical detection with a single-walled carbon nanotube capacitor. *Science* **2005**, *307*, 1942-1945.

(3) Avouris, P.; Chen, Z.; Perebeinos, V.: Carbon-based electronics. *Nature Nanotech.* **2007**, *2*, 605-615.

(4) Misewich, J. A.; Martel, R.; Avouris, P.; Tsang, J. C.; Heinze, S.; Tersoff, J.: Electrically induced optical emission from a carbon nanotube FET. *Science* **2003**, *300*, 783-786.

(5) Chen, J.; Perebeinos, V.; Freitag, M.; Tsang, J.; Fu, Q.; Liu, J.; Avouris, P.: Bright infrared emission from electrically induced excitons in carbon nanotubes. *Science* **2005**, *310*, 1171-1174.

(6) Essig, S.; Marquardt, C. W.; Vijayaraghavan, A.; Ganzhorn, M.; Dehm, S.; Hennrich, F.; Ou, F.; Green, A. A.; Sciascia, C.; Bonaccorso, F.; Bohnen, K. P.; von Loehneysen, H.; Kappes, M. M.; Ajayan, P. M.; Hersam, M. C.; Ferrari, A. C.; Krupke, R.: Phonon-assisted electroluminescence from metallic carbon nanotubes and graphene. *Nano Lett.* **2010**, *10*, 1589-1594.

(7) Freitag, M.; Martin, Y.; Misewich, J. A.; Martel, R.; Avouris, P. H.: Photoconductivity of single carbon nanotubes. *Nano Lett.* **2003**, *3*, 1067-1071.

(8) Qiu, X. H.; Freitag, M.; Perebeinos, V.; Avouris, P.: Photoconductivity spectra of single-carbon nanotubes: Implications on the nature of their excited states.

Nano Lett. **2005**, *5*, 749-752.

(9) Bachilo, S. M.; Strano, M. S.; Kittrell, C.; Hauge, R. H.; Smalley, R. E.; Weisman, R. B.: Structure-assigned optical spectra of single-walled carbon nanotubes. *Science* **2002**, *298*, 2361-2366.

(10) O'Connell, M. J.; Bachilo, S. M.; Huffman, C. B.; Moore, V. C.; Strano, M. S.; Haroz, E. H.; Rialon, K. L.; Boul, P. J.; Noon, W. H.; Kittrell, C.; Ma, J. P.; Hauge, R. H.; Weisman, R. B.; Smalley, R. E.: Band gap fluorescence from individual single-walled carbon nanotubes. *Science* **2002**, *297*, 593-596.

(11) Thess, A.; Lee, R.; Nikolaev, P.; Dai, H. J.; Petit, P.; Robert, J.; Xu, C. H.; Lee, Y. H.; Kim, S. G.; Rinzler, A. G.; Colbert, D. T.; Scuseria, G. E.; Tomanek, D.; Fischer, J. E.; Smalley, R. E.: Crystalline ropes of metallic carbon nanotubes. *Science* **1996**, *273*, 483-487.

(12) Maultzsch, J.; Pomraenke, R.; Reich, S.; Chang, E.; Prezzi, D.; Ruini, A.; Molinari, E.; Strano, M. S.; Thomsen, C.; Lienau, C.: Exciton binding energies in carbon nanotubes from two-photon photoluminescence. *Phys. Rev. B* **2005**, *72*, 241402.

(13) Hartschuh, A.; Pedrosa, H. N.; Novotny, L.; Krauss, T. D.: Simultaneous fluorescence and Raman scattering from single carbon nanotubes. *Science* **2003**, *301*, 1354-1356.

(14) Wang, F.; Dukovic, G.; Brus, L. E.; Heinz, T. F.: The optical resonances in carbon nanotubes arise from excitons. *Science* **2005**, *308*, 838-841.

(15) Korovyanko, O. J.; Sheng, C. X.; Vardeny, Z. V.; Dalton, A. B.; Baughman, R. H.: Ultrafast spectroscopy of excitons in single-walled carbon

nanotubes. *Phys. Rev. Lett.* **2004**, *92*, 017403.

(16) Brennan, M. E.; Coleman, J. N.; Drury, A.; Lahr, B.; Kobayashi, T.; Blau, W. J.: Nonlinear photoluminescence from van Hove singularities in multiwalled carbon nanotubes. *Opt. Lett.* **2003**, *28*, 266-268.

(17) Kasha, M.: Characterization of electronic transitions in complex molecules. *Discuss. Faraday Soc.* **1950**, 14-19.

(18) Yanagi, K.; Kataura, H.: Carbon nanotubes: Breaking Kasha's rule. *Nature Photon.* **2010**, *4*, 200-201.

(19) Loi, M. A.; Gao, J.; Cordella, F.; Blondeau, P.; Menna, E.; Bartova, B.; Hebert, C.; Lazar, S.; Botton, G. A.; Milko, M.; Ambrosch-Draxl, C.: Encapsulation of conjugated oligomers in single-walled carbon nanotubes: Towards nanohybrids for photonic devices. *Adv. Mater.* **2010**, *22*, 1635-1639.

(20) Coleman, J. N.; Dalton, A. B.; Curran, S.; Rubio, A.; Davey, A. P.; Drury, A.; McCarthy, B.; Lahr, B.; Ajayan, P. M.; Roth, S.; Barklie, R. C.; Blau, W. J.: Phase separation of carbon nanotubes and turbostratic graphite using a functional organic polymer. *Adv. Mater.* **2000**, *12*, 213-216.

Chapter 7: Conclusions and future work

7.1 Conclusions

This thesis discussed field-enhanced optical phenomena with plasmonic nanostructures using two nonlinear optical processes, multiphoton-absorption-induced luminescence (MAIL) and metal-enhanced multiphoton absorption polymerization (MEMAP), with ultrafast near-infrared (NIR) pulses. A variety of nanostructures, such as gold nanoparticles, nanowires, nanoplates, and silver nanowires were used to observe MAIL and MEMAP. MAIL and its strong correlation to MEMAP were demonstrated by employing different types of prepolymer resins and different excitation wavelengths.

As described in Chapter 2, MAIL and MEMAP were examined using randomly distributed gold nanoparticles. The MAIL from aggregated particles was intense due to localized surface plasmon resonance (LSPR). This MAIL emission ranges from the near-ultraviolet to the visible region of the spectrum. When this broadband MAIL emission excites a photoinitiator, polymerization can be driven. Polymer shells around the nanoparticles were created using excitation wavelengths for which direct two-photon excitation of the photoinitiator cannot be driven. This result demonstrates that MAIL is essential to inducing photopolymerization around the plasmonic nanostructures.

Polymerization induced by MAIL was demonstrated again using uniform gold nanowires in Chapter 3. Consistent MAIL signals were observed at both ends of the

nanowires due to LSPR and the "lightning rod" nanoantenna effect. Polymer features created by MAIL using three different types of prepolymer resins confirmed that MAIL excited photoinitiators and induced polymerization.

Chapter 4 showed the strong correlation between MAIL and MEMAP using gold nanoplates. MAIL intensity was strong at the edges of the nanoplates and these localized luminescence signals were sensitive to the polarization of the excitation light. This MAIL emission created polymer features at the localized nanoplate areas.

MAIL was observed at remote positions when one end of a silver nanowire was excited with NIR light because the incident light coupled to surface plasmons, which propagated along the nanowire. The guided MAIL emission induced polymerization at remote positions. When another nanostructure contacted the nanowire, guided luminescence coupled to the nanostructure and created thin polymer film at the contact point. This method was used to assemble nanostructures in a controlled manner, as shown in one example in Chapter 5.

The correlation between MAIL and MEMAP was also observed using carbon nanostructures in Chapter 6. MAIL from individual multiwalled carbon nanotubes was observed due to the strong Coulomb interaction between the excited electrons and holes, and to the existence of high density of electron states. The broadband of the MAIL emission excited a photoinitiator and polymer features were created where the NIR light was scanned. MAIL-driven polymerization was also observed using single-walled carbon nanotubes and multilayer graphene sheets.

7.2 Future work

7.2.1 MAIL in biological applications

We have demonstrated that nonlinear luminescence can be observed directly from metal nanostructures using NIR light. The luminescence patterns can be manipulated by employing different polarization states. For example, linearly, azimuthally, and radially polarized NIR light can generate different luminescence patterns from the metal nanostructures.

When gold nanorods, about 60 nm in length and about 30 nm in diameter (Figure 7.1), are excited with linearly polarized NIR light, we can see the MAIL intensity pattern, as seen in Figures 7.2a and 7.2b. The coupling of NIR light into surface plasmons is the most efficient when the polarization of light is parallel to the

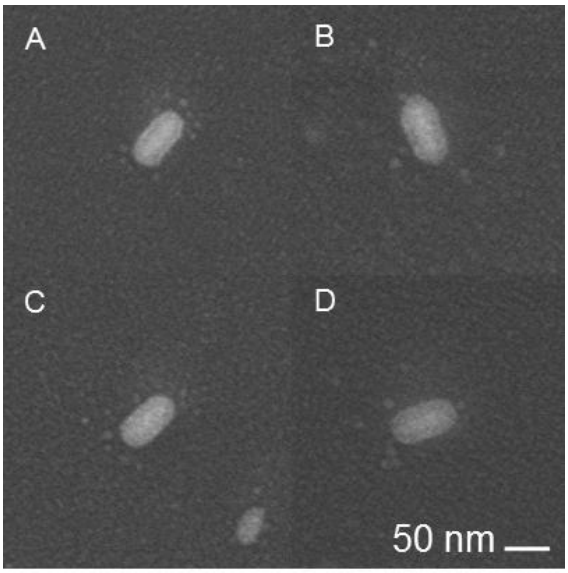

Figure 7.1. SEM images of gold nanorods that were excited with linearly, azimuthally, and radially polarized NIR light.

long axis of the gold nanorods. Therefore, the MAIL signals are sensitive to the orientation of the nanorods and the direction of linearly polarized light. For example, MAIL from a nanorod A was not observed using the excitation polarization parallel to the x-axis, but detected using the polarization perpendicular to the x-axis, as seen in the Figure 7.2.

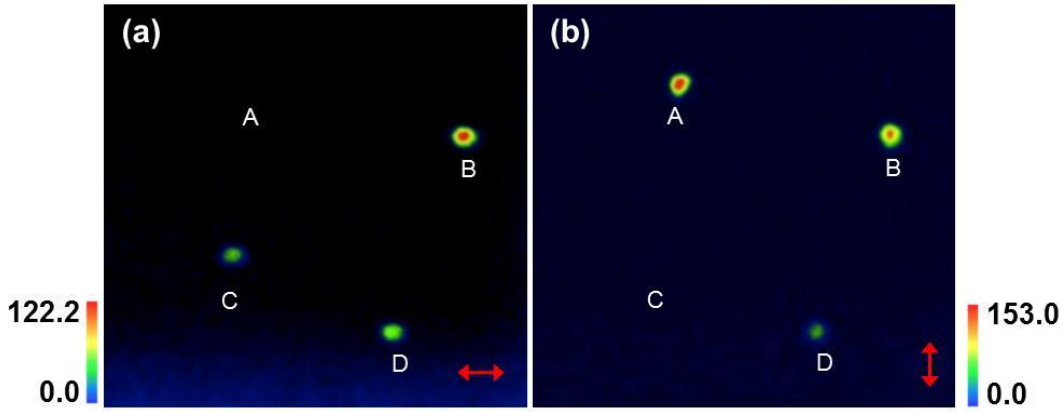

Figure 7.2. MAIL excitation images of the nanorods of Figure 7.1 with a polarization direction parallel to the x-axis (a) and the y-axis (b).

When azimuthally and radially polarized light are employed, we can observe two-lobe MAIL signals from all nanorods.[1-4] For instance, when azimuthally polarized light excites the nanorods that were used in Figure 7.2, MAIL signals are observed at both sides of each nanorod in which electric fields are parallel to the long axis of the nanorod, as shown in Figures 7.3a. In Figure 7.3b, radially polarized light generates MAIL signals at both ends of the nanorods, where electric fields are parallel to the long axis of the nanorod.

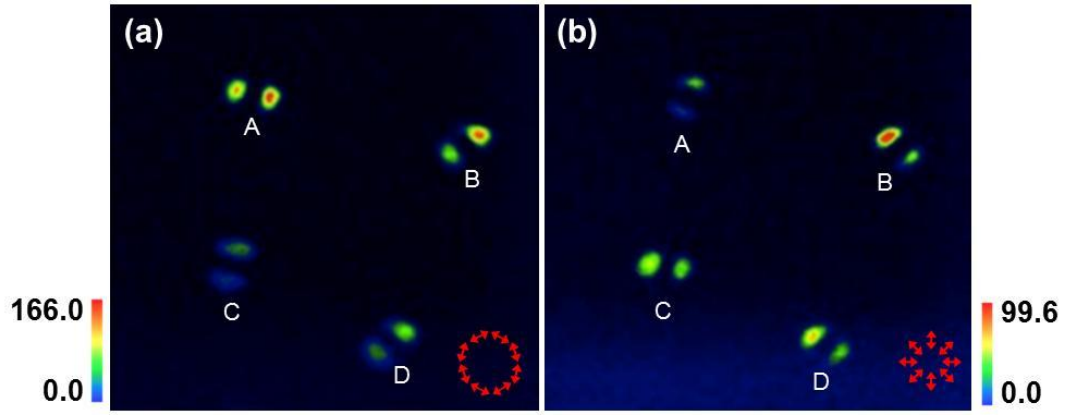

Figure 7.3. MAIL excitation images of the nanorods of Figure 7.1 with azimuthally polarized light (a) and radially polarized light (b).

This polarization-dependent MAIL can be used for biological imaging.[5-7] Gold nanorods[8-12] have been used for cellular imaging due to their bright optical signals. Linearly polarized light can generate MAIL from the nanorods that align parallel to the polarization.[13] However, azimuthally and radially polarized light can show bright two-lobe MAIL signals from individual nanorods in any orientations. Polarization-dependent MAIL can increase the sensitivity of the optical imaging and the efficiency of photothermal therapy.[6,7]

7.2.2 Biocompatible gold nanorods

Despite the strong MAIL intensity from gold nanorods, their biological applications are limited due to the surfactant of the nanorods, cetyl trimethylammonium bromide (CTAB), is cytotoxic.[14-16] Nanorods have been treated with polymers[17,18] or bioconjugates[19] to replace CTAB for biological applications. However, the chemical treatment for new functionalization of the nanorods requires

multiple chemical reactions for several hours. When ultrafast NIR pulses excite gold nanorods, they can be encapsulated in polymers within a second.

Gold nanorods in a water-based prepolymer resin can be added into a microfluidic channel. The microfluidic channel can be prepared between a polydimethyl siloxane (PDMS) mold and a glass coverslip. When the PDMS mold is prepared using a three-dimensional master structure fabricated by a multiphoton absorption polymerization (MAP) method, the microfluidic device can have multiple channels that can combine and form one main channel. When the nanorod-included water-soluble prepolymer resin flows in the microfluidic channel and water is added from four side of the channel, the flow rate and the volume of the resin can be adjusted by controlling the flow rate of water. This method can lead to the nanorod resin flowing in the middle of the channel.

Figure 7.4 shows such a microfluidic channel including the nanorod-included prepolymer resin and water. The nanorod prepolymer resin flows in the middle of the channel. When the resin meets water coming from four directions, the resin is confined in the middle of the channel so that the nanorods are not stuck in the PDMS walls and the glass substrate. When a large area of the resin is scanned with NIR light, hundreds of polymer-encapsulated nanorods can be fabricated in a few seconds. Scanning speed, scanning dimensions, and the concentration of the nanorods in the resin can determine the efficiency of producing polymer-coated nanorods. This method can provide a quick method fabricating biocompatible gold nanorods.

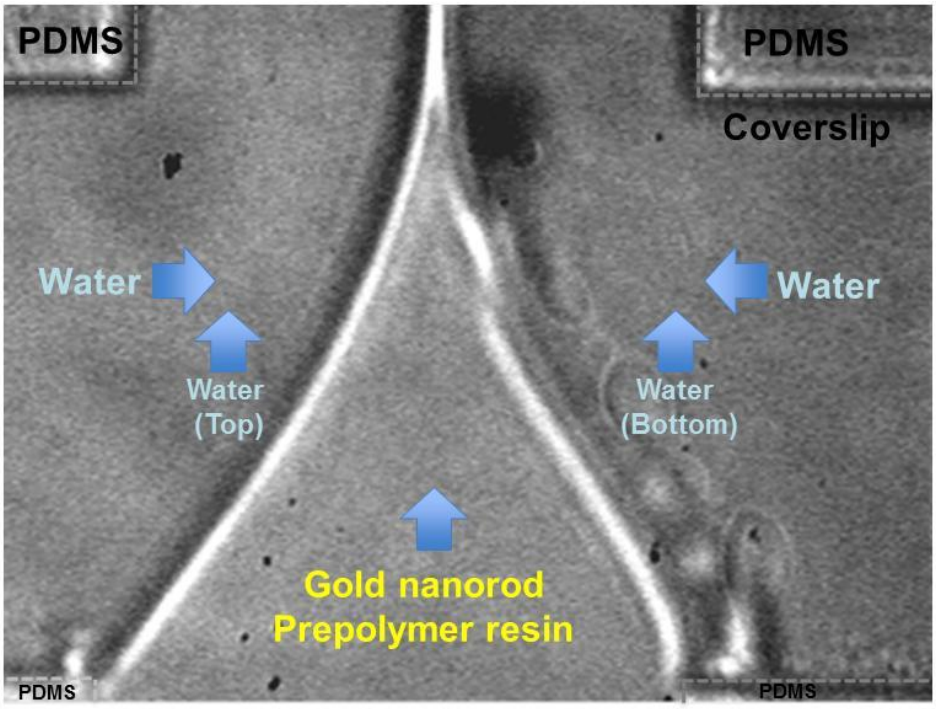

Figure 7.4. Optical image of microfluidic channel including gold nanorods in a water-based prepolymer resin, and water. Blue arrows indicate additional water coming from four channels.

7.2.3 Nanolithography with NIR light

NIR excitation on one end of silver nanowires can generate luminescence at remote positions. This luminescence emission created polymer features that were smaller than the nanowire diameter. This method can be used for nanolithography that currently uses an expensive and complex UV light excitation source.

Silver nanowire arrays can be prepared using an anodized aluminum oxide template using electrochemical deposition method.[20,21] An example of silver nanowire arrays is shown in Figure 7.5a. This scanning electron microscope (SEM) image shows the top view of the nanowire arrays. Using a microtome, the height of the nanowire arrays can be made more uniform, as seen in Figure 7.5b. When one

end of the nanowire array is excited with NIR light, the other end of the nanowire array can generate nanometer-scale polymer features, as shown in Figure 7.6. As the nanowires have small diameters, high-resolution nanolithography can be achieved.

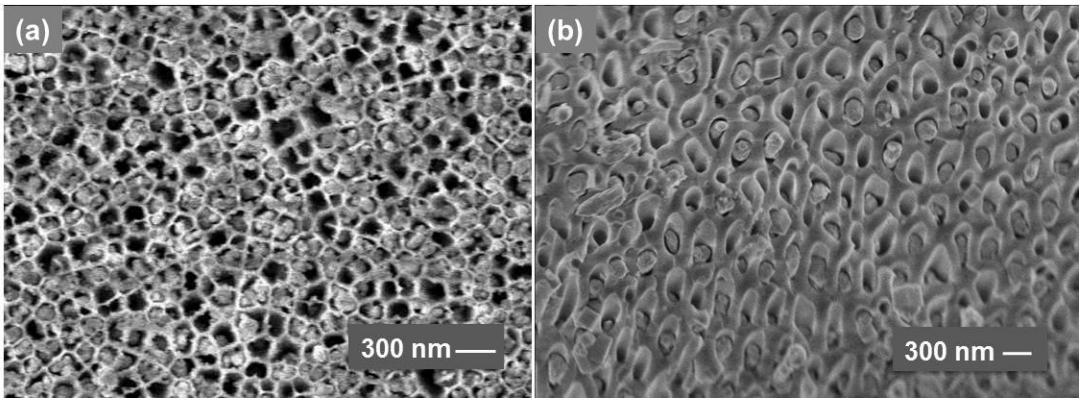

Figure 7.5. SEM images of silver nanowire arrays in an anodized aluminum oxide template (a) and that after cut with microtome (b).

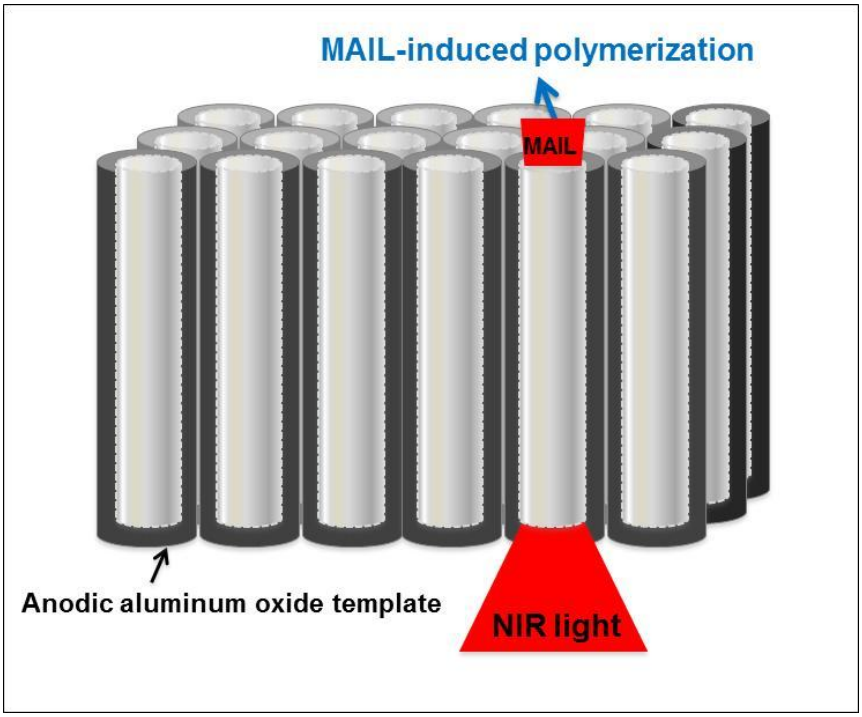

Figure 7.6. Schematic of nanolithography using silver nanowire arrays with NIR excitation.

7.2.4 Fabrication of optical field-enhancing substrates

Gold nanoplates can be used as substrates for surface-enhanced Raman scattering (SERS). When metal nanostructures are assembled on the nanoplate, the scattering intensity can be significantly increased due to the crowded electric fields and surface plasmon resonance. This SERS-active substrate can be fabricated using a microfluidic channel. When NIR light excites gold nanoplates while a gold nanoparticle solution is inside the microfluidic channel, gold nanoparticles can be assembled on the nanoplates by thin polymer films created by MAIL. If a quantum dot (QD) solution is inside the channel, QD-nanoplate assemblies can be fabricated. When QDs absorb MAIL, they can generate near-ultraviolet to near-infrared light with narrow bandwidth.[22,23]

7.3 Conclusion

Plasmonic nanostructures have the capability of enhancing optical fields and manipulating light to induce localized photochemistry. As shown in this dissertation, nonlinear luminescence and photopolymerization have been observed from different shapes of plasmonic nanostructures using ultrafast NIR pulses. These results demonstrate the potential of using nonlinear optical properties of the nanostructures in applications such as nanolithography, optical sensing, biological imaging, and phototherapy.

References

(1) Failla, A. V.; Qian, H.; Qian, H.; Hartschuh, A.; Meixner, A. J.: Orientational imaging of subwavelength au particles with higher order laser modes. *Nano Lett.* **2006**, *6*, 1374-1378.

(2) Zuechner, T.; Failla, A. V.; Steiner, M.; Meixner, A. J.: Probing dielectric interfaces on the nanoscale with elastic scattering patterns of single gold nanorods. *Opt. Express* **2008**, *16*, 14635-14644.

(3) Ishitobi, H.; Nakamura, I.; Hayazawa, N.; Sekkat, Z.; Kawata, S.: Orientational imaging of single molecules by using azimuthal and radial polarizations. *J. Phys. Chem. B* **2010**, *114*, 2565-2571.

(4) Chizhik, A. M.; Chizhik, A. I.; Gutbrod, R.; Meixner, A. J.; Schmidt, T.; Sommerfeld, J.; Hulsken, F.: Imaging and spectroscopy of defect luminescence and electron-phonon coupling in single SiO(2) nanoparticles. *Nano Lett.* **2009**, *9*, 3239-3244.

(5) Kang, H.; Jia, B.; Li, J.; Morrish, D.; Gu, M.: Enhanced photothermal therapy assisted with gold nanorods using a radially polarized beam. *Appl. Phys. Lett.* **2010**, *96*, 063702.

(6) von Maltzahn, G.; Park, J.-H.; Agrawal, A.; Bandaru, N. K.; Das, S. K.; Sailor, M. J.; Bhatia, S. N.: Computationally guided photothermal tumor therapy using long-circulating gold nanorod antennas. *Cancer Res.* **2009**, *69*, 3892-3900.

(7) Li, J. L.; Day, D.; Gu, M.: Ultra-low energy threshold for cancer photothermal therapy using transferrin-conjugated gold nanorods. *Adv. Mater.* **2008**, *20*, 3866-3871.

(8) Tong, L.; Wei, Q.; Wei, A.; Cheng, J.-X.: Gold nanorods as contrast agents for biological imaging: optical properties, surface conjugation and photothermal effects. *Photochem. Photobiol.* **2009**, *85*, 21-32.

(9) Wang, H. F.; Huff, T. B.; Zweifel, D. A.; He, W.; Low, P. S.; Wei, A.; Cheng, J. X.: In vitro and in vivo two-photon luminescence imaging of single gold nanorods. *Proc. Natl. Acad. Sci. U.S.A.* **2005**, *102*, 15752-15756.

(10) Bardhan, R.; Grady, N. K.; Cole, J. R.; Joshi, A.; Halas, N. J.: Fluorescence enhancement by Au nanostructures: nanoshells and nanorods. *Acs Nano* **2009**, *3*, 744-752.

(11) Durr, N. J.; Larson, T.; Smith, D. K.; Korgel, B. A.; Sokolov, K.; Ben-Yakar, A.: Two-photon luminescence imaging of cancer cells using molecularly targeted gold nanorods. *Nano Lett.* **2007**, *7*, 941-945.

(12) Ni, W.; Kou, X.; Yang, Z.; Wang, J.: Tailoring longitudinal surface plasmon wavelengths, scattering and absorption cross sections of gold nanorods. *Acs Nano* **2008**, *2*, 677-686.

(13) Chang, W.-S.; Ha, J. W.; Slaughter, L. S.; Link, S.: Plasmonic nanorod absorbers as orientation sensors. *Proc. Natl. Acad. Sci. U.S.A.* **2010**, *107*, 2781-2786.

(14) Mirska, D.; Schirmer, K.; Funari, S. S.; Langer, A.; Dobner, B.; Brezesinski, G.: Biophysical and biochemical properties of a binary lipid mixture for DNA transfection. *Colloid. Surface. B* **2005**, *40*, 51-59.

(15) Zimmer, A.: Antisense oligonucleotide delivery with polyhexyl cyanoacrylate nanoparticles as carriers. *Methods.* **1999**, *18*, 286-295.

(16) Takahashi, H.; Niidome, Y.; Niidome, T.; Kaneko, K.; Kawasaki, H.; Yamada, S.: Modification of gold nanorods using phospatidylcholine to reduce cytotoxicity. *Langmuir* **2006**, *22*, 2-5.

(17) Leonov, A. P.; Zheng, J.; Clogston, J. D.; Stern, S. T.; Patri, A. K.; Wei, A.: Detoxification of gold nanorods by treatment with polystyrenesulfonate. *Acs Nano* **2008**, *2*, 2481-2488.

(18) Thierry, B.; Ng, J.; Krieg, T.; Griesser, H. J.: A robust procedure for the functionalization of gold nanorods and noble metal nanoparticles. *Chem. Comm.* **2009**, 1724-1726.

(19) Liao, H. W.; Hafner, J. H.: Gold nanorod bioconjugates. *Chem. Mater.* **2005**, *17*, 4636-4641.

(20) Liu, R.; Lee, S. B.: MnO2/Poly(3,4-ethylenedioxythiophene) coaxial nanowires by one-step coelectrodeposition for electrochemical energy storage. *J. Am. Chem. Soc.* **2008**, *130*, 2942-2943.

(21) Xiao, R.; Il Cho, S.; Liu, R.; Lee, S. B.: Controlled electrochemical synthesis of conductive polymer nanotube structures. *J. Am. Chem. Soc.* **2007**, *129*, 4483-4489.

(22) Steckel, J. S.; Zimmer, J. P.; Coe-Sullivan, S.; Stott, N. E.; Bulovic, V.; Bawendi, M. G.: Blue luminescence from (CdS)ZnS core-shell nanocrystals. *Angew. Chem. Int. Ed.* **2004**, *43*, 2154-2158.

(23) Kim, S.; Lim, Y. T.; Soltesz, E. G.; De Grand, A. M.; Lee, J.; Nakayama, A.; Parker, J. A.; Mihaljevic, T.; Laurence, R. G.; Dor, D. M.; Cohn, L.

H.; Bawendi, M. G.; Frangioni, J. V.: Near-infrared fluorescent type II quantum dots for sentinel lymph node mapping. *Nature Biotech.* **2004**, *22*, 93-97.

References

(1) Ah, C. S.; Yun, Y. J.; Park, H. J.; Kim, W. J.; Ha, D. H.; Yun, W. S.: Size-controlled synthesis of machinable single crystalline gold nanoplates. *Chem. Mater.* **2005**, *17*, 5558-5561.

(2) Akimov, A. V.; Mukherjee, A.; Yu, C. L.; Chang, D. E.; Zibrov, A. S.; Hemmer, P. R.; Park, H.; Lukin, M. D.: Generation of single optical plasmons in metallic nanowires coupled to qquantum dots. *Nature* **2007**, *450*, 402-406.

(3) Avouris, P.; Chen, Z.; Perebeinos, V.: Carbon-based electronics. *Nature Nanotech.* **2007**, *2*, 605-615.

(4) Avouris, P.; Freitag, M.; Perebeinos, V.: Carbon-nanotube photonics and optoelectronics. *Nature Photon.* **2008**, *2*, 341-350.

(5) Bachilo, S. M.; Strano, M. S.; Kittrell, C.; Hauge, R. H.; Smalley, R. E.; Weisman, R. B.: Structure-assigned optical spectra of single-walled carbon nanotubes. *Science* **2002**, *298*, 2361-2366.

(6) Baigorri, R.; Garcia-Mina, J. M.; Aroca, R. F.; Alvarez-Puebla, R. A.: Optical enhancing properties of anisotropic gold nanoplates prepared with different fractions of a natural humic substance. *Chem. Mater.* **2008**, *20*, 1516-1521.

(7) Baldacchini, T.; LaFratta, C. N.; Farrer, R. A.; Teich, M. C.; Saleh, B. E. A.; Naughton, M. J.; Fourkas, J. T.: Acrylic-based resin with favorable properties for three-dimensional two-photon polymerization. *J. Appl. Phys.* **2004**, *95*, 6072-6076.

(8) Bardhan, R.; Grady, N. K.; Cole, J. R.; Joshi, A.; Halas, N. J.: Fluorescence enhancement by Au nanostructures: nanoshells and nanorods. *Acs Nano*

2009, *3*, 744-752.

(9) Barnes, W. L.: Surface plasmon-polariton length scales: A route to sub-wavelength optics. *J. Opt. a-Pure Appl. Opt.* **2006**, *8*, S87-S93.

(10) Bell, S. E. J.; Sirimuthu, N. M. S.: Quantitative surface-enhanced Raman spectroscopy. *Chem. Soc. Rev.* **2008**, *37*, 1012-1024.

(11) Beversluis, M. R.; Bouhelier, A.; Novotny, L.: Continuum generation from single gold nanostructures through near-field mediated intraband transitions. *Phys. Rev. B* **2003**, *68*, 115433.

(12) Biagioni, P.; Celebrano, M.; Savoini, M.; Grancini, G.; Brida, D.; Matefi-Tempfli, S.; Matefi-Tempfli, M.; Duo, L.; Hecht, B.; Cerullo, G.; Finazzi, M.: Dependence of the two-photon photoluminescence yield of gold nanostructures on the laser pulse duration. *Phys. Rev. B* **2009**, *80*, 045411.

(13) Bouhelier, A.; Bachelot, R.; Lerondel, G.; Kostcheev, S.; Royer, P.; Wiederrecht, G. P.: Surface plasmon characteristics of tunable photoluminescence in single gold nanorods. *Phys. Rev. Lett.* **2005**, *95*, 267405.

(14) Boyd, G. T.; Yu, Z. H.; Shen, Y. R.: Photoinduced luminescence from the noble-metals and its enhancement on roughened surfaces *Phys. Rev. B* **1986**, *33*, 7923-7936.

(15) Brennan, M. E.; Coleman, J. N.; Drury, A.; Lahr, B.; Kobayashi, T.; Blau, W. J.: Nonlinear photoluminescence from van Hove singularities in multiwalled carbon nanotubes. *Opt. Lett.* **2003**, *28*, 266-268.

(16) Brongersma, M. L.; Kik, P. G.: *Surface plasmon nanophotonics*; Springer: Dordrecht, 2007.

(17) Brown, E. B.; Campbell, R. B.; Tsuzuki, Y.; Xu, L.; Carmeliet, P.; Fukumura, D.; Jain, R. K.: In vivo measurement of gene expression, angiogenesis and physiological function in tumors using multiphoton laser scanning microscopy. *Nature Med.* **2001**, *7*, 864-868.

(18) Cai, W. B.; Amano, T.; Osawa, M.: A comparison of surface-enhanced infrared and surface-enhanced Raman spectra of pyrazine adsorbed on polycrystalline gold electrodes. *J. Electroanal. Chem.* **2001**, *500*, 147-155.

(19) Camden, J. P.; Dieringer, J. A.; Wang, Y.; Masiello, D. J.; Marks, L. D.; Schatz, G. C.; Van Duyne, R. P.: Probing the structure of single-molecule surface-enhanced Raman scattering hot spots. *J. Am. Chem. Soc.* **2008**, *130*, 12616-12617.

(20) Chang, W.-S.; Ha, J. W.; Slaughter, L. S.; Link, S.: Plasmonic nanorod absorbers as orientation sensors. *Proc. Natl. Acad. Sci. U.S.A.* **2010**, *107*, 2781-2786.

(21) Chen, J.; Perebeinos, V.; Freitag, M.; Tsang, J.; Fu, Q.; Liu, J.; Avouris, P.: Bright infrared emission from electrically induced excitons in carbon nanotubes. *Science* **2005**, *310*, 1171-1174.

(22) Chizhik, A. M.; Chizhik, A. I.; Gutbrod, R.; Meixner, A. J.; Schmidt, T.; Sommerfeld, J.; Hulsken, F.: Imaging and spectroscopy of defect luminescence and electron-phonon coupling in single SiO(2) nanoparticles. *Nano Lett.* **2009**, *9*, 3239-3244.

(23) Coleman, J. N.; Dalton, A. B.; Curran, S.; Rubio, A.; Davey, A. P.; Drury, A.; McCarthy, B.; Lahr, B.; Ajayan, P. M.; Roth, S.; Barklie, R. C.; Blau, W. J.: Phase separation of carbon nanotubes and turbostratic graphite using a functional organic polymer. *Adv. Mater.* **2000**, *12*, 213-216.

(24) Curto, A. G.; Volpe, G.; Taminiau, T. H.; Kreuzer, M. P.; Quidant, R.; van Hulst, N. F.: Unidirectional emission of a quantum dot coupled to a nanoantenna. *Science* **2010**, *329*, 930-933.

(25) Denk, W.; Strickler, J. H.; Webb, W. W.: Two-photon laser scanning fluorescence microscopy. *Science* **1990**, *248*, 73-76.

(26) Dickson, R. M.; Lyon, L. A.: Unidirectional plasmon propagation in metallic nanowires. *J. Phys. Chem. B* **2000**, *104*, 6095-6098.

(27) Diebold, E. D.; Peng, P.; Mazur, E.: Isolating surface-enhanced Raman scattering hot spots using multiphoton lithography. *J. Am. Chem. Soc.* **2009**, *131*, 16356-16357.

(28) Ditlbacher, H.; Hohenau, A.; Wagner, D.; Kreibig, U.; Rogers, M.; Hofer, F.; Aussenegg, F. R.; Krenn, J. R.: Silver nanowires as surface plasmon resonators. *Phys. Rev. Lett.* **2005**, *95*, 257403.

(29) Durr, N. J.; Larson, T.; Smith, D. K.; Korgel, B. A.; Sokolov, K.; Ben-Yakar, A.: Two-photon luminescence imaging of cancer cells using molecularly targeted gold nanorods. *Nano Lett.* **2007**, *7*, 941-945.

(30) Eichelbaum, M.; Kneipp, J.; Schmidt, B. E.; Panne, U.; Rademann, K.: SERS and multiphoton-induced luminescence of gold micro- and nanostructures fabricated by NIR femtosecond-laser irradiation. *Chemphyschem* **2008**, *9*, 2163-2167.

(31) Engheta, N.: Circuits with light at nanoscales: Optical nanocircuits inspired by metamaterials. *Science* **2007**, *317*, 1698-1702.

(32) Essig, S.; Marquardt, C. W.; Vijayaraghavan, A.; Ganzhorn, M.; Dehm, S.; Hennrich, F.; Ou, F.; Green, A. A.; Sciascia, C.; Bonaccorso, F.; Bohnen,

K. P.; von Loehneysen, H.; Kappes, M. M.; Ajayan, P. M.; Hersam, M. C.; Ferrari, A. C.; Krupke, R.: Phonon-assisted electroluminescence from metallic carbon nanotubes and graphene. *Nano Lett.* **2010**, *10*, 1589-1594.

(33) Eustis, S.; El-Sayed, M. A.: Why gold nanoparticles are more precious than pretty gold: Noble metal surface plasmon resonance and its enhancement of the radiative and nonradiative properties of nanocrystals of different shapes. *Chem. Soc. Rev.* **2006**, *35*, 209-217.

(34) Failla, A. V.; Qian, H.; Qian, H.; Hartschuh, A.; Meixner, A. J.: Orientational imaging of subwavelength au particles with higher order laser modes. *Nano Lett.* **2006**, *6*, 1374-1378.

(35) Falk, A. L.; Koppens, F. H. L.; Yu, C. L.; Kang, K.; Snapp, N. d. L.; Akimov, A. V.; Jo, M.-H.; Lukin, M. D.; Park, H.: Near-field electrical detection of optical plasmons and single-plasmon sources. *Nature Phys.* **2009**, *5*, 475-479.

(36) Fang, Y.; Wei, H.; Hao, F.; Nordlander, P.; Xu, H.: Remote-excitation surface-enhanced Raman scattering using propagating Ag nanowire plasmons. *Nano Lett.* **2009**, *9*, 2049-2053.

(37) Fang, Y. R.; Li, Z. P.; Huang, Y. Z.; Zhang, S. P.; Nordlander, P.; Halas, N. J.; Xu, H. X.: Branched silver nanowires as controllable plasmon routers. *Nano Lett.* **2010**, *10*, 1950-1954.

(38) Farrer, R. A.; Butterfield, F. L.; Chen, V. W.; Fourkas, J. T.: Highly efficient multiphoton-absorption-induced luminescence from gold nanoparticles. *Nano Lett.* **2005**, *5*, 1139-1142.

(39) Fourkas, J. T.: Nanoscale photolithography with visible light. *J. Phys.*

Chem. Lett. **2010**, *1*, 1221-1227.

(40) Freitag, M.; Martin, Y.; Misewich, J. A.; Martel, R.; Avouris, P. H.: Photoconductivity of single carbon nanotubes. *Nano Lett.* **2003**, *3*, 1067-1071.

(41) Garcia-Santamaria, F.; Salgueirino-Maceira, V.; Lopez, C.; Liz-Marzan, L. M.: Synthetic opals based on silica-coated gold nanoparticles. *Langmuir* **2002**, *18*, 4519-4522.

(42) GarciaVidal, F. J.; Pendry, J. B.: Collective theory for surface enhanced Raman scattering. *Phys. Rev. Lett.* **1996**, *77*, 1163-1166.

(43) Gong, H. M.; Zhou, Z. K.; Xiao, S.; Su, X. R.; Wang, Q. Q.: Strong near-infrared avalanche photoluminescence from Ag nanowire arrays. *Plasmonics* **2008**, *3*, 59-64.

(44) Göppert-Mayer, M.: Über elementarakte mit zwei quantensprüngen. *Annalen der Physik* **1931**, *9*, 273-295.

(45) Goutev, N.; Futamata, M.: Attenuated total reflection surface-enhanced infrared absorption spectroscopy of carboxyl terminated self-assembled monolayers on gold. *Appl. Spectrosc.* **2003**, *57*, 506-513.

(46) Gramotnev, D. K.; Bozhevolnyi, S. I.: Plasmonics beyond the diffraction limit. *Nature Photon.* **2010**, *4*, 83-91.

(47) Han, Y.; Sun, J.; Ye, H.; Wu, W.; Shi, G.: Nonlinear refraction of silver nanowires from nanosecond to femtosecond laser excitation. *Appl. Phys. B: Lasers and Optics* **2009**, *94*, 233-237.

(48) Hartschuh, A.; Pedrosa, H. N.; Novotny, L.; Krauss, T. D.: Simultaneous fluorescence and Raman scattering from single carbon nanotubes.

Science **2003**, *301*, 1354-1356.

(49) Haynes, C. L.; Van Duyne, R. P.: Nanosphere lithography: A versatile nanofabrication tool for studies of size-dependent nanoparticle optics. *J. Phys. Chem. B* **2001**, *105*, 5599-5611.

(50) Haynes, C. L.; Van Duyne, R. P.: Plasmon-sampled surface-enhanced Raman excitation spectroscopy. *J. Phys. Chem. B* **2003**, *107*, 7426-7433.

(51) Huang, J.-S.; Callegari, V.; Geisler, P.; Bruening, C.; Kern, J.; Prangsma, J. C.; Wu, X.; Feichtner, T.; Ziegler, J.; Weinmann, P.; Kamp, M.; Forchel, A.; Biagioni, P.; Sennhauser, U.; Hecht, B.: Atomically flat single-crystalline gold nanostructures for plasmonic nanocircuitry. *Nature Comm.* **2010**, *1*:150.

(52) Huang, X. H.; El-Sayed, I. H.; Qian, W.; El-Sayed, M. A.: Cancer cell imaging and photothermal therapy in the near-infrared region by using gold nanorods. *J. Am. Chem. Soc.* **2006**, *128*, 2115-2120.

(53) Hulteen, J. C.; Vanduyne, R. P.: Nanosphere lithography - A materials general fabrication process for periodic particle array surfaces. *J. Vac. Sci. Technol. A-Vac. Surf. Films* **1995**, *13*, 1553-1558.

(54) Hutchison, J. A.; Centeno, S. P.; Odaka, H.; Fukumura, H.; Hofkens, J.; Uji-i, H.: Subdiffraction limited, remote excitation of surface enhanced Raman scattering. *Nano Lett.* **2009**, *9*, 995-1001.

(55) Imura, K.; Nagahara, T.; Okamoto, H.: Photoluminescence from gold nanoplates induced by near-field two-photon absorption. *Appl. Phys. Lett.* **2006**, *88*, 023104.

(56) Ishitobi, H.; Nakamura, I.; Hayazawa, N.; Sekkat, Z.; Kawata, S.:

Orientational imaging of single molecules by using azimuthal and radial polarizations. *J. Phys. Chem. B* **2010**, *114*, 2565-2571.

(57) Jain, P. K.; Eustis, S.; El-Sayed, M. A.: Plasmon coupling in nanorod assemblies: Optical absorption, discrete dipole approximation simulation, and exciton-coupling model. *J. Phys. Chem. B* **2006**, *110*, 18243-18253.

(58) Jang, S. M.; Park, J. S.; Shin, S. M.; Yoon, C. J.; Choi, B. K.; Gong, M. S.; Joo, S. W.: Adsorption of 4-biphenylmethanethiolate on different-sized gold nanoparticle surfaces. *Langmuir* **2004**, *20*, 1922-1927.

(59) Jensen, T. R.; Malinsky, M. D.; Haynes, C. L.; Van Duyne, R. P.: Nanosphere lithography: Tunable localized surface plasmon resonance spectra of silver nanoparticles. *J. Phys. Chem. B* **2000**, *104*, 10549-10556.

(60) Jones, M. R.; Macfarlane, R. J.; Lee, B.; Zhang, J.; Young, K. L.; Senesi, A. J.; Mirkin, C. A.: DNA-nanoparticle superlattices formed from anisotropic building blocks. *Nature Mater.* **2010**, *9*, 913-917.

(61) Juluri, B. K.; Chaturvedi, N.; Hao, Q.; Lu, M.; Velegol, D.; Jensen, L.; Huang, T. J.: Scalable manufacturing of plasmonic nanodisk dimers and Cusp nanostructures using salting-out quenching method and colloidal lithography. *Acs Nano* **2011**, *5*, 5838-5847.

(62) Kaiser, W.; Garrett, C. G. B.: Two-photon excitation in CaF2:Eu2+. *Phys. Rev. Lett.* **1961**, *7*, 229-232.

(63) Kang, H.; Jia, B.; Li, J.; Morrish, D.; Gu, M.: Enhanced photothermal therapy assisted with gold nanorods using a radially polarized beam. *Appl. Phys. Lett.* **2010**, *96*, 063702.

(64) Kasha, M.: Characterization of electronic transitions in complex molecules. *Discuss. Faraday Soc.* **1950**, 14-19.

(65) Kawata, S.; Inouye, Y.; Verma, P.: Plasmonics for near-field nano-imaging and superlensing. *Nature Photon.* **2009**, *3*, 388-394.

(66) Kelly, K. L.; Coronado, E.; Zhao, L. L.; Schatz, G. C.: The optical properties of metal nanoparticles: The influence of size, shape, and dielectric environment. *J. Phys. Chem. B* **2003**, *107*, 668-677.

(67) Kempa, T.; Farrer, R. A.; Giersig, M.; Fourkas, J. T.: Photochemical synthesis and multiphoton luminescence of monodisperse silver nanocrystals. *Plasmonics* **2006**, *1*, 45-51.

(68) Kim, H.; Xiang, C.; Guell, A. G.; Penner, R. M.; Potma, E. O.: Tunable two-photon excited luminescence in single gold nanowires fabricated by lithographically patterned nanowire electrodeposition. *J. Phys. Chem. C* **2008**, *112*, 12721-12727.

(69) Kim, J.-W.; Galanzha, E. I.; Shashkov, E. V.; Moon, H.-M.; Zharov, V. P.: Golden carbon nanotubes as multimodal photoacoustic and photothermal high-contrast molecular agents. *Nature Nanotech.* **2009**, *4*, 688-694.

(70) Kim, S.; Lim, Y. T.; Soltesz, E. G.; De Grand, A. M.; Lee, J.; Nakayama, A.; Parker, J. A.; Mihaljevic, T.; Laurence, R. G.; Dor, D. M.; Cohn, L. H.; Bawendi, M. G.; Frangioni, J. V.: Near-infrared fluorescent type II quantum dots for sentinel lymph node mapping. *Nature Biotech.* **2004**, *22*, 93-97.

(71) Kinkhabwala, A.; Yu, Z.; Fan, S.; Avlasevich, Y.; Muellen, K.; Moerner, W. E.: Large single-molecule fluorescence enhancements produced by a

bowtie nanoantenna. *Nature Photon.* **2009**, *3*, 654-657.

(72) Kneipp, J.; Kneipp, H.; Kneipp, K.: SERS - a single-molecule and nanoscale tool for bioanalytics. *Chem. Soc. Rev.* **2008**, *37*, 1052-1060.

(73) Kneipp, K.; Kneipp, H.; Itzkan, I.; Dasari, R. R.; Feld, M. S.: Ultrasensitive chemical analysis by Raman spectroscopy. *Chem. Rev.* **1999**, *99*, 2957-2976.

(74) Kneipp, K.; Wang, Y.; Kneipp, H.; Perelman, L. T.; Itzkan, I.; Dasari, R.; Feld, M. S.: Single molecule detection using surface-enhanced Raman scattering (SERS). *Phys. Rev. Lett.* **1997**, *78*, 1667-1670.

(75) Knight, M. W.; Grady, N. K.; Bardhan, R.; Hao, F.; Nordlander, P.; Halas, N. J.: Nanoparticle-mediated coupling of light into a nanowire. *Nano Lett.* **2007**, *7*, 2346-2350.

(76) Knoll, W.: Interfaces and thin films as seen by bound electromagnetic waves. *Annu. Rev. Phys. Chem.* **1998**, *49*, 569-638.

(77) Kojima, K.; Ito, M.; Morishita, H.; Hayashi, N.: A novel water-soluble photoinitiator for the acrylic photopolymerization type resist system. *Chem. Mater.* **1998**, *10*, 3429-3433.

(78) Korovyanko, O. J.; Sheng, C. X.; Vardeny, Z. V.; Dalton, A. B.; Baughman, R. H.: Ultrafast spectroscopy of excitons in single-walled carbon nanotubes. *Phys. Rev. Lett.* **2004**, *92*, 017403.

(79) Kravets, V. G.; Zoriniants, G.; Burrows, C. P.; Schedin, F.; Geim, A. K.; Barnes, W. L.; Grigorenko, A. N.: Composite Au nanostructures for fluorescence studies in visible light. *Nano Lett.* **2010**, *10*, 874-879.

(80) LaFratta, C. N.; Fourkas, J. T.; Baldacchini, T.; Farrer, R. A.: Multiphoton fabrication. *Angew. Chem. Int. Ed.* **2007**, *46*, 6238-6258.

(81) Lal, S.; Grady, N. K.; Kundu, J.; Levin, C. S.; Lassiter, J. B.; Halas, N. J.: Tailoring plasmonic substrates for surface enhanced spectroscopies. *Chem. Soc. Rev.* **2008**, *37*, 898-911.

(82) Larson, D. R.; Zipfel, W. R.; Williams, R. M.; Clark, S. W.; Bruchez, M. P.; Wise, F. W.; Webb, W. W.: Water-soluble quantum dots for multiphoton fluorescence imaging in vivo. *Science* **2003**, *300*, 1434-1436.

(83) Leonov, A. P.; Zheng, J.; Clogston, J. D.; Stern, S. T.; Patri, A. K.; Wei, A.: Detoxification of gold nanorods by treatment with polystyrenesulfonate. *Acs Nano* **2008**, *2*, 2481-2488.

(84) Li, J. L.; Day, D.; Gu, M.: Ultra-low energy threshold for cancer photothermal therapy using transferrin-conjugated gold nanorods. *Adv. Mater.* **2008**, *20*, 3866-3871.

(85) Li, L.; Gattass, R. R.; Gershgoren, E.; Hwang, H.; Fourkas, J. T.: Achieving lambda/20 resolution by one-color initiation and deactivation of polymerization. *Science* **2009**, *324*, 910-913.

(86) Liao, H. W.; Hafner, J. H.: Gold nanorod bioconjugates. *Chem. Mater.* **2005**, *17*, 4636-4641.

(87) Liu, N.; Tang, M. L.; Hentschel, M.; Giessen, H.; Alivisatos, A. P.: Nanoantenna-enhanced gas sensing in a single tailored nanofocus. *Nature Mater.* **2011**, *10*, 631-636.

(88) Liu, R.; Lee, S. B.: MnO2/Poly(3,4-ethylenedioxythiophene) coaxial

nanowires by one-step coelectrodeposition for electrochemical energy storage. *J. Am. Chem. Soc.* **2008**, *130*, 2942-2943.

(89) Liz-Marzan, L. M.; Giersig, M.; Mulvaney, P.: Synthesis of nanosized gold-silica core-shell particles. *Langmuir* **1996**, *12*, 4329-4335.

(90) Loi, M. A.; Gao, J.; Cordella, F.; Blondeau, P.; Menna, E.; Bartova, B.; Hebert, C.; Lazar, S.; Botton, G. A.; Milko, M.; Ambrosch-Draxl, C.: Encapsulation of conjugated oligomers in single-walled carbon nanotubes: Towards nanohybrids for photonic devices. *Adv. Mater.* **2010**, *22*, 1635-1639.

(91) Louden, R.: *The quantum theory of light*. 2nd ed.; Oxford University Press: New York, 1983.

(92) Maier, S. A.: *Plasmonics: Fundamentals and applications*; Springer: New York, 2007.

(93) Maiti, S.; Shear, J. B.; Williams, R. M.; Zipfel, W. R.; Webb, W. W.: Measuring serotonin distribution in live cells with three-photon excitation. *Science* **1997**, *275*, 530-532.

(94) Maruo, S.; Fourkas, J. T.: Recent progress in multiphoton microfabrication. *Laser Photon. Rev.* **2008**, *2*, 100-111.

(95) Maultzsch, J.; Pomraenke, R.; Reich, S.; Chang, E.; Prezzi, D.; Ruini, A.; Molinari, E.; Strano, M. S.; Thomsen, C.; Lienau, C.: Exciton binding energies in carbon nanotubes from two-photon photoluminescence. *Phys. Rev. B* **2005**, *72*, 241402.

(96) Michaels, A. M.; Jiang, J.; Brus, L.: Ag nanocrystal junctions as the site for surface-enhanced Raman scattering of single Rhodamine 6G molecules. *J.*

Phys. Chem. B **2000**, *104*, 11965-11971.

(97) Michaels, A. M.; Nirmal, M.; Brus, L. E.: Surface enhanced Raman spectroscopy of individual rhodamine 6G molecules on large Ag nanocrystals. *J. Am. Chem. Soc.* **1999**, *121*, 9932-9939.

(98) Miller, M. M.; Lazarides, A. A.: Sensitivity of metal nanoparticle surface plasmon resonance to the dielectric environment. *J. Phys. Chem. B* **2005**, *109*, 21556-21565.

(99) Millstone, J. E.; Hurst, S. J.; Metraux, G. S.; Cutler, J. I.; Mirkin, C. A.: Colloidal gold and silver triangular nanoprisms. *Small* **2009**, *5*, 646-664.

(100) Millstone, J. E.; Park, S.; Shuford, K. L.; Qin, L. D.; Schatz, G. C.; Mirkin, C. A.: Observation of a quadrupole plasmon mode for a colloidal solution of gold nanoprisms. *J. Am. Chem. Soc.* **2005**, *127*, 5312-5313.

(101) Mirska, D.; Schirmer, K.; Funari, S. S.; Langer, A.; Dobner, B.; Brezesinski, G.: Biophysical and biochemical properties of a binary lipid mixture for DNA transfection. *Colloid. Surface. B* **2005**, *40*, 51-59.

(102) Misewich, J. A.; Martel, R.; Avouris, P.; Tsang, J. C.; Heinze, S.; Tersoff, J.: Electrically induced optical emission from a carbon nanotube FET. *Science* **2003**, *300*, 783-786.

(103) Mock, J. J.; Barbic, M.; Smith, D. R.; Schultz, D. A.; Schultz, S.: Shape effects in plasmon resonance of individual colloidal silver nanoparticles. *J. Chem. Phys.* **2002**, *116*, 6755-6759.

(104) Mohamed, M. B.; Volkov, V.; Link, S.; El-Sayed, M. A.: The 'lightning' gold nanorods: fluorescence enhancement of over a million compared to

the gold metal. *Chem. Phys. Lett.* **2000**, *317*, 517-523.

(105) Muhlschlegel, P.; Eisler, H. J.; Martin, O. J. F.; Hecht, B.; Pohl, D. W.: Resonant optical antennas. *Science* **2005**, *308*, 1607-1609.

(106) Murazawa, N.; Ueno, K.; Mizeikis, V.; Juodkazis, S.; Misawa, H.: Spatially selective nonlinear photopolymerization induced by the near-field of surface plasmons localized on rectangular gold nanorods. *J. Phys. Chem. C* **2009**, *113*, 1147-1149.

(107) Nah, S.; Li, L.; Fourkas, J. T.: Field-enhanced phenomena of gold nanoparticles. *J. Phys. Chem. A* **2009**, *113*, 4416-4422.

(108) Nah, S.; Li, L.; Liu, R.; Hao, J.; Lee, S. B.; Fourkas, J. T.: Metal-enhanced multiphoton absorption polymerization with gold nanowires. *J. Phys. Chem. C* **2010**, *114*, 7774-7779.

(109) Nakamura, O.: Fundamental of two-photon microscopy. *Microsc. Res. Tech.* **1999**, *47*, 165-171.

(110) Nelayah, J.; Gu, J.; Sigle, W.; Koch, C. T.; Pastoriza-Santos, I.; Liz-Marzan, L. M.; van Aken, P. A.: Direct imaging of surface plasmon resonances on single triangular silver nanoprisms at optical wavelength using low-loss EFTEM imaging. *Opt. Lett.* **2009**, *34*, 1003-1005.

(111) Nelayah, J.; Kociak, M.; Stephan, O.; Garcia de Abajo, F. J.; Tence, M.; Henrard, L.; Taverna, D.; Pastoriza-Santos, I.; Liz-Marzan, L. M.; Colliex, C.: Mapping surface plasmons on a single metallic nanoparticle. *Nature Phys.* **2007**, *3*, 348-353.

(112) Ni, W.; Kou, X.; Yang, Z.; Wang, J.: Tailoring longitudinal surface

plasmon wavelengths, scattering and absorption cross sections of gold nanorods. *Acs Nano* **2008**, *2*, 677-686.

(113) Nie, S. M.; Chiu, D. T.; Zare, R. N.: Probing individual molecules with confocal fluorescence microscopy. *Science* **1994**, *266*, 1018-1021.

(114) Nie, S. M.; Emery, S. R.: Probing single molecules and single nanoparticles by surface-enhanced Raman scattering. *Science* **1997**, *275*, 1102-1106.

(115) Nordlander, P.; Oubre, C.; Prodan, E.; Li, K.; Stockman, M. I.: Plasmon hybridization in nanoparticle dimers. *Nano Lett.* **2004**, *4*, 899-903.

(116) Novotny, L.; Beversluis, M. R.; Youngworth, K. S.; Brown, T. G.: Longitudinal field modes probed by single molecules. *Phys. Rev. Lett.* **2001**, *86*, 5251-5254.

(117) O'Connell, M. J.; Bachilo, S. M.; Huffman, C. B.; Moore, V. C.; Strano, M. S.; Haroz, E. H.; Rialon, K. L.; Boul, P. J.; Noon, W. H.; Kittrell, C.; Ma, J. P.; Hauge, R. H.; Weisman, R. B.; Smalley, R. E.: Band gap fluorescence from individual single-walled carbon nanotubes. *Science* **2002**, *297*, 593-596.

(118) Osawa, M.: *Surface-enhanced infrared absorption. In near-field optics and surface plasmon polaritons.* Springer: New York, 2001; Vol. 81; pp 163.

(119) Osawa, M.; Ataka, K.; Yoshii, K.; Nishikawa, Y.: Surface-enhanced infrared-spectroscopy - The origin of the absorption enhancement and band selection rule in the infrared-spectra of molecules adsorbed on fine metal particles. *Appl. Spectrosc.* **1993**, *47*, 1497-1502.

(120) Park, J.; Estrada, A.; Sharp, K.; Sang, K.; Schwartz, J. A.; Smith, D. K.; Coleman, C.; Payne, J. D.; Korgel, B. A.; Dunn, A. K.; Tunnell, J. W.: Two-

photon-induced photoluminescence imaging of tumors using near-infrared excited gold nanoshells. *Opt. Express* **2008**, *16*, 1590-1599.

(121) Pieczonka, N. P. W.; Aroca, R. F.: Single molecule analysis by surfaced-enhanced Raman scattering. *Chem. Soc. Rev.* **2008**, *37*, 946-954.

(122) Pompa, P. P.; Martiradonna, L.; Della Torre, A.; Della Sala, F.; Manna, L.; De Vittorio, M.; Calabi, F.; Cingolani, R.; Rinaldi, R.: Metal-enhanced fluorescence of colloidal nanocrystals with nanoscale control. *Nature Nanotech.* **2006**, *1*, 126-130.

(123) Postnikova, B. J.; Currie, J.; Doyle, T.; Hanes, R. E.; Anslyn, E. V.; Shear, J. B.; Vanden Bout, D. E.: Towards nanoscale three-dimensional fabrication using two-photon initiated polymerization and near-field excitation. *Microelectron. Eng.* **2003**, *69*, 459-465.

(124) Pyayt, A. L.; Wiley, B.; Xia, Y. N.; Chen, A.; Dalton, L.: Integration of photonic and silver nanowire plasmonic waveguides. *Nature Nanotech.* **2008**, *3*, 660-665.

(125) Qian, X. M.; Nie, S. M.: Single-molecule and single-nanoparticle SERS: from fundamental mechanisms to biomedical applications. *Chem. Soc. Rev.* **2008**, *37*, 912-920.

(126) Qiu, X. H.; Freitag, M.; Perebeinos, V.; Avouris, P.: Photoconductivity spectra of single-carbon nanotubes: Implications on the nature of their excited states. *Nano Lett.* **2005**, *5*, 749-752.

(127) Rechberger, W.; Hohenau, A.; Leitner, A.; Krenn, J. R.; Lamprecht, B.; Aussenegg, F. R.: Optical properties of two interacting gold nanoparticles. *Opt.*

Comm. **2003**, *220*, 137-141.

(128) Ropp, C.; Cummins, Z.; Probst, R.; Qin, S.; Fourkas, J. T.; Shapiro, B.; Waks, E.: Positioning and immobilization of individual quantum dots with nanoscale precision. *Nano Lett.* **2010**, *10*, 4673–4679.

(129) Ropp, C.; Probst, R.; Cummins, Z.; Kumar, R.; Berglund, A. J.; Raghavan, S. R.; Waks, E.; Shapiro, B.: Manipulating quantum dots to nanometer precision by control of flow. *Nano Lett.* **2010**, *10*, 2525-2530.

(130) Rumi, M. B., S.; Wang, J.; Perry, J. W.; Marder, S. R. : *Two-photon absorbing materials and two-photon-induced chemistry. In photoresponsive polymers I.* Springer: Berlin, 2008; Vol. 213; pp 1.

(131) Sanders, A. W.; Routenberg, D. A.; Wiley, B. J.; Xia, Y.; Dufresne, E. R.; Reed, M. A.: Observation of plasmon propagation, redirection, and fan-out in silver nanowires. *Nano Lett.* **2006**, *6*, 1822-1826.

(132) Schatz, G. C.: Theoretical-studies of surface enhanced Raman-scattering. *Accounts Chem. Res.* **1984**, *17*, 370-376.

(133) Schuller, J. A.; Barnard, E. S.; Cai, W.; Jun, Y. C.; White, J. S.; Brongersma, M. L.: Plasmonics for extreme light concentration and manipulation. *Nature Mater.* **2010**, *9*, 193-204.

(134) Schumacher, T.; Kratzer, K.; Molnar, D.; Hentschel, M.; Giessen, H.; Lippitz, M.: Nanoantenna-enhanced ultrafast nonlinear spectroscopy of a single gold nanoparticle. *Nature Comm.* **2011**, *2*:333.

(135) Schwartzberg, A. M.; Zhang, J. Z.: Novel optical properties and emerging applications of metal nanostructures. *J. Phys. Chem. C* **2008**, *112*, 10323-

10337.

(136) Shalaev, V. M.; Kawata, S.: *Nanophotonics with surface plasmons*; Elsevier: Amsterdam, 2007.

(137) Snow, E. S.; Perkins, F. K.; Houser, E. J.; Badescu, S. C.; Reinecke, T. L.: Chemical detection with a single-walled carbon nanotube capacitor. *Science* **2005**, *307*, 1942-1945.

(138) So, P. T. C.; Dong, C. Y.; Masters, B. R.; Berland, K. M.: Two-photon excitation fluorescence microscopy. *Annu. Rev. Biomed. Eng.* **2000**, *2*, 399-429.

(139) Squirrell, J. M.; Wokosin, D. L.; White, J. G.; Bavister, B. D.: Long-term two-photon fluorescence imaging of mammalian embryos without compromising viability. *Nature Biotech.* **1999**, *17*, 763-767.

(140) Srituravanich, W.; Fang, N.; Sun, C.; Luo, Q.; Zhang, X.: Plasmonic nanolithography. *Nano Lett.* **2004**, *4*, 1085-1088.

(141) Steckel, J. S.; Zimmer, J. P.; Coe-Sullivan, S.; Stott, N. E.; Bulovic, V.; Bawendi, M. G.: Blue luminescence from (CdS)ZnS core-shell nanocrystals. *Angew. Chem. Int. Ed.* **2004**, *43*, 2154-2158.

(142) Storhoff, J. J.; Lucas, A. D.; Garimella, V.; Bao, Y. P.; Muller, U. R.: Homogeneous detection of unamplified genomic DNA sequences based on colorimetric scatter of gold nanoparticle probes. *Nature Biotech.* **2004**, *22*, 883-887.

(143) Su, X.; Li, M.; Zhou, Z.; Zhai, Y.; Fu, Q.; Huang, C.; Song, H.; Hao, Z.: Microstructure and multiphoton luminescence of Au nanocrystals prepared by using glancing deposition method. *J. Lumin.* **2008**, *128*, 642-646.

(144) Sun, Y. G.; Yin, Y. D.; Mayers, B. T.; Herricks, T.; Xia, Y. N.:

Uniform silver nanowires synthesis by reducing $AgNO_3$ with ethylene glycol in the presence of seeds and poly(vinyl pyrrolidone). *Chem. Mater*. **2002**, *14*, 4736-4745.

(145) Sundaramurthy, A.; Schuck, P. J.; Conley, N. R.; Fromm, D. P.; Kino, G. S.; Moerner, W. E.: Toward nanometer-scale optical photolithography: Utilizing the near-field of bowtie optical nanoantennas. *Nano Lett.* **2006**, *6*, 355-360.

(146) Takahara, J.; Yamagishi, S.; Taki, H.; Morimoto, A.; Kobayashi, T.: Guiding of a one-fimensional optical beam with nanometer fiameter. *Opt. Lett.* **1997**, *22*, 475-477.

(147) Takahashi, H.; Niidome, Y.; Niidome, T.; Kaneko, K.; Kawasaki, H.; Yamada, S.: Modification of gold nanorods using phospatidylcholine to reduce cytotoxicity. *Langmuir* **2006**, *22*, 2-5.

(148) Tao, A. R.; Yang, P.: Polarized surface-enhanced Raman spectroscopy on coupled metallic nanowires. *J. Phys. Chem. B* **2005**, *109*, 15687-15690.

(149) Thess, A.; Lee, R.; Nikolaev, P.; Dai, H. J.; Petit, P.; Robert, J.; Xu, C. H.; Lee, Y. H.; Kim, S. G.; Rinzler, A. G.; Colbert, D. T.; Scuseria, G. E.; Tomanek, D.; Fischer, J. E.; Smalley, R. E.: Crystalline ropes of metallic carbon nanotubes. *Science* **1996**, *273*, 483-487.

(150) Thierry, B.; Ng, J.; Krieg, T.; Griesser, H. J.: A robust procedure for the functionalization of gold nanorods and noble metal nanoparticles. *Chem. Comm.* **2009**, 1724-1726.

(151) Tian, Z. Q.; Ren, B.; Wu, D. Y.: Surface-enhanced Raman scattering: From noble to transition metals and from rough surfaces to ordered nanostructures. *J. Phys. Chem. B* **2002**, *106*, 9463-9483.

(152) Tong, L.; Wei, Q.; Wei, A.; Cheng, J.-X.: Gold nanorods as contrast agents for biological imaging: Optical properties, surface conjugation and photothermal effects. *Photochem. Photobiol.* **2009**, *85*, 21-32.

(153) Ueno, K.; Juodkazis, S.; Shibuya, T.; Yokota, Y.; Mizeikis, V.; Sasaki, K.; Misawa, H.: Nanoparticle plasmon-assisted two-photon polymerization induced by incoherent excitation source. *J. Am. Chem. Soc.* **2008**, *130*, 6928-6929.

(154) von Maltzahn, G.; Park, J.-H.; Agrawal, A.; Bandaru, N. K.; Das, S. K.; Sailor, M. J.; Bhatia, S. N.: Computationally guided photothermal tumor therapy using long-circulating gold nanorod antennas. *Cancer Res.* **2009**, *69*, 3892-3900.

(155) Walker, D. A.; Browne, K. P.; Kowalczyk, B.; Grzybowski, B. A.: Self-assembly of nanotriangle super lattices facilitated by repulsive electrostatic interactions. *Angew. Chem. Int. Ed.* **2010**, *49*, 6760-6763.

(156) Wang, F.; Dukovic, G.; Brus, L. E.; Heinz, T. F.: The optical resonances in carbon nanotubes arise from excitons. *Science* **2005**, *308*, 838-841.

(157) Wang, H. F.; Huff, T. B.; Zweifel, D. A.; He, W.; Low, P. S.; Wei, A.; Cheng, J. X.: In vitro and in vivo two-photon luminescence imaging of single gold nanorods. *Proc. Natl. Acad. Sci. U.S.A.* **2005**, *102*, 15752-15756.

(158) Wang, Y.; Zou, X.; Ren, W.; Wang, W.; Wang, E.: Effect of silver nanoplates on Raman spectra of p-aminothiophenol assembled on smooth macroscopic gold and silver surface. *J. Phys. Chem. C* **2007**, *111*, 3259-3265.

(159) Willets, K. A.; Van Duyne, R. P.: Localized surface plasmon resonance spectroscopy and sensing. *Annu. Rev. Phys. Chem.* **2007**, *58*, 267-297.

(160) Wu, X.; Ming, T.; Wang, X.; Wang, P.; Wang, J.; Chen, J.: High-

photoluminescence-yield gold nanocubes: for cell imaging and photothermal therapy. *Acs Nano* **2010**, *4*, 113-120.

(161) Xiao, R.; Il Cho, S.; Liu, R.; Lee, S. B.: Controlled electrochemical synthesis of conductive polymer nanotube structures. *J. Am. Chem. Soc.* **2007**, *129*, 4483-4489.

(162) Xing, J.-F.; Dong, X.-Z.; Chen, W.-Q.; Duan, X.-M.; Takeyasu, N.; Tanaka, T.; Kawata, S.: Improving spatial resolution of two-photon microfabrication by using photoinitiator with high initiating efficiency. *Appl. Phys. Lett.* **2007**, *90*.

(163) Xu, H. X.; Aizpurua, J.; Kall, M.; Apell, P.: Electromagnetic contributions to single-molecule sensitivity in surface-enhanced Raman scattering. *Phys. Rev. E* **2000**, *62*, 4318-4324.

(164) Xue, P.; Lu, R.; Yang, X.; Zhao, L.; Xu, D.; Liu, Y.; Zhang, H.; Nomoto, H.; Takafuji, M.; Ihara, H.: Self-assembly of a chiral lipid gelator controlled by solvent and speed of gelation. *Chem.-Eur. J.* **2009**, *15*, 9824-9835.

(165) Yan, R.; Pausauskie, P.; Huang, J.; Yang, P.: Direct photonic-plasmonic coupling and routing in single nanowires. *Proc. Natl. Acad. Sci. U.S.A.* **2009**, *106*, 21045-21050.

(166) Yanagi, K.; Kataura, H.: Carbon nanotubes: Breaking Kasha's rule. *Nature Photon.* **2010**, *4*, 200-201.

(167) Yang, W. H.; Schatz, G. C.; Vanduyne, R. P.: Discrete dipole approximation for calculating extinction and Raman intensities for small particles with arbitrary shapes. *J. Chem. Phys.* **1995**, *103*, 869-875.

(168) Yanik, M. F.; Cinar, H.; Cinar, H. N.; Chisholm, A. D.; Jin, Y. S.;

Ben-Yakar, A.: Neurosurgery - Functional regeneration after laser axotomy. *Nature* **2004**, *432*, 822-822.

(169) Yin, X. F., Nicholas; Zhang, Xiang; Martini, Ignacio B.; Schwartz, Benjamin J.: Near-field multiphoton nanolithography using an apertureless optical probe. *In nonlinear optical transmission and multiphoton processes in organics.* ; Yeates, A. T., Belfield, K. D., Kajzar, F., Lawson, C. M., Ed., 2003; Vol. 5211; pp 96-103

(170) Yu, P.; Huang, J.; Tang, J.: Observation of coalescence process of silver nanospheres during shape transformation to nanoprisms. *Nanoscale Res. Lett.* **2011**, *6*, 46.

(171) Zheng, Y. B.; Yang, Y.-W.; Jensen, L.; Fang, L.; Juluri, B. K.; Flood, A. H.; Weiss, P. S.; Stoddart, J. F.; Huang, T. J.: Active molecular plasmonics: controlling plasmon resonances with molecular switches. *Nano Lett.* **2009**, *9*, 819-825.

(172) Zijlstra, P.; Chon, J. W. M.; Gu, M.: Five-dimensional optical recording mediated by surface plasmons in gold nanorods. *Nature* **2009**, *459*, 410-413.

(173) Zimmer, A.: Antisense oligonucleotide delivery with polyhexyl cyanoacrylate nanoparticles as carriers. *Methods.* **1999**, *18*, 286-295.

(174) Zipfel, W. R.; Williams, R. M.; Webb, W. W.: Nonlinear magic: multiphoton microscopy in the biosciences. *Nature Biotech.* **2003**, *21*, 1368-1376.

(175) Zou, S. L.; Schatz, G. C.: Silver nanoparticle array structures that produce giant enhancements in electromagnetic fields. *Chem. Phys. Lett.* **2005**, *403*,

62-67.

(176) Zou, X.; Dong, S.: Surface-enhanced Raman scattering studies on aggregated silver nanoplates in aqueous solution. *J. Phys. Chem. B* **2006**, *110*, 21545-21550.

(177) Zuechner, T.; Failla, A. V.; Steiner, M.; Meixner, A. J.: Probing dielectric interfaces on the nanoscale with elastic scattering patterns of single gold nanorods. *Opt. Express* **2008**, *16*, 14635-14644.